THE UNIVERSITY OF MANITOBA

THE DEFORMATION BEHAVIOR OF PRECIPITATION HARDENED Co - Ni - Cr - Ti SUPERALLOYS

by

D. W. CHUNG

A THESIS

SUBMITTED TO THE FACULTY OF GRADUATE STUDIES

IN PARTIAL FULFILMENT OF THE REQUIREMENTS FOR THE DEGREE

OF DOCTOR OF PHILOSOPHY

DEPARTMENT OF MECHANICAL ENGINEERING

METALLURGY

WINNIPEG, MANITOBA

February, 1976

"THE DEFORMATION BEHAVIOR OF PRECIPITATION HARDENED
Co - Ni - Cr - Ti SUPERALLOYS"

by

D. W. CHUNG

A dissertation submitted to the Faculty of Graduate Studies of the University of Manitoba in partial fulfillment of the requirements of the degree of

DOCTOR OF PHILOSOPHY

ABSTRACT

The Deformation Behavior of Co - Ni - Cr - Ti Alloys

by

D. W. Chung

The deformation behavior of three Co - Ni - Cr base precipitation hardenable alloys with different Ti contents has been studied. On ageing at 700, 800 and 900° C the main precipitating phase was found to be the γ' phase, with an ordered F.C.C. structure, in a F.C.C. matrix. The γ' phase precipitated coherently along <100> matrix directions in cuboid shape and the precipitate-lattice mismatch was 1.3%. The coarsening kinetics of γ' precipitate in all the three alloys followed the time-law predictions of the Lifshitz-Wagner theory of diffusion controlled growth at all the ageing temperatures. The particle size distribution of γ' was significantly broader than the distribution predicted by the Lifshitz-Wagner theory. This appears to be in agreement with previous studies on other alloy systems and may be attributable to the relatively large lattice mismatch between the precipitate and the matrix. The effect of volume fraction of γ' on its coarsening rate was negligible and thus the present system did not follow the "Modified Lifshitz-Wagner theory", which takes into consideration the volume fraction of the growing phase.

The strengthening mechamisms in terms of dislocation-particle interaction, have also been studied. It was observed that when the γ' particle size is smaller than 28 $\mathring{A}$ they are sheared by

the glide dislocations, which move in pairs, and when it is larger than 56 Å they are passed by the single glide dislocations leaving loops around the precipitate particles. Both types of interactions were observed when the particle size was between 28 - 56 Å. During the early stages of ageing, when the particles are sheared by pairs of dislocations, the tensile test results seem to fit both the coherence hardening model of Gerold and Haberkorn and the order hardening model of Brown and Ham. However, the nature of the $\Delta\tau$ - $r_s^{1/2}$ curves and the determination of antiphase boundary energy from them seemed to favour the order hardening mechanism. During the Orowan hardening the suggestion of Hirsch and Humphreys that both edge and screw dislocations require the same stress to by-pass the particles, seems to be correct.

Serrated yielding was also observed in the temperature range of 300 $\sim$ 600° C. The onset of serrated yielding is shown to be in agreement with the static strain ageing model. The critical strain to serrations decreases with increasing solute concentration in the solid-solution and with ageing time in aged conditions. This behavior can be explained in terms of a change in obstacles spacing if solute atoms are the major obstacles to dislocation motion in the solid solution condition and if γ' particles are the obstacles in the aged condition. The results also indicate a consistancy with Saada's model for vacancy production and a negligible change in the mobile dislocation density with strain.

The flow stresses in the temperature range of 23 to 900° C at various strain rates was also determined. In the temperature range

where serrated yielding was observed the 0.2% offset yield stress showed a characteristic temperature independence and also an inverse strain rate effect.

SYMBOLS

C	An average concentration in a system with a different particle size.
C_r	The equilibrium solutility of a one component particle with a radius r.
C_e	The equilibrium solubility of a particle of infinite radius in the external phase.
γ_s	The interfacial free energy of the particle-matrix interface.
Ω	Molar volume of a particle.
t	Ageing time of a system.
D	Diffusion coefficient of solute atoms in the matrix phase.
R	Gas constant; 1.987 cal/mole° K.
T	Absolute temperature.
r	The particle radius.
r^*	The critical particle radius; $\Sigma r_i / \Sigma r_i^2 = 1/r^*$ where i = 0, 1, 2, 3, ...
$\bar{r}$	The mean particle radius.
$\bar{r}_{(o)}$	The mean particle radius at t = 0.
$\bar{r}_{(t)}$	The mean particle radius at time t.
f_v	Volume fraction of particles.
$f(r,t)$	The distribution function of particle size, r, at time t.
Q	Activation energy for the coarsening process.
Z	The total number of particles per unit volume.
$g'(r,t)$; $f(r,t)/z$	
ρ	The dimensionless measure of particle size; $r/r^*_{(t)}$.

K	A rate constant of the coarsening process for the spherical particle.
K'	A rate constant of the coarsening process for the cuboid particles.
$g(t)$, $h(\rho)$	Help functions defined for growth kinetics in section (1.2).
ρ_M	The maximum reduced particle size in dimensionless unit.
$\Gamma(f_v)$	A function of f_v; $\int_{8f_v}^{\infty} x^{-2/3} e^{-x} dx$.
$\bar{a}(t)$	The mean edge length of the cubic particles at time t.
$\bar{a}(o)$	The mean edge length of the cubic particle at time 0. t = 0.
F	The force on an obstacle due to a dislocation and vice versa.
T^*	The Dewit-Koehler approximation for the line tension.
τ	Applied shear stress resolved in the slip direction in the slip plane.
ϕ	Included angle between the arms of a dislocation at an obstacle.
b	Burgers vector of a dislocation.
N_A	The number of particle per unit area.
L	Spacing between two obstacles.
L_o	The mean planar spacing of obstacles; Orowan spacing.
L_s	The square lattice spacing; $N_A^{-1/2}$.
L_1	The effective particle spacing at the first dislocation of a pair.
L''	The average distance between the force centers.
L_f	The Friedel spacing.
τ_f	The Friedel stress.
N_V	The number of particles per unit volume

τ_o	The Orowan stress.
τ_1	The shear stress required to cut the particle by the first dislocation.
γ_{APB}	Anti-phase boundary energy.
r_s	The average radius of particle intersected by a slip band; $(\frac{2}{3})^{1/2} r$.
$\Delta\tau$	The increment of flow stress.
K_r	The maximum repelling force of the strain field of a single particle on a moving dislocation.
θ	The angle between the Burgers vector and the normal to the tangent of a curved segment of dislocation; $1/2\ (\pi - \phi)$.
ε	The "constrained" strain; coherency strain.
τ_m	The shear yield stress of the matrix phase.
τ_{edge}	The shear stress for edge dislocation
τ_{screw}	The shear stress for screw dislocation
G	Shear modulus.
X	Dipole width of a dislocation.
r_o	Inner cut off radius.
ν	Poisson ratio.
σ, σ_{edge}, σ_{screw}, σ_m	The macroscopic flow stress; for two phases edge dislocation, screw dislocation, and the matrix phase.
T_c	The ordering temperature.
S	The Bragg-Williams long range order parameter.
τ_p	The extra-hardening stress due to particle.
V_s	The velocity of the solute atoms.

ℓ	The effective radius of the solute atmosphere.
U_m	The solute-dislocation binding energy.
ε	Strain.
$\dot{\varepsilon}$	Strain rate.
V_D	The velocity of a dislocation around solute atmosphere.
Φ	An orientation factor upon which $\dot{\varepsilon}$ depends.
ρ_m	Mobile dislocation density.
ρ_T	Total dislocation density.
C_V	Vacancy concentration of alloy.
Q_m	Vacancy migration energy.
D_o	Pre-exponential diffusion coefficient.
ε_c	Critical strain for the onset of serrated yielding.
t_w	Waiting time of a dislocation at obstacles.
t_a	Ageing time of a dislocation.
t_f	Dislocation flight time.
$\bar{V}_j$	Jumping velocity of a dislocation during serrated yielding.
C_1	Solute concentration at the dislocation line.
C_o	Solute concentration of the alloy.
ℓ_d	Length between attractive trees of defect.
ρ_o	The density of randomly distributed dislocation network.
σ_y, σ_o	0.2% tensile yield stress of the alloy and solid solution.
a_o	A lattice parameter.
F_A, F_B	The atomic fraction of A and B atoms.
τ_{AP}	The applied shear stress.
$\bar{L}$	The mean planar particle spacing.

α, α_1, A, A_1, A_2, A_s, β, B_1, B_2, B_3, K', m, n, N
Constants arising in the analysis of serrated yielding process.

κ Boltzmann's constant; 1.381×10^{-16} erg/K°.

A_o The area occupied by a loop.

dN The number of attractive trees per unit volume

β_1, B, δ, $N_{hk\ell}$, $\bar{V}_{LI_2}$ Constants arising in the particle strengthening process.

γ_θ The dislocation loop radius.

Z_{AB} The number of first nearest neighbor atoms in crystal.

$\Delta\sigma_f$ The discontinuous increase in flow stress prior to the yield drop.

$\Delta\sigma_d$ The displacement of the level of the force-elongation curve accompanying each serration.

ε_s The strain between successive periodic locking serrations.

e Engineering strain.

v, β', $\bar{A}$ Constants arising in the analysis of coarsening process.

$f(\bar{r}, \bar{f}_v)$ A function of particle size and volume fraction of γ'.

a_p, a_m Lattice parameters of the precipitate particle and the matrix respectively.

ε_p Plastic strain.

ACKNOWLEDGMENTS

I wish to express my sincere thanks to my supervisor, Dr. M. C. Chaturvedi whose guidance and assistance made this work possible. In addition, I am indebted to Dr. D. J. Lloyd for making many helpful suggestions for the improvement of this thesis. I also acknowledge the University of Manitoba for financial support in the form of a scholarship.

Above all, I am grateful to my wife, Myong Hi for her faithful patience and encouragement during the course of this study.

CONTENTS

CONTENTS

CONTENTS

I. INTRODUCTION

The empirical development of an alloy for the improvement of its mechanical properties has led to introducing a variety of alloying element into the more complex alloying system. During the past several years many nickel and cobalt based superalloys have been developed. These alloys have been extensively used in exacting thermal conditions because of their good mechanical and corrosion properties. Cobalt based superalloys have a flatter stress-rupture/time temperature parameters, can provide a better hot corrosion resistance, and also they can be used at temperature a few hundred degrees higher than Nickel base alloys[1]. Most of the strength of these high temperature superalloys is derived by the precipitation of γ' phase. The γ' precipitate is of Ni_3X type with an ordered F.C.C. structure (LI_2), and precipitates coherently in the F.C.C. matrix of nickel base alloys. The magnitude of the strength of these alloys is dependent mainly on the volume fraction and size of γ' precipitate and also on their growth kinetics.

The coarsening process of spherical particles in a fluid matrix has been explained in terms of a diffusion controlled process[2,3]. A similar explanation has been successfully applied to the growth of γ' particles in the solid state in several binary Ni - base alloys[4-7]. In addition, this type of precipitate has also been shown to possess the diffusion controlled coarsening characteristics in a low volume fraction alloy Nimonic 80A[8], as well as in a high volume fraction alloy, Udimet 700[9].

Following the coarsening kinetics of γ' phase, several strengthening mechanisms by γ' particles in terms of dislocation interaction with particles have been widely investigated in Nickel-base high temperature alloys[10-12]. When the γ' particles are small the moving dislocation tends to shear the particle and when the particle size is large it by-passes them by the Orowan mechanism.

During the particle shearing, the strength of the alloy seems to be governed mainly, by two factors, viz. (1) chemical or order hardening and (2) coherency or misfit hardening. The chemical hardening originates from the anti-phase boundary which is created within the ordered particles during the shearing process[12]. The coherency hardening is attributed to the interaction of glide dislocations with the elastic coherency stresses around coherent γ' precipitates. A great deal of doubt exists regarding the relative contribution of these two factors to the strength of alloys. Mihalison and Decker[13], and Fine[14] emphasize the coherency strains while Raynor and Silcock[15] and Phillips[16] consider A.P.B. energy to be the main strengthening factor. On the other hand, Singhal and Martin[17] found the two factors to be additive. However, at large misfit, coherency strain will be more significant than at low misfit.

During the course of the deformation studies serrated yielding has been noted in superalloys[18]. An extensive literature has been developed regarding the serrated yielding in F.C.C. and B.C.C. alloys[19-21], but there has been no detailed investigation of the phenomenon in alloys precipitation hardened by γ' phase. In the case of Udimet 520[19],

Doi and Shimanuki attributed the effect to solute atom-dislocation interaction, similar to the mechanism suggested for the majority of F.C.C. alloys. However, serrated yielding in a series of metastable austenitic alloys has been attributed to carbide precipitation. But, the influence of large amount of second phase particle on serrated flow has not been investigated in any detail. In Al alloys Phillips[22] and Matsuura et al[23] have shown that ageing increases the critical strain to serrations and may also modify the nature of serrations observed. Experiments on Alpha-beta brass[24] have also shown that the critical strain to serrations increases with increasing volume fractions of second phase. However, the mechanism by which precipitation influences serrated yielding is not understood at present.

Recently in a Co - Ni - Cr - Ti alloy[25], the main strengthening phase was identified as the γ' ordered, Ni_3Ti, which precipitates coherently in a Co - Ni - Cr F.C.C. matrix and on overageing γ' transforms to a hexagonal η- type, Ni_3Ti phase. The lattice misfit between γ and γ' was found to be 1.3%, which is one of the higher values in comparison with those of other high temperature alloys[25].

This alloy was chosen as the basic composition to investigate the coarsening behavior of γ' precipitate as well as its influence on the deformation behavior in a series of Co - Ni - Cr - Ti alloys.

II LITERATURE REVIEW

1. Coarsening process of precipitate particles.

The mechanical properties of precipitation strengthened alloys have been understood in terms of the morphological changes through the thermal interaction between the two phases. These changes usually involve the shapes and sizes of the second phase particles and their distribution. The shape changes may be related to diffusion along the interface of the particles while the change in size is controlled by the volume diffusion of the particles and/or by the volume diffusion within the matrix surrounding the particles. The change in size distribution may also be controlled by the mechanism of transport across the interface of the particles, and/or by the diffusion in the matrix. Early in 1900, Ostwald[26] first reported a systematic study of the increased solubility of small particles due to their reduction in total particle surface (Ostwald ripening). Later, Lifshitz and Slyozov[2] and Wagner[3] developed the basic theory of particle coarsening (LSW theory). Several reviews on this problem have recently appeared in the literature, e.g. by Greenwood, [27] by Che-Yu Li and Oriani[28] and by Ardell[29].

The basic theory of LSW is concerned primarily with the fact that if there is enough atomic mobility in a solid matrix, a dispersion of particles will coarsen by the transfer of matter from small to large particles in order to reduce the free energy associated with the particle/matrix interface area. In other words, at any given moment, particles smaller than a critical size r* will dissolve, surrounding themselves with an excess amount of solute atom which will diffuse to particles larger than r*. Thus, if the diffusion of atoms between

the particles is the slowest step, then the coarsening will be diffusion controlled, whereas if the deposition or dissolution of atoms at the particle interfaces is the slowest step then the growth kinetics will be the reaction controlling process. Based on these definitions the concentration profile between particles can be constructed as shown in Figure (1), and several growth rates of the particle can be formulated. (The case of interface controlled transfer also developed by Wagner[3] will not be considered here.)

1.1 Diffusion controlled growth kinetics.

The coarsening process where the rate determining step is the diffusion through the matrix has been analysed by Wagner[3].

He began with the old classic Gibbs-Thomson equation

$$C_r = C_e \exp (2 \gamma_s \Omega / r RT) \quad \ldots \quad (1)$$

relating C_r, the equilibrium solubility of a one component particle of radius r, to C_e, the equilibrium solubility of a particle of infinite radius in the given external fluid phase. γ_s is the specific interfacial free energy between the external phase and the particle of molar volume Ω, R is the gas constant and T the absolute temperature.

Using Zener's expression[30] for the concentration gradient at the interface between the particle and solution, he obtained the rate of change in particle radius,

$$\frac{dr}{dt} = D\Omega \frac{C - C_r}{r} = \frac{\gamma_s C_e D \Omega}{RTr} \left(\frac{1}{r^*} - \frac{1}{r}\right) \quad \ldots \quad (2)$$

Figure (1) Schematic concentration profiles for growing and shrinking particles.

(a) pure surface control,

(b) fast diffusion or large particle spacings,

(c) slow diffusion or small spacings.

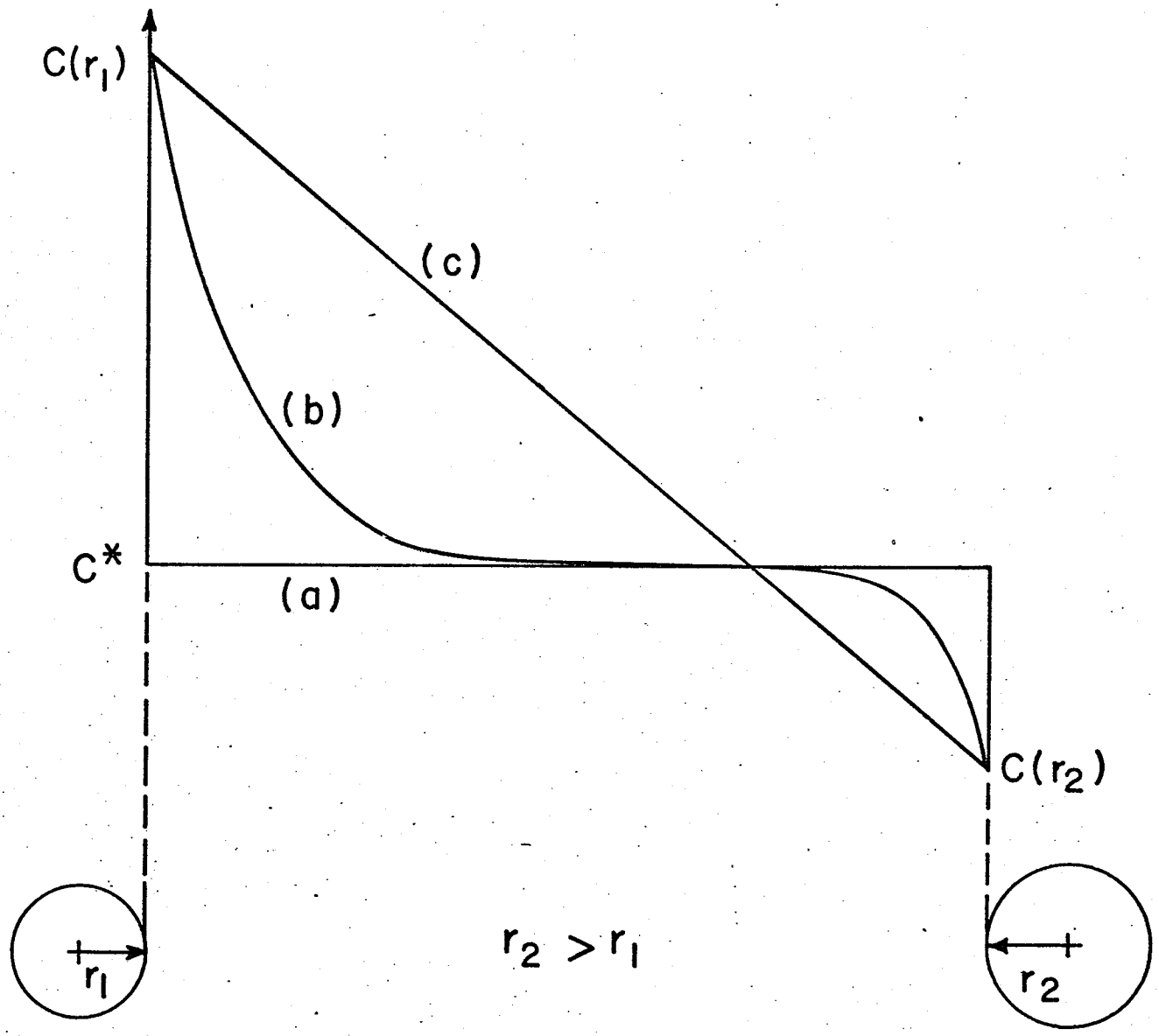

FIG. (1)

where D is the diffusivity in the matrix phase and r* is the critical radius given by

$$\Sigma\ r_i/\Sigma r_i^{\,2} = \frac{1}{r^*}$$

Provided the number of particle/unit volume is not too large the equation (2) may be applied to any one particle in an assembly of particles distributed at random over a range of size. It, however, should be noted that C denotes the mean concentration at the periphery of a sphere and also that the particle is drawn with a diameter equal to the mean separation between particles. Thus, the particle characterized by $C_r < C$, ie. larger than average particles in their immediate neighbourhood, will grow, and the particle characterized by $C_r > C$ ie. smaller than average will lose substance.

Wagner also solved the complex statistical problem for the variation of the mean radius $\bar{r}$ with time in an assembly of particles by introducing the size distribution function f(r,t). This function is such that f(r,t) dr is the number of particles at time t having radii between r and r + dr. (Details of solution are in Ref. (2) and (3).

The final form of LSW equation for the diffusion controlled process is thus given by

$$\bar{r}(t)^3 - \bar{r}(0)^3 = \left(\frac{8r_s DC_e\Omega^2}{9RT}\right)t = Kt \qquad \ldots\ (3)$$

where $\bar{r}(0)$ is the particle radius at the onset of coarsening.

This equation is valid only after the time required to deplete the concentration of matrix down to the C_e, and when the transfer of matter between particles is controlled by diffusion in the matrix.

1.2 Distribution of particle size.

Wagner[3] further showed that the distribution function of particle size f(r,t) is proportional to r^2, by

$$f(r,t) = g(t)\ \rho^2\ h(\rho) \qquad \ldots . \qquad (4)$$

where $g(t) = 1/(1 + t/\tau')^{4/3}$, $\tau' = \dfrac{9(\bar{r}(o))^3 RT}{8\gamma_s D C_e\ \Omega^2}$

$= (\bar{r}_{(o)})^3/K$, $\rho = r/r^*(t)$, and he also found $h(\rho)$ as

$$h(\rho) = \left(\frac{3}{3+\rho}\right)^{7/3} \left(\frac{3/2}{3/2-\rho}\right)^{11/3} \exp\left(\frac{-\rho}{3/2-\rho}\right) \text{ when } \rho < 3/2$$

$$h(\rho) = 0 \qquad \text{when } \rho > 3/2$$

The function $\rho^2 h(\rho)$ has the following characteristic features;

(a) a sharp cut-off at $\rho = 3/2$

(b) maximum at $\rho = 1.135$

(c) $\int_o^\infty \rho^2 h(\rho) d\rho = 9/4$ .... (5)

It has also been shown that, the distribution function f(r,t) is so defined that $\int_o^\infty f(r,t)\ dr = Z$, where Z is the number of particle/unit volume.

For the empirical purposes it is convenient to normalize f(r,t) by defining a new function g'(r,t) such that $\int_o^\infty g'(r,t)\ dr = 1$.

Upon substitution of equation (4) into the defining expression for Z, and making use of equation (5)

$$g'(r,t) = f(r,t)/Z$$

which then becomes

$$g'(r,t) = \frac{\rho^2 h(\rho)}{(9/4)\bar{r}}$$

Thus, for "steady-state" distribution the experimental histogram $g'(r,t)$ need only be multiplied by $(9/4)\bar{r}$ for comparison with the theoretical time-invariant function $\rho^2 h(\rho)$.

1.3 The effect of volume fraction on the particle coarsening process.

The theory of diffusion controlled particle coarsening developed by LSW is applicable only when the volume fraction, f_V, of the dispersed phase is very low. Just how small f_V must be is not precisely defined in the LSW theory. However it is assumed that it is small enough so that the mean distance between particle centers is larger than the particle dimension.

Sarian and Weart[31] suggested that the general growth law of LSW theory was still valid with a finite fraction f_V of precipitates. The only difference was that the rate constant in equation (3) had to be multiplied by a f_V dependent enhancement factor given by $4/3[(1 - f_V)/f_V]^{-1}$. Recently Ardell[32] modified the LSW theory in that the coarsening rate should increase with increasing volume fraction of precipitate, whereas the basic $(1/t)^3$ kinetics are unaffected. According to this modification, even at very small volume fraction ($f_V < 0.01$) the effect of f_V on the

coarsening rate is significant as shown in Fig. (2). It was clearly indicated that Ardell's approximation for critical radius, r*, would exaggerate the effect of particle interaction and therefore could be considered as an upper bound. Furthermore Ardell predicted that the theoretical distribution function of particle size should also be affected by f_V. Figure (3) shows the effect of volume fraction on the diffusion controlled growth. It is seen that $h(\rho)$ broadens rapidly with increasing f_V, and approaches the particle size distribution for interface coarsening in the limit $f_V = 1$.

1.4 Experimental observations of coarsening kinetics.

The first experimental evidence supporting the theory of diffusion controlled particle growth in a solid was obtained by Livingston[33]. Working on Co precipitate in Cu - Co alloys, he found a cubic growth kinetics by magnetic technique. A later study by Servi and Turnbull[34] verified that the growth of precipitate in this system is diffusion controlled. Both studies, however, deal with early stages of precipitate growth, and it is not certain that Livingston's result pertain to stationary Ostwald ripening.

Speich and Oriani[35] found that the growth of Cu precipitate is Cu - Fe matrix follows a cubic rate law, even though the precipitates are rod shaped. However, a number of complicating features were left in the application of LSW theory in this system since the precipitates are semi coherent in the matrix. A considerable amount of attention has recently been given to the influence of coherency strain on the particle growth kinetics[36-38]. It has been

Figure (2) Effect of Volume fraction of particles on rate constant, $K^{(32)}$.

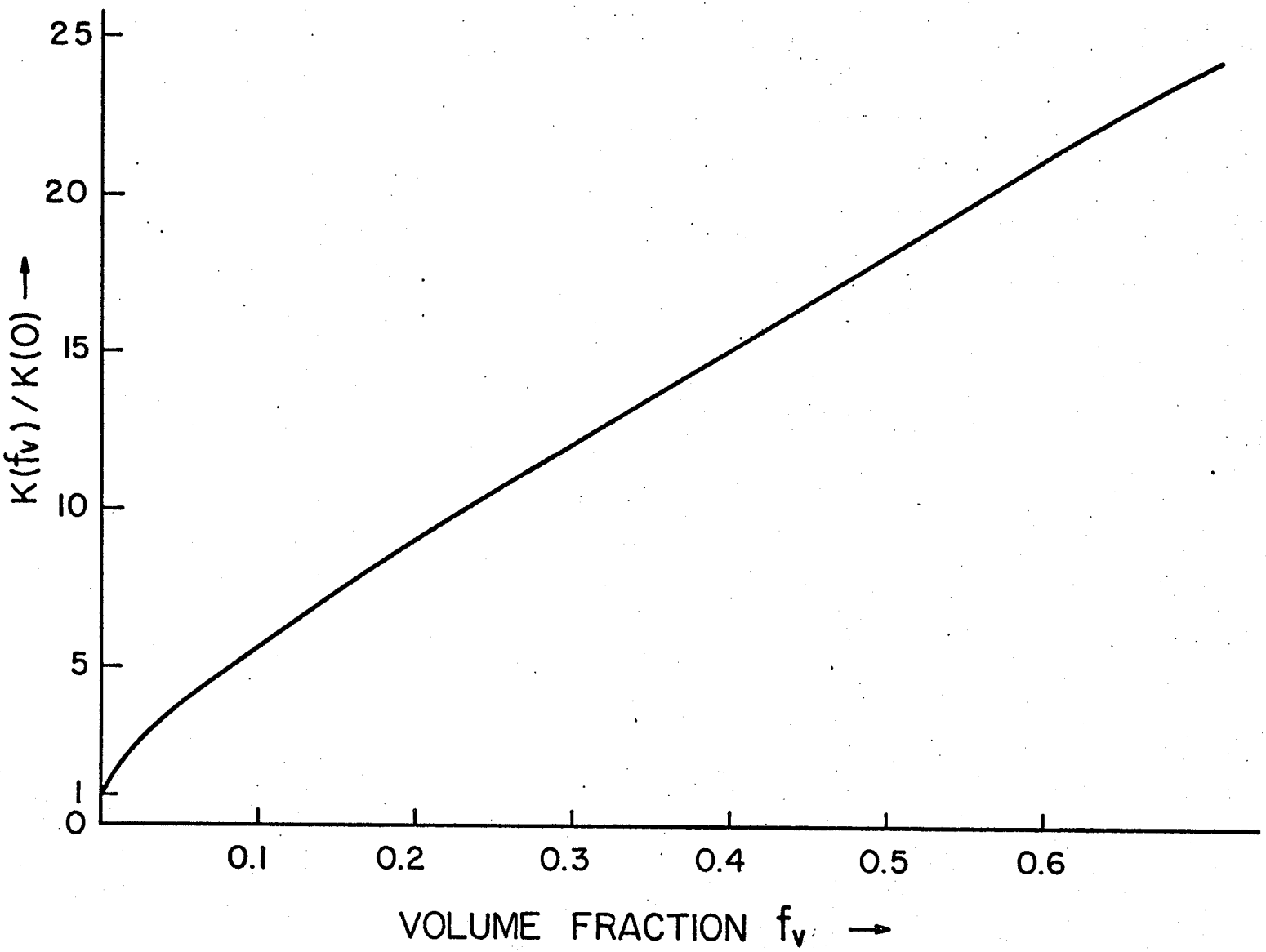

FIG. (2)

Figure (3) Stationary size distributions[2,3] and the effect of volume fraction in diffusion controlled growth[32].

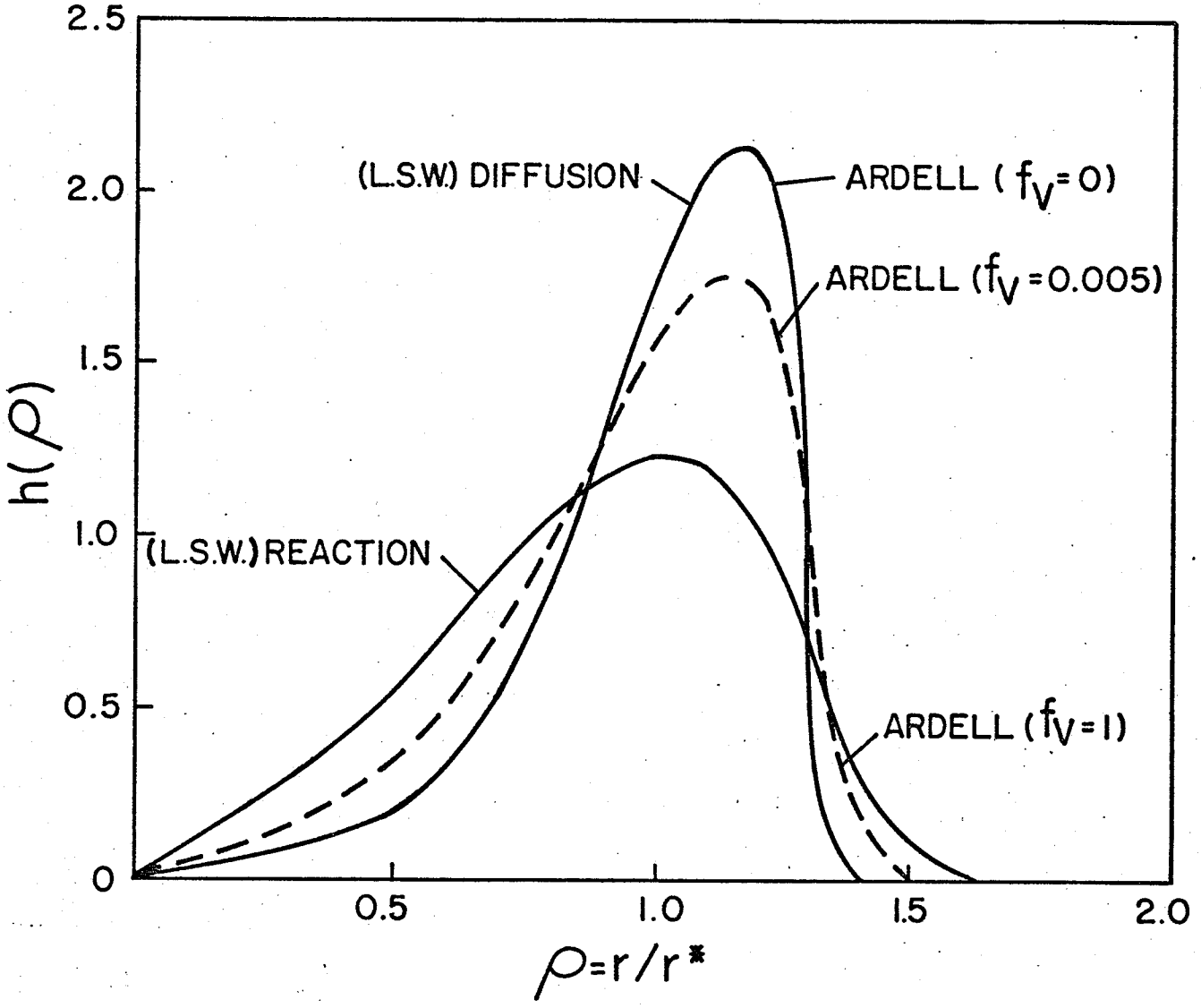
2.5
2.0
1.5
1.0
0.5
0
h(ρ)
(L.S.W.) DIFFUSION
ARDELL (f_V = 0)
ARDELL (f_V = 0.005)
(L.S.W.) REACTION
ARDELL (f_V = 1)
0.5
1.0
1.5
2.0
ρ = r/r*

FIG. (3)

argued that a coherent precipitate, because of its associated strain energy, must have a higher solubility than a non-coherent precipitate of the same phase. Although some alteration in the growth parameter has been made, serious modification to the general form of the growth analysis is not expected to be required[38].

Most of the coarsening studies on metal - intermetallic systems have been concerned with γ' phase [Ni_3(Al, Ti)] particles in nickel based alloys. This subject has been well reviewed by Ardell[29] and Hornbogen and Roth[39]. Generally the γ' particles are coherent with the matrix, but in Ni - Cr - Al alloy, by adjusting the matrix composition the misfit can be made zero. It is also found that the particle/matrix interface energy is very low since only second nearest neighbor interactions are involved. With increasing misfit the particle shape can change from spherical to cubic and finally plate or rod-like. Frequently a large volume fraction of γ' precipitate is developed in these alloys. The precipitate particles, then, align themselves along <100> directions owing to the interaction of coherency stresses. Eshelby[40] has discussed these interactions in detail and a mechanism for alignment by preferential growth of favorably situated particles has been proposed[4]. However, irrespective of particle shape and misfit, growth of the γ' precipitate obeys a diffusion controlled coarsening model where the average particle radius increases linearly with time to the one-third power, $t^{1/3}$. i.e. $\bar{r} \propto t^{1/3}$.

In the case of superalloy containing γ' phase Mitchell[8] has shown that the coarsening of γ' in the relatively simple, low volume fraction superalloy Nimonic 80A is also diffusion - controlled.

Recently, using the technique of γ' separation, refined by Kriege and co-workers[41,42], Molen et al[43] determined chemical composition, volume fraction and particle size of the γ' precipitate in Udimet 700 as a function of temperature and time. They showed that the growth of γ' particles precisely follows $t^{1/3}$ diffusion controlled coarsening kinetics. Using their coarsening data a method was developed to estimate the volume fraction and average particle size of the γ' precipitate for any given heat treatment. It was then suggested that this approach could be applied to other γ' strengthened superalloys.

2. Strengthening mechanisms in alloys containing the precipitate particles.

Hardening by precipitate particles has been an important mechanism in high strength materials. Investigations in this field have recently been reviewed by Brown and Ham[12].

It was suggested that in materials containing small ordered particles, dislocations move in pairs. In cutting through a particle the first dislocation creates an anti-phase boundary, when the second dislocation passes through the same particle, the order is restored. For large particles, the glide dislocations bow-out and by-pass them following the Orowan mechanism.

Several theories have been published describing the dependence of the critical shear stress on the particle size and volume fraction of the particles, but the basic mechanisms are mainly dependent on calculating the force interaction between a moving dislocation

and the particle in its path. Suppose a dislocation moves through a field of dispersed particles. This dislocation must bend to an angle, ϕ, which depends on the particle strength, as shown in Figure (4). At a certain critical point where the dislocation breakes away from the particles, the particle strength, F, is related to the dislocation line tension, T*, by

$$F = 2T^* \cos\left(\frac{\phi}{2}\right) \quad \ldots. \quad (6)$$

The shear stress, τ, needed to cause the dislocation to break away from the particle will thus be:

$$\tau b = \frac{F}{L} \text{ or } \tau = \frac{F}{bL} = \frac{2T^* \cos\left(\frac{\phi}{2}\right)}{bL} \quad \ldots. \quad (6a)$$

where L is the effective particle spacing and b the Burgers vector.

In a real two phase alloy the calculation of flow stress mainly involves selecting some average value of F and L and then substituting these values into equation (6). For example, the most commonly used expression for the obstacle spacing is that of Friedel[44]

$$L_f = \left(\frac{2T^*}{\tau_f b N_A}\right)^{1/3} = \left(\frac{2T^* L_s^2}{\tau_f b}\right)^{1/3} \quad \ldots. \quad (7)$$

where L_s is the square lattice spacing, (= $N_V^{1/2}$ where N_V is the number of particles per unit volume), and τ_f is the stress required to cause the dislocation to break through the arrays of particles and N_A the number of particle intersecting unit area of slip plane.

Substituting this value of L_f into (6) gives the τ

$$\tau = \frac{2T}{b} (N_A)^{1/2} \left[\cos\left(\frac{\phi}{2}\right)\right]^{3/2} = \frac{2T^*}{bL_s} \left[\cos\left(\frac{\phi}{2}\right)\right]^{3/2} \quad \ldots. \quad (8)$$

Figure (4) Dislocation pairs interacting with ordered particles, showing effect of bend angle ϕ on obstacle spacing. Shaded area represents Anti-phase boundaries[12].

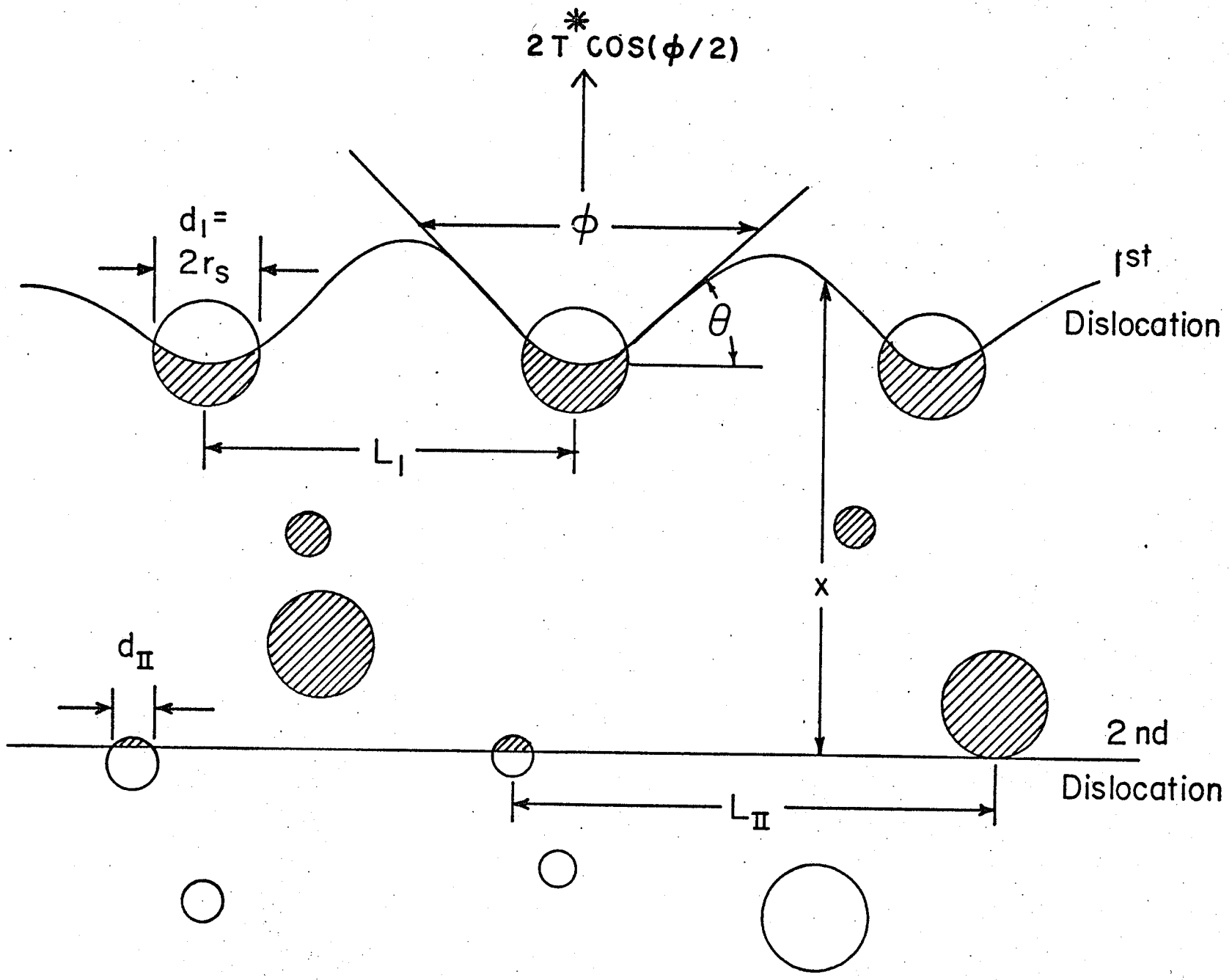
2T* COS(φ/2)
φ
d_I = 2r_S
θ
1st Dislocation
L_I
x
d_II
2nd Dislocation
L_II

FIG. (4)

The exact value of particle spacing has been the subject of considerable discussion in the literature[45,50]. For a regular square array of impenetrable particles on the slip plane $L_f = L_s$, for the random array of particles, Kocks[46-48] gives $L_f = 1.19\ L_s$ and Foreman and Makin[49,50] give $L_f = 1.23\ L_s$.

2.1 Particle shearing models.

In the case where particles are cut by glide dislocation ($\phi > 0$), the force, F, required to cut the particle or the breaking angle ϕ must be calculated and substituted into equation (6) and (8). These calculations have been based on two strengthening models, viz. a) order strengthening b) misfit or coherency strengthening.

(a) Order strengthening model.

When the glide dislocation cuts an ordered particle, Ham[51] suggested that, neglecting the particle matrix interfacial energy, the force $\tau_1 b$, on the dislocation must balance the anti-phase boundary energy created, which is $2\ r_s\ \gamma_{APB}/L_1$ where γ_{APB} is the anti phase boundary (APB) energy, thus

$$\tau_1 = \frac{2r_s\ \gamma_{APB}}{L_1\ b} \qquad \ldots . \qquad (9)$$

where r_s is the average radius of particle intersected by a slip plane [$r_s = (\frac{2}{3})^{1/2}\ r$ where r is the particle radius]. Since $N_A = \frac{f_v}{\pi r_s^2}$, $L = (\frac{\pi}{f_v})\ r_s$ where f_v is the volume fraction of the particles. The Friedel spacing becomes:

$$L_1 = (\frac{2T^*\pi\ r_s}{f_v \tau_1\ b})^{1/3} \qquad \ldots . \qquad (10)$$

Substituting L_1 into equation (9), the stress necessary to force the dislocation through the particle is

$$\tau_1 = \frac{\gamma_{APB}^{3/2}}{b} \left(\frac{4f_v r_s}{\pi T^*}\right)^{1/2} \quad \ldots \quad (11)$$

While the first dislocation can cause an A.P.B. in the ordered particle, the second dislocation then removes the A.P.B., and therefore moves without external shear stress until it is repelled by the first dislocation which has caused the A.P.B. The force due to the A.P.B., therefore, always connects two dislocations as a dislocation pair[51] as shown in Figure (4). Following the single dislocation shearing process developed by Ham[51], Brown and Ham[12] calculated an equation for the case of superlattice dislocation pairs interacting with ordered particles, (see Appendix)

$$\tau = \frac{\gamma_{APB}}{2b} \left[\left(\frac{4\gamma_{APB} f_v r_s}{\pi T^*}\right)^{1/2} - f_v\right] \quad \ldots \quad (12)$$

for

$$\frac{\pi T^* f_v}{4\gamma_{APB}} < r_s < \frac{T^*}{\gamma_{APB}}$$

$$\tau = \frac{\gamma_{APB}}{2b} \left[\left(\frac{4f_v}{\pi}\right)^{1/2} - f_v\right] \quad \ldots \quad (13)$$

for

$$r_s > T^*/\gamma_{APB}$$

and $\tau = 0$ for $r_s \leq \pi \dfrac{T^* f_v}{4\gamma_{APB}}$

The flow stress given by equation (12) would then reduce to one-half of the stress given in equation (11) for single dislocation. The

basic features of this model are summarized schematically in Figure (5) and have been applied successfully to a number of austenitic alloys[10, 12,15,51,52].

(b) Misfit strengthening model.

There have been attempts[53] to calculate the influence of coherency strains on the critical shear stress but they failed to explain the observed dependence of the critical shear stress on the particle size. Recently a model has been proposed by Gerold and Haberkorn[54] where the interaction between the dislocation and strain field around the precipitate particles plays a dominant role. The equation begins with the increase in flow stress due to the interaction of the dislocation with the strain field i.e.

$$\Delta\tau = \frac{K_r}{bL''} \qquad \ldots\ldots \qquad (14)$$

where K_r is the maximum repelling force of the strain field of a single particle on a moving dislocation and L'' is the average distance between the force center. As in the first section of this chapter, the problem in the equation is to find appropriate expressions for K_r and L''. K_r is found to be equal to or less than the line tension, T* of an edge dislocation. But, for L'', instead of using the Friedel spacing as in the case of ordering model they used an expression of Fleischer[55] spacing for L'' in which the obstacle spacing depends on the bend angle $\theta = \frac{1}{2}(\pi - \phi)$ by

$$L'' = \frac{r_s \pi^{1/2}}{(\theta f_v)^{1/2}}, \quad \frac{9\pi f_v}{16} < \theta < \frac{3}{2} \qquad \ldots\ldots \qquad (15)$$

Figure (5) Schematic age-hardening curves illustrating relation between order strengthening and Orowan bowing as a function of particle size.

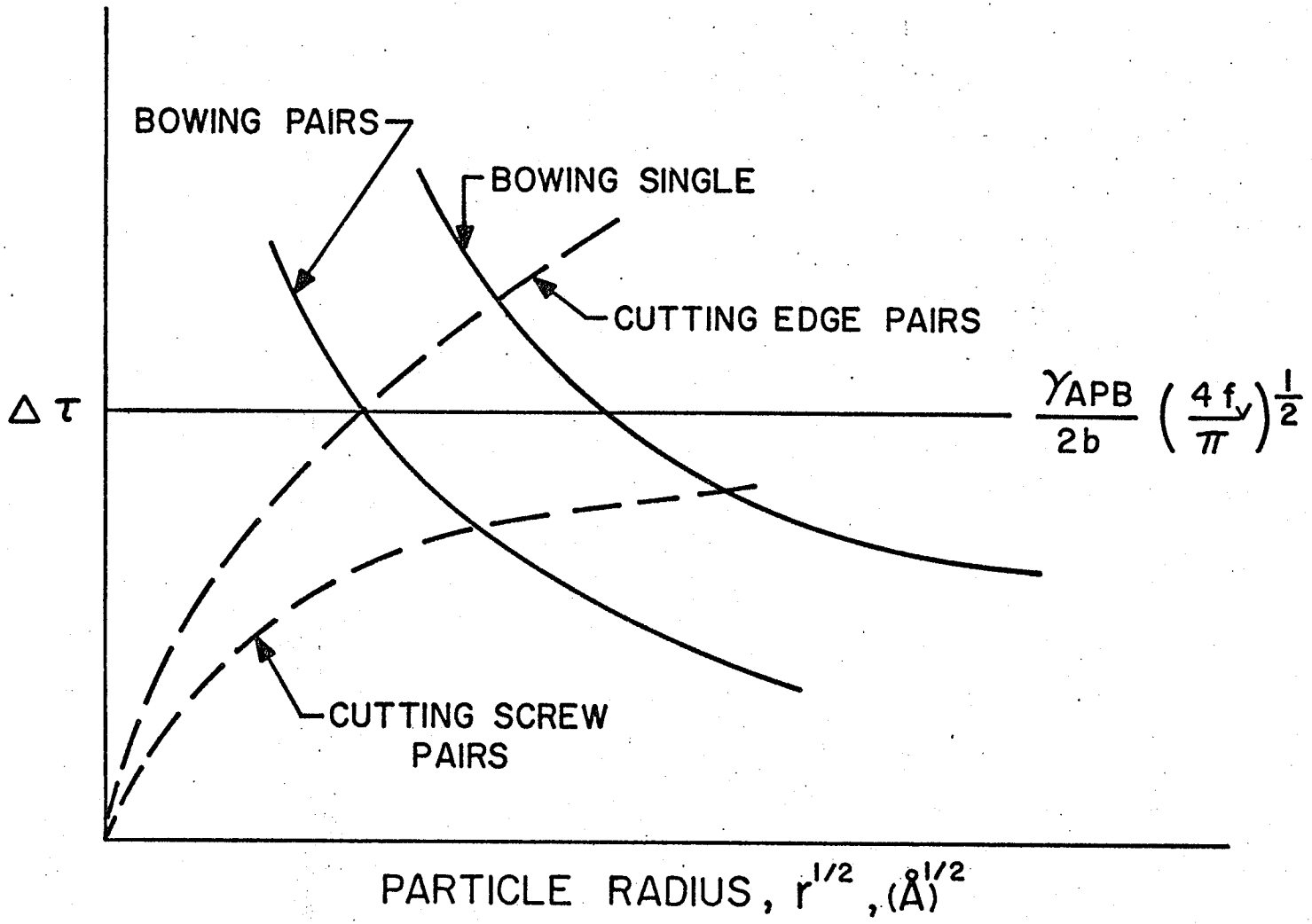
BOWING PAIRS
BOWING SINGLE
CUTTING EDGE PAIRS
Δτ
$\frac{\gamma_{APB}}{2b}\left(\frac{4f_v}{\pi}\right)^{\frac{1}{2}}$
CUTTING SCREW PAIRS
PARTICLE RADIUS, $r^{1/2}$, $(Å)^{1/2}$

FIG. (5)

The angle to which a dislocation is bent by the force, K_r before escaping the particles is given by

$$2 \sin \theta \simeq \frac{K_r}{2T^*} \quad \ldots \quad (16)$$

Combining equation (14), (15) and (16) the critical shear stress for the edge dislocation is obtained by

$$\Delta\tau = 3G\varepsilon^{3/2} \left(\frac{r_s f_v}{b}\right)^{1/2}, \quad \frac{9\pi f_v}{16} < \frac{3|\varepsilon| r_s}{b} < \frac{1}{2} \quad \ldots \quad (17)$$

and for a screw dislocation as

$$\Delta\tau = G\varepsilon^{3/2} \left(\frac{r_s f_v}{b}\right)^{1/2}, \quad \frac{9\pi f_v}{26} < |\varepsilon| \, r_s < \frac{1}{2} \quad \ldots \quad (18)$$

Based on experimental data for Cu, Co and Al-Zn alloy, it was concluded that edge dislocations control the critical shear stress and, while for small particles $r_s/b < 20$, the dislocations cut the particles, and for the larger particle size dislocations by-pass the particles by the Orowan mechanism.

2.2 Particle by-passing model.

As the particle size increases the dislocation-precipitate interaction changes from "cutting" to "bowing" i.e., the particles act as impenetrable obstacles and force the glide dislocation to bow out and by-pass them. This mechanism was first analysed by Orowan[56] who suggested that the flow stress of the alloy is given by

$$\tau_o = \tau_m + \frac{2T^*}{bL_o}$$

where τ_m is the yield stress of the matrix, T* is the line tension, b is the Burgers vector and L_o is the mean planar spacing of the particles.

According to Ashby[57], this equation should be modified in order to take into account the effect of the variation of line tension with dislocation character on the shape of the dislocation loop, via the interaction of the two arms of dislocation on opposite sides of the particle. The critical or Orowan stress, assuming elastic isotropy, is then that stress which is just capable of elongating appropriate dipoles of width, X, spaced L_o apart.

$$\tau_{edge} = \frac{1}{2\pi}\left(\frac{Gb}{L_o}\right) \ln\left(\frac{X}{r_o}\right), \text{ and,} \quad \ldots. \quad (19)$$

$$\tau_{screw} = \frac{1}{2\pi(1-\nu)}\,\frac{Gb}{L_o} \ln\left(\frac{X}{r_o}\right) \quad \ldots. \quad (20)$$

where X can be replaced by 2 r_s, the particle diameter, r_o is the inner cut-off radius, b is the Burgers vector and G and ν are the matrix shear modulus and Poisson's ratio respectively. In real crystals, however, a distribution of particle spacing will exist and the yield stress will then be associated with some mean value of the particle spacing. Kocks[46] and Foreman and Makin[49] have proposed that extensive slip can first occur at the critical value of the applied stress such that about one third of the spacing between particles is transparent. If the critical configuration is that at which the angle, ϕ, between two arms of dislocation is zero, then a statistical factor about 0.85, relates the macroscopic flow stress σ of the random array to the average local Orowan stress,

τ_o, i.e.

$$\sigma = 0.85\ \tau_o.$$

Therefore the empirical expression leading to the increase in the critical stress due to non deformable particle; is given by

$$\sigma_{edge} - \sigma_m = 0.85\ \frac{Gb}{2\pi L_o} \ln\left(\frac{2r_s}{r_o}\right) \quad .... \quad (21)$$

$$\sigma_{screw} - \sigma_m = 0.85\ \frac{Gb}{2\pi L_o\ (1-\nu)} \ln\left(\frac{2r_s}{r_o}\right) \quad .... \quad (22)$$

The particle size $2r_s$ is usually much smaller than their spacing L_o, when this is not so, L_o should be replaced by $(L_o - 2r_s)$. Hirsch and Humphreys[58] pointed out that the best estimate of the critical flow stress should be the geometric mean of equation (21) and (22). Taking $L_o^{-1} = 0.81\ N_A^{1/2}$ of the Foreman and Makin's result and assuming the shape of the loop to be an ellipse, the yield stress is expressed by

$$\sigma = \frac{0.81\ Gb}{2\pi L_o (1-\nu)^{1/2}} \ln\left(\frac{2r_s}{r_o}\right) \quad .... \quad (23)$$

Recently Bacon et. al.[59] have developed a new treatment of line tension approximation for the dislocation undergoing a looping process around the precipitate particle. In this model they assumed that a bowing dislocation is not an elastic string with a well defined line tension because it will interact with itself due to its own stress field. Based on the self interaction of dislocation, the following equation for the flow stress was derived:

$$\sigma = \sigma_m + \left(\frac{\ln 2r_s}{\ln L_o}\right)^{1/2} \frac{Gb}{2\pi L_o} \ln\left(\frac{2r_s}{r_o}\right) \quad .... \quad (24)$$

where Gb/L_o is the classical Orowan expression. The implication of this equation is that the last two factors are the expression for the dipole extension as proposed by Ashby in equation (19), which accounts for the mutual loop interaction, while the first factor describes the effect of the random array. The correction factors for randomness of the obstacle array in equation (24) gives a value substantially less than 0.84 derived by Kocks[48] without the consideration of the self-interaction of the dislocation. However, the equation (24) seems to be well justified to take into account the effect of obstacle spacing. In the looping process, since greater hardening may occur if the particle spacing is reduced by means of the coherency strain round them this effect has been observed in many precipitation hardened alloys[12,73].

2.3 Experimental evaluations of strengthening mechanism in precipitation hardened alloys.

The strengthening behaviour of Ni - Al alloy containing γ' phase has been extensively investigated by Davis and Stoloff[60] and by Phillips[16,61]. Recently Brown and Ham[12] analysed the data of Phillips according to their order strengthening model, and found that the flow stress was a linear function of $r_s^{1/2}$, where r_s is the effective mean particle radius. From the slope of this plot they also calculated the anti-phase boundary energy to be $\gamma_{APB} \simeq 153$ erg/cm^2. At the ageing peak, using equation (12) the observed flow stress gave $\gamma_{APB} \simeq 148$ erg/cm^2, which is in excellent

agreement with the values of 164 erg/cm^2 estimated by Copley and Kear[62] from the Flimn's[63] relation given by,

$$\gamma_{APB}\ (<110>\{111\}) = 0.7\ (\frac{\kappa T_c}{b^2})\ s^2, \qquad \ldots \qquad (24a)$$

where T_c is the ordering temperature, taken as the melting point of Ni_3Al, and s is the long range order parameter, measured to be 0.803 in bulk γ' of composition Ni - 23.33 at % Al.

Raynor and Silcock[15] have determined γ_{APB} in a series of Fe - Cr - Ni - Al - Ti alloys by finding the pinched-off loop that could be supported by particles by-passed by the Orowan process and also by measuring the spacing of dislocation pairs. The effective γ_{APB} increased from 240 erg/cm^2 with Ti/Al ratio = 1 to 300 erg/cm^2 with Ti/Al $\simeq$ 8. These values, however, are much higher than those obtained for Ni - Al alloys (ie. Ti/Al ratio = 0 in γ'). This indicates that the effect of Ti addition upon the effective A.P.B. energy seems to be important.

Brown and Ham[12] have also analysed the result of Hornbogen and his co-worker[52,64]. In Ni - Cr - Al alloys, using equation (12), they found $\gamma_{APB} \simeq 104$ erg/cm^2 by Hornbogen and Mukheigee's results and $\gamma_{APB} \simeq 90$ erg/cm^2 by Gleiter and Hornbogen's results. The mean effective γ_{APB} was thus 97 erg/cm^2 which was much smaller than 145 erg/cm^2 for Ni - Al alloys. Brown and Ham attributed this to the presence of Cr in the alloys of Hornbogen and his co-workers. The substitution of Cr atoms for either Ni or Al in γ' would reduce the effective degree of order and hence the value of A.P.B. energy[12].

In the high temperature superalloys, Castagné and his co-worker[65] have studied a wrought alloy of Ni - Cr - Co - Mo - Ti - Al containing several other impurities such as C, Fe, Mn, S and B. Ageing of this alloy also produced dislocation pairs and pile-ups of pairs at small particles. For alloys deformed after ageing at higher temperature and large particle sizes single pinched-off loops were observed. For still higher ageing temperature (> 900° C) and very large particle size ($2r_s$ > 1000 Å), double pinched-off loops were reported. However, they applied their pile-up computation to the alloys in a condition giving $r_s \sim 40$ Å, L = 130 Å, and deduced a value of $\gamma_{APB} \simeq 220$ erg/cm^2. This value appears to be larger than the values of 153 and 97 erg/cm^2 estimated for Ni - Al and Ni - Cr - Al respectively, but close to the results of Raynor and Silcock[15]. According to Guard and Westbrook[66], cobalt is soluble in the γ' as a Ni substitute, and also in the matrix, while in some alloys the partitioning of cobalt favours the matrix. Mo is also soluble in γ', probably as an Al substitute (Ni_3Mo is stable) and W dissolves in γ' as an Al substitute as well as in the matrix. Thus the effect of these element and Ti upon the partitioning of Cr between γ' and matrix may be even more important[67,68].

Some examples of the Orowan process will now be considered. Lewis and Martin[69,70] studied the tensile flow stress at -183° C and at 20° C of Cu polycrystals containing sphere of SiO_2 particles and found that the flow stress was inversely proportional to the

particle spacing, L. The value of L was calculated from the mean particle radius and the volume fraction of the particles. Since they did not observe any shearing of particles during deformation, they concluded that the Orowan process was in operation. Ebeling and Ashby[71] also measured the critical shear stress at -195° C and 20° C of Cu single crystals containing sphere of SiO_2 particles. They found that the extra-hardening due to particles, τ_p, was proportional to $f_v^{1/2}$ at constant r_s, while for constant f_v, $\tau_p \propto 1/r_s$ at small flow stresses and $\tau_p \propto (\frac{1}{r_s})^{1/2}$ at higher flow stress. This means that at small stress $\tau_p \propto f_v^{1/2}/r_s \propto 1/L$, while at larger stresses $\tau_p \propto (f_v/r_s)^{1/2} \propto r_s^{1/2}/L$. The critical shear stresses varied with temperature only as G in the range of -196° to 20° C, and were independent of strain rate, in agreement with Orowan's prediction.

Jones and Kelley[72] have conducted similar tests on single crystals of copper containing BeO particles in the temperature range of -196° to 200° C. The transmission electron microscopy revealed large coherency strains near the BeO particles, while these were not present near the SiO_2 particles in Ebeling and Ashby's work. They found, in agreement with Ebeling and Ashby's result of flow stress relationship that $\tau_p \propto f_v^{1/2}$ for constant particle size and $\tau_p \propto 1/r_s^{1/2}$ at higher flow stresses. But their total flow stress were much higher than those of Ebeling and Ashby's alloys. The explanation for this discrepancy lies in the fact that the BeO particles contain large coherency strains, at least around small particles, which may increase the effective particle size[12,73] of BeO and, hence, the flow stress[12,73].

3.0 Serrated yielding behavior.

Serrated yielding, also known as Portevin - Le Chatalier effect and jerky flow, has been observed in a number of solid solutions. During deformation these alloys first deform smoothly and then develop serrations or jerks in their stress-strain diagram. These serrations are influenced by the temperature of testing, strain rate and grain size. The onset of serrated yielding has been explained on the basis of:

(1) Dynamic strain ageing and (2) static strain ageing models.

3.1 Dynamic strain ageing model.

The dynamic strain ageing model, as proposed by Cottrell[74] and modified by Ham and Jaffrey[75], is the earliest model for the explanation of the serrated yielding phenomenon. According to this model for the serrated yielding to occur the deformation conditions should be such that the solute mobility is high enough and the average dislocation velocity low enough to allow the solute atoms to reach the mobile dislocations. These solute atoms form an atmosphere around dislocations and exert a drag on them if dislocations move at less than some critical velocity v_s, given by

$$V_s \simeq \frac{4D}{\ell} \qquad \ldots \qquad (25)$$

where D is the diffusion coefficient of the solute and ℓ is the "effective radius" of the solute atmosphere and is equal to $\frac{U_m b}{\kappa T}$

where U_m is the solute-dislocation binding energy, b is the burger vector and κ, T have their usual meaning.

Orowan[56] [76] has suggested that during deformation the applied strain rate, $\dot{\varepsilon}$, should be balanced with the mobile dislocation density, ρ_m, in order to maintain a constant velocity, V_D, i.e.,

$$\dot{\varepsilon} = \phi \; b \; \rho_m \; V_D \qquad \ldots \qquad (26)$$

where ϕ is a geometrical factor ($\sim$ 1.0) and b is the burgers vector. When V_D is too small to satisfy this equation instability occurs and stress rises rapidly until, in order to maintain the strain rate, there is a sudden increase in the mobile dislocation density, ρ_m, leading to a stress drop[75]. The critical condition for this instability is that the velocity of dislocations, V_D, be equal to that of the solute atoms V_S, i.e.,

$$\frac{\dot{\varepsilon}}{\phi \; b \; \rho_m} = \frac{4D}{\ell}$$

or

$$\dot{\varepsilon} = \frac{4 \; b \; D \; \rho_m}{\ell}$$

or

$$\dot{\varepsilon} = \frac{4 \; b \; \rho_m \; D_o \; C_V \exp(-Q_m/\kappa T)}{\ell} \qquad \ldots \qquad (27)$$

where C_V is the concentration of vacancies, D_o is the pre-exponential diffusion constant, Q_m is the vacancy migration energy.

In experiments conducted at normal temperatures and involving plastic deformation the concentration of vacancies produced

by straining is much greater[77] than the thermal equilibrium vacancy concentration, which may then be neglected. Therefore, the concentration of vacancies, C_v, can be related to the plastic strain, ε, by Van Bueren's empirical relationship[78].

$$C_v = A\ \varepsilon^m \qquad \ldots. \qquad (28)$$

where A and m are constants.

The mobile dislocation density, ρ_m, may also be related to the plastic strain ε, unfortunately the precise relationship is not known. According to Ham and Jafferey[75], however, the mobile dislocation density should be related to ε by

$$\rho_m = N\ \varepsilon^\beta \qquad \ldots. \qquad (29)$$

where N and β are constants.

Substituting equations (28) and (29) in (27) gives the critical strain for the onset of serrations

$$\varepsilon_c^{m+\beta} = \frac{\ell\ \dot{\varepsilon}\ \exp(Q_m/\kappa T)}{4\ b\ D_o\ N\ A} \qquad \ldots. \qquad (30)$$

3.2 Static strain ageing model.

Working on the carbon steel alloys. Sleeswyk[93] suggested that moving dislocations do not drag along their carbon atmospheres. He argued that if a stationary dislocation is an obstacle in the path of the moving one, then the moving dislocation will be arrested temporarily before cutting through the stationary dislocation. If

the time is sufficiently long, then carbon may diffuse from stationary to the moving dislocation and thus carbon would impede the movement of the moving dislocation.

Recently McCormick[94] has subsequently developed the static strain ageing model. According to this model, during deformation a mobile dislocation spends most of its time in surpassing obstacles, (t_w), and once the dislocation surpasses the obstacles, then, jumps at high velocity, (t_f), over a distance, L, to the next obstacles by

$$\bar{V}_j \approx L/t_w + t_f \qquad \ldots \qquad (31)$$

He then used the condition for locking to be $t_w \approx t_a$ where t_a is the ageing time required to lock the arrested dislocation. If t_w is less than t_a at the start of plastic deformation the dislocations arrested at obstacles will not be locked and the stress-strain curves will be continuous. Furthermore, during straining t_a will decrease due to vacancy production while t_w will increase as a result of dislocation multiplication so that, at the critical strain, ε_c, t_a becomes equal to t_w, and the few remaining unlocked dislocation will multiply causing the formation of a Lüder's front, and thus the start of serrated yielding.

Following the above arguement, using equation (26) and (31), and assuming $t_w >> t_f$, he equated the arrest time, t, in terms of the strain rate and dislocation density by

$$t_w \simeq \frac{L \rho_m b}{\dot{\varepsilon}} \qquad \ldots \qquad (32)$$

Using Friedel's[44] equation for ageing time of the elastic solute and dislocation interaction:

$$t_w \simeq \left(\frac{C_1}{C_o}\right)^{3/2} \frac{\kappa T\, b^2}{3\, D\, U_m} \qquad \ldots\ldots \quad (33)$$

where C_1 is the solute concentration at the dislocation line which is required to lock it, C_o the solute concentration of the alloy ($C_1 >> C_o$), and $\alpha \simeq 3$, the time required to age an arrested dislocation, t_a, was obtained to be

$$t_a \simeq t_w$$

Therefore, combining equation (32) and (33)

$$\dot{\varepsilon} = \left(\frac{C_o}{C_1}\right)^{3/2} \frac{3L\, \rho_m\, C_v\, U_m\, D_o}{kTb} \exp\left(\frac{-Q_m}{\kappa T}\right) \qquad \ldots\ldots \quad (34)$$

or, in terms of the critical strain, as in the Cottrell model, using (28) and (29)

$$\varepsilon_c^{m+\beta} = \left(\frac{C_1}{\alpha C_o}\right)^{3/2} \frac{\dot{\varepsilon}\, \kappa T\, b \exp\left(\frac{Q_m}{\kappa T}\right)}{3L\, N_A\, U_m\, D_o} \qquad \ldots\ldots \quad (35)$$

3.3 The relation between vacancy concentration and plastic strain.

It has been observed that the values of C_v and ρ_m are critical for solving equation (30) and (34) of serrated yielding since the critical strain, ε_c, prior to the onset of serrations is explained in terms of the strain dependence of $C_v = A\varepsilon^m$ and $\rho_m = N\varepsilon^\beta$. The values of $m + \beta$ can be easily obtained from the gradient of a strain rate vs critical strain for onset of serrations, ε_c, but the individual value of m and β can not be resolved unless one of these

values is known. Unfortunately, it is not possible at present to experimentally measure ρ_m. However, there are many models proposed for the formation of vacancies by moving dislocations. They are mainly based either on the mutual annihilation of dislocations others than screw, or on the non conservative motion of jogs in dislocations with a screw component. Most appropriate models are based on the annihilation of dipole dislocations. Van Bueren[78] considered that jogs move only non-conservatively leaving behind them rows of point defects and the generation of point defects are completed when the dipole pinch off and form point defects clusters. In this procedure, if the density of randomly distributed dislocations in the crystal is ρ_o and a loop of area A_o is swept out, then for each expanding loop the number of jogs will be proportional to $\rho_o A_o$. The number of intersected dislocations, and the number of vacancies or interstials left in the wake of these jogs is then proportional to the radius of expansion of loop with a jog travel distance $A_o^{1/2}$, and thus the vacancy concentration $\propto A_o^{3/2} \rho_o/b \propto \varepsilon^{3/2}$. By considering the formation of new loops and the energy balance Van Bueren[78] also showed that the total concentration of vacancies should be proportional to $\varepsilon^{5/4}$ at small strain and to ε^2 at larger strain.

Alternatively, Friedel[44] suggested that for small dislocation velocities, the jogs should move along the edge of the dislocation rather than produce point defects. The production of point defect occurs only when a mobile dislocation loop cuts through an attractive "tree" of the dislocation "forest". This model has been presented in detail by Saada[95].

When a mobile loop meets an attractive tree, the loop will be divided in two parts separated by an immobile junction dislocation.

If the Burger's vector of the trees is not parallel to the slip plane of the loop, then the two parts of the loop will be in different slip planes.

If they subsequently bow out until they meet and recombine over a certain length, then a row of point defects of length ℓ_d which is proportional to the size of the dislocation network ρ_o will be created, i.e. $\ell_d = A_o \rho_o$. The atomic fraction of point defects generated after dN attractive trees/unit volume are cut is thus $dC \propto \ell_d b^2 \, dN \propto [(\frac{\ell_d}{b}) d N/(\frac{1}{b^3})]$. The corresponding increase in strain is then $d\varepsilon = b \ell_d^2 \, d N$. Thus $\frac{dC}{d\varepsilon} \propto \frac{b}{\ell_d}$. If the cutting of the attractive trees is the dominant work-hardening, then the stress required to break the junction is $\sigma \propto Gb/\ell_d$. By combining two equations $dc/d\varepsilon \propto \sigma/G$. Therefore the total concentration of vacancies produced is (assuming equal amount of vacancy or interstials are produced)

$$C_V \propto \frac{1}{G} \int_o^{\varepsilon} \sigma \, d\varepsilon \qquad \ldots . \qquad (36)$$

This indicates that the vacancy concentration produced by cold working is proportional to the work done.

Various attempts have been made to obtain a theoretical value of m. Van Bueren obtained values of m = 1.25 and 2.0 for the single and multiple glide, respectively. Saada found m to be equal to 2.0 and suggested it to be in good agreement with the resistivity work on copper single crystals[96,97]. At low strains Lenasen obtained a value of 2.0[98]. However using equation (38) the static strain ageing experiments have yielded values for m of 1.35 in Cu - Zn[99] and 2.16 in Cu - Sn[100] alloys.

Several investigation have also measured the dependence of dislocation density, ρ_m, on strain, ε, and gave values for β of 1.0 in Al[101], 1.0 in Cu crystal, 1.17 in Cu - Sn[75], 1.2 in Cu - Zn[102] 1.0 in Fe[103] and 1.0 in LiF[104].

It appears reasonable to conclude from these results that $\beta \approx 1.0 - 1.2$. By combining $\beta = 1.0 - 1.2$ and the theoretical value of $m = 2$, it is apparant that the value of $m + \beta$ obtained from serrated yielding experiment, as shown in Table (1), are invariably rather low. This discrepancy, however, could be due to the fact that the mobile dislocation density, ρ_m, is assumed to be proportional or equal to the total dislocation density, ρ_T.

Recently Lloyd[105] has suggested that, if stress-strain curves give the correct value of n, where n is work-hardening coefficient, then using Saada's expression $m = n + 1$, the value of $\beta \approx 0$ in Al - 5.6 wt% Mg and Al - 8.6 Mg[23], and Mg - 10 wt% Ag alloys[106]. It should be noted that the value of m can be reduced below the theoretical value when vacancies are annihilated at sinks during straining. This may also account for the slightly lower value of $(m + \beta)$ reported for some Al - Mg alloys.

3.4 The relation between the critical strain, ε_c, obstacles spacing, L and the concentration of solute atoms, C_o.

It has been shown that in the static strain ageing model, ε_c is a function of the effective obstacles spacing and concentration

Table 1

Values of $(m + \beta)$ reported from serrated yielding experiments.

Materials	$(m+\beta)$	References
Al-Mg	1.7	MacEwen and Ramaswami (79)
Al-Mg	1.82	Mukherjee, D'Antonio and Maciag (80)
Al-Mg	1.69-2.07	Miura and Yamauchi (85)
Al-Mg	2.12-3.21	Tensi and Pless (86)
Al-Mg	3.3	Tensi, Dropmann and Borchers (87)
Al-Mg	1.8	Roberts, Lenasson and Bergström (88)
Al-Mg-Si	1.6	McCormick (114)
Al-Mg-Zn	3.33	Mukherjee, D'Antonio, Maciag and Fischer (89)
Au-In	2.14	Soler-Gomez and Tegart (83)
Cu-Al	1.77-2.61	
Cu-As	2.99-3.50	
Cu-Ga	2.28	Räuchle, Vöhringer and Macherauch (90)
Cu-Ge	1.45-1.88	
Cu-In	3.07	
Cu-Sn	2.2	Russell (84)
Cu-Sn	2.8-3.17	Vöhringer and Macherauch (82)
Cu-Zn	1.94-3.70	Munz and Macherauch (81)
Cu-Zn	1.9	Charnock (109)
Cu-Zn	2.1-3.4	Adams (24)
Cu_3Au	2.18-2.93	Mohamed, Murty and Langdon (133)

of solute atoms. McCormick[94] has explained that the obstacle spacing will depend on the density and distribution of the rate controlling obstacles. In alloys that exhibit serrated yielding these obstacles may be dislocations, solute atoms or precipitate particles. If dislocations are the controlling obstacles, then L will be a function of strain. Thus assuming $L \propto \rho^{-1/2}$, the strain exponent in equation can be obtained to be $m + \beta/2$. Whereas, if solute atoms are the controlling obstacles, L will be independent of strain.

Working on the Cu - Sn alloy Lloyd et al[107] suggested that the rate of dislocation motion could be controlled by dislocation interaction at low solute concentrations and by solute interaction at higher concentration.

If dislocations are the controlling obstacles, then L may also be dependent on the grain size since the mobile dislocation density is a function of grain size[81,82,108, 109]. In certain alloys studies have shown a grain size dependence of ε_c[109,110].

In static strain ageing equation L is also expected to decrease with increasing solute concentration, thus decreasing the concentration dependence of ε_c. In Cu - Sn alloys Russel found $\varepsilon_c \propto C_o^{-1/2}$ [84], for $m + \beta = 2.2$, and Vohringer and Macherauch[82] also found $\varepsilon_c \propto C_o^{-1/2}$ for $m + \beta = 2.8$, which is in reasonable agreement with equation (35). The value of L, in case of dislocation and/solute atom controlling obstacles, is not precisely revealed in strain ageing process since it is not a directly measurable quantity.

In alloys with high concentration it, however, appears[94,102] that the multiple obstacles are present, and thus in some system the controlling obstacles may be a function of strain. Whereas in dilute alloys, it appears that dislocation interaction is the primary process controlling the rate of dislocation motion.

III EXPERIMENTAL PROCEDURES

1. Preparations of materials.

The following three compositions (weight %) of a new alloy system were chosen:

1) 39.50 Co - 37.60 Ni - 16.82 Cr - 6.0 Ti

2) 40.00 Co - 38.00 Ni - 17.00 Cr - 5.0 Ti

3) 40.42 Co - 38.40 Ni - 17.17 Cr - 4.0 Ti

650 grams of each of the three alloys, using 99.99% pure materials except Ti which was 99.7% pure, were melted in vacuum induction furnace, and cast into 3/4" diameter square rods in silica sand molds. All the ingots were then homogenized at 1250° C for 3 days, and rolled down to appropriate thicknesses, ie. 0.06" thick strip for tensile specimen, 1/4" diameter rod for optical microscope examination, carbon extraction reprica technique, electrolytic extraction for X - Ray analysis, and chemical analysis and 0.005" thick strip for thin foil technique. All the heat treatments were carried out in a argon filled vycor capsules. The final solid solution treatment was conducted at 1250° C followed by an iced water quench. During quenching the Vycor tube was broken underwater to minimize the precipitation reaction. The oxide layer from the specimens was always removed by electropolishing after the heat treatment. Ageing treatment was carried out at 700° C, 800° C, and 900° C for times up to 1200 hours.

1.1 Electro-polishing and etching.

After the appropriate heat treatments the specimens were electropolished at 10V in a bath of 10% sulfuric acid, 90% methanol which was maintained at just $\sim 0^\circ$ C and stirred slowly. After polishing for 8 to 10 minutes, the specimen was quickly washed in running water and then dried with absolute alcohol.

The etching reagents used for the optical microscopic investigation were 30 ml lactic acid, 20 ml hydrochloric acid, 10 ml nitric acid for γ' phase, and two parts HCl, three parts HNO_3, and four parts glycerine for the overaged specimens. After etching the specimen was quickly washed in alcohol, then in running cold water, and finally washed again in pure alcohol and dried. Etching time and etchant required depended upon the heat treatment.

1.2 Carbon extraction replication.

After the etching process a thin film of carbon was evaporated on the specimen in vacuum. It was then electro-etched for a few seconds in a solution of 5% sulfuric acid and 95% methanol at 5 Volts, until the carbon layer was loosened. The exact etching time was dependent on the particle size. After carefuly washing in alcohol, the carbon film was floated in a disc of distilled water and collected on a 200 mesh copper grid and then dried in air.

1.3 Electrolytic extraction of particles.

An extraction cell containing an electrolyte composed of 10% acetic acid in water was used to extract the precipitate particles

at a current density of about 0.05 A/cm^2. The specimen was weighed accurately in an electronic balance and the extraction was carried out. In about 20 hours the matrix was completely dissolved. The electrolyte was centrifuged and the solvent was then removed by a suction pump. The particles were washed first in distilled water and then in alcohol with intermediate centrifuging. These well dried extracted particles were weighed in a fine electronic scale to calculate the volume fraction of particles.

In order to obtain the values of the lattice misfit between the matrix and the precipitate, the lattice parameter of the matrix and that of the precipitate in bulk samples and also the extracted particles were measured using a Phillips powder camera with Co k_α radiation and Fe filter.

1.4 Thin foil technique.

The electrolytic jet polishing technique was used to prepare thin foils. A heat treated 0.005" thick x 0.25" square strip was carefully polished mechanically and its edges were then lacquered. The specimen was then mounted anodically in a jet polishing cell, and polished in a bath contained 10% perchloric acid and 90% methanol at -50° C at 10 $\sim$ 15 volts until a hole appeared. The specimen was then quickly removed from the electrolyte and put in cold alcohol for washing, cleaned of lacquer and rewashed in alcohol. After drying, the specimen was held between two clean tissue papers and a suitable area was cut out with a sharp knife. Care had to be taken in handling

the specimen to avoid deformation. The thin foil was mounted in between two "75" mesh copper grids and examined in a Phillips 300G electron microscope.

2. The measurement of particle sizes.

The measurement of particle size was conducted using carbon extraction replicas, as well as thin foil electron microscopy at an accelerating voltage of 100 K.V. In the case of thin foil measurements, a dark - field micrograph was taken using the super-lattice reflections from the ordered γ' precipitate. Whenever possible, the particle sizes were measured in (100) foil orientation, otherwise in (110) orientation along <100> directions, since these γ' particles were cuboids in shape and align themselves in <100> matrix direction[25].

All the precautions were taken to ensure the aberrations free image by employing the standard procedures. The mean particle edge length, $\bar{a}$, was determined either from a histogram incorporating 500 measurements or was taken as the arithmatic mean of 200 measurements of individual particles. These two methods yielded a close value of $\bar{a}$ whenever both were used for a given sample. It is important to note that the average sizes reported here refer to the cube shape that exists prior to coalescence since as ageing proceeds the particles become aligned along <100> eventually coalesce into plate - like shape[25].

The volume fractions of precipitate were also determined by thin foil electron micrographs by determining the thickness of

the foil using the slip trace method. The measurement of volume fraction were also carried out by carbon replica as well as by weighing the extracted particles. These results were in good agreement with each other except for slightly greater scattering in the data obtained from replicas, indicating that the extraction and foil methods were more reliable.

The extracted precipitate particles were also employed for the composition analysis by atomic absorption techniques, whose accuracy was estimated to be within $\pm$ 5%.

3. Deformation method.

Flat sheets of (0.08 x 0.6 x 7.62) cms were shaped by a spark cutting machine into a tensile sample with a gauge length of as shown in Fig. (6). Prior to the test, all the tensile samples were electro-polished to obtain a scratch free surface in a bath of 10% sulfuric acid and 90% methanol at 0° C. The tensile test was performed using an Instron "tensile testing machine". The high temperature testing was done in a three zone vacuum furnace in the strain rate range of 3.28×10^{-5} to 3.28×10^{-3}/sec. The furnace temperature was thermostatically controlled to within $\pm$ 1° of the reported values. The specimens were held in cylindrical self-aligning grips which also held the thermocouple at the bottom of the specimen.

Load-time curves were plotted on an x-y load-extension recorder, adjusted to give a 9 mv full scale deflection and 9 mv switched

Figure (6) Standard tensile specimen used for deformation studies

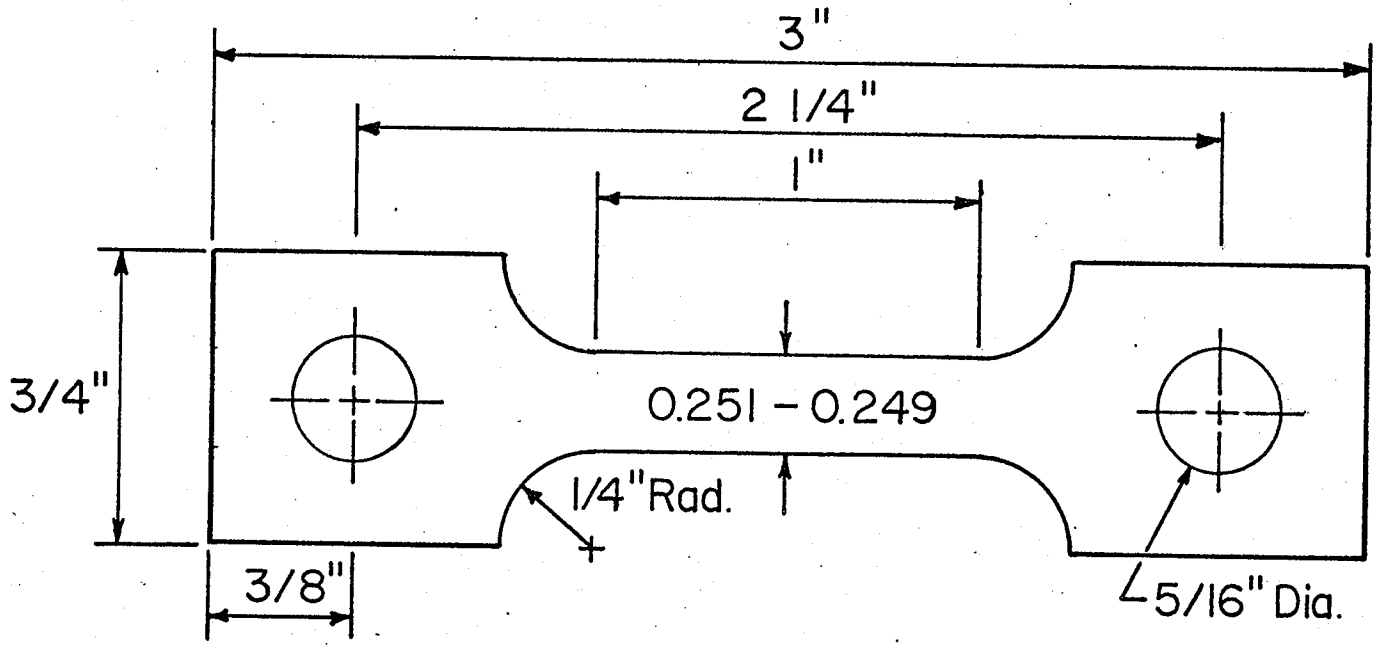

FIG. (6)

zero suppression steps (10 steps) were employed to extend the range of load. The nominal stress were calculated from the tensile loads and original cross-sectional areas to an accuracy of $\pm$ 0.1 kg/mm^2. The strains were deduced from elongation data and initial gage lengths to an accuracy of better than 0.002. When required, the true strain, ε, and true stress, σ, were calculated from the relationship $\varepsilon = \ln (1 + e)$ and $\sigma = \sigma_o(1 + e)$, where e is the engineering strain and σ_o is the nominal stress respectively.

Most tests were carried out to fracture, while others, from which thin foils for electron microscopy, were prepared, were stopped at various strains. The deformed tensile sample were then spark cut into section and hand polished lightly to a thickness of $\sim$ 0.003". Thin foil from these strips were then made as discussed in section (1.4).

IV EXPERIMENTAL RESULTS

1. Precipitation behavior of alloys.

The as-quenched structure of all the three alloys was austenitic F.C.C. disordered phase. The main precipitate at ageing temperatures of 700, 800 and 900° C, within the grains was γ' phase, which has an ordered LI_2 type of structure, with a composition of $(Co, Ni)_3 Ti$. Occasionally some hexagonal Ni_3Ti, η precipitate formed at the grain boundaries. The shape of γ' precipitate was cubic with a precipitate matrix orientation relationship of <100> γ'//<100> γ, $(010)\gamma'$// $(010)\gamma$. The lattice parameters of the austenite matrix and γ' phase were determined to be 3.5513 Å and 3.5750 Å respectively, and their misfit was calculated to be + 1.3%. Fig. (7) and (8) show typical structures of γ' phase in 4% Ti alloy aged at 800° C and 6% Ti alloys aged at 900° C, respectively. These are the dark-field structures, taken with the help of [100] superlattice reflection of γ', and show the cubic shape of γ' particles. It is also seen that the particles align themselves along <100> matrix directions.

The variation in the volume fraction of γ' precipitate with ageing time, at 800° C in 5% Ti alloy, is shown in figure 9. It is seen that after 5 hours of ageing the volume fraction of γ' phase remains constant. The variation in the volume fraction of γ' with the ageing temperautre, in this alloy, is shown in figure 10. Figure 11, whereas, shows the variation in volume fraction of γ' with Ti in 4,5 and 6 wt% Ti alloys aged at 800° C and 900° C. It is observed that within

the temperature investigated (700-900° C), the volume fraction of γ' in 5% Ti alloy decreases linearly with an increase in the ageing temperature (Fig. 10) and within the composition of 4 $\sim$ 6% Ti the volume fraction of γ' increase significantly with increase in the Ti content of the alloys (Fig. 11).

The chemical composition of electrochemically extracted γ' phase in 5% Ti alloy was also determined by atomic absorption technique. Table (2) shows the chemical composition of γ' precipitated at 700°, 800° and 900° C. The titanium content of the precipitate formed at all the three ageing temperatures is the same, however, nickel and chromium content decrease, while cobalt content increases as the ageing temperature is increased from 700° C to 900° C. The chemical composition of γ' and its weight fraction were used to compute the amount of titanium left in the solid solution matrix (C_e) during the growth of the γ' precipitate. The computed amounts of C_e are given in Table (3) and were used to construct a pseudo γ - γ' binary phase diagram shown in Fig. (12).

Table 2

Chemical Composition and Volume fraction of γ' of 5% Ti alloy at various ageing temperatures.

Temperature °K	Volume fraction	Chemical Composition (w/o)			
		Co	Ni	Cr	Ti
973	17.36	10.39	57.35	10.58	21.68
1023	16.33	-----	-----	-----	-----
1073	14.09	13.57	54.91	9.88	21.64
1123	12.12	-----	-----	-----	-----
1173	10.01	17.50	53.93	7.02	21.55

Figure (7) Dark-field micrograph of γ' phase in a 4% Ti alloy aged for 120 hours at 800° C.

Figure (8) Dark-field micrograph of γ' phase in a 6% Ti alloy aged for 6 hours at 900° C.

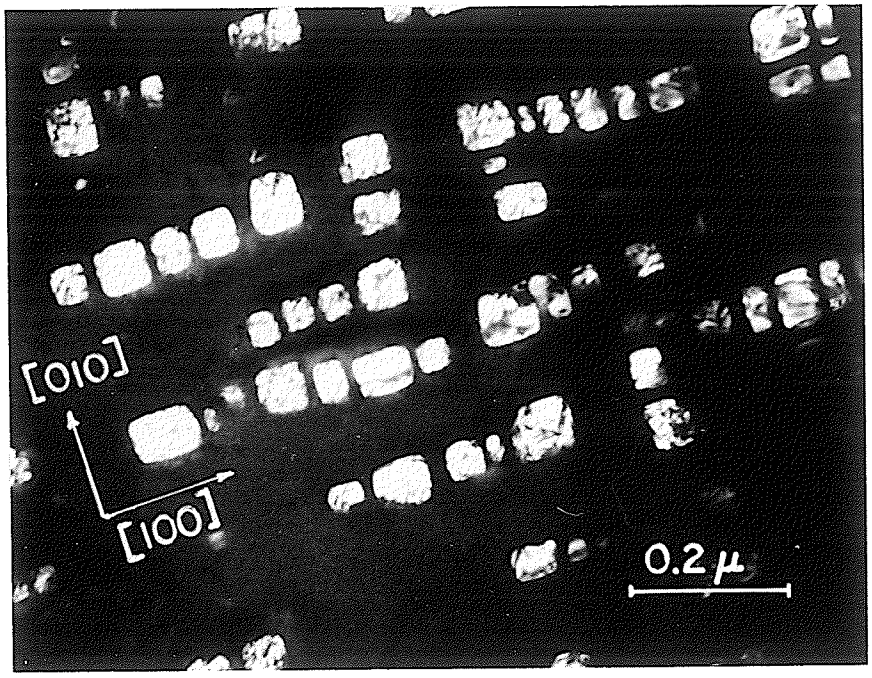

FIG. 7

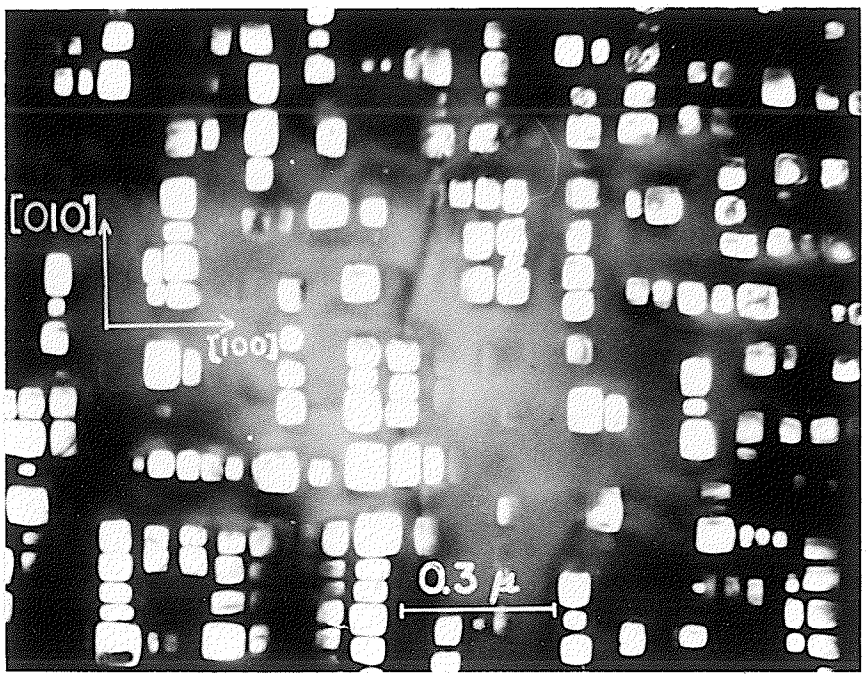

FIG. 8

Figure (9) The variation in volume fraction of γ' precipitate with ageing time, at 800° C in 5% Ti alloy.

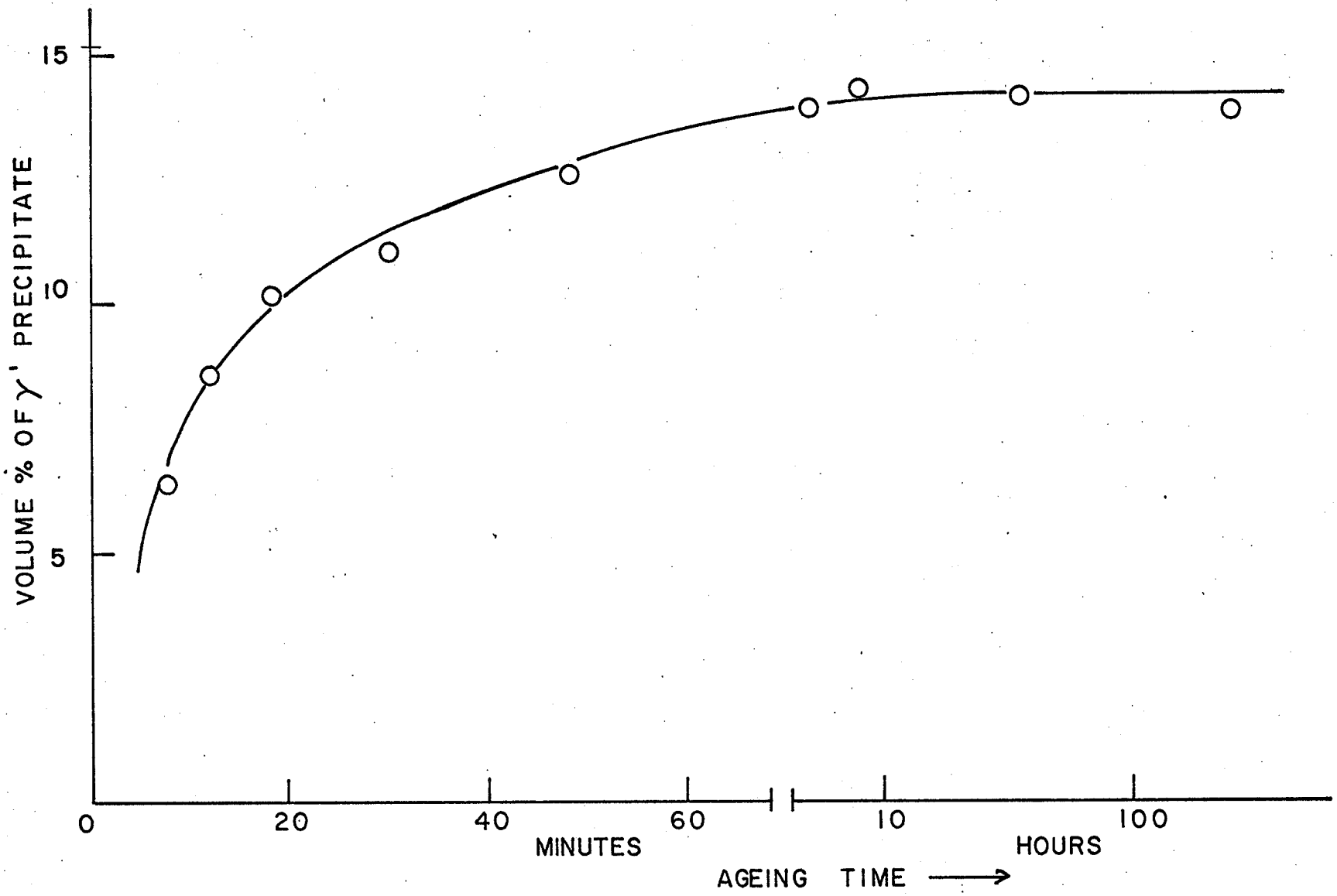
VOLUME % OF γ' PRECIPITATE
15
10
5
0
20
40
60
10
100
MINUTES
HOURS
AGEING TIME

FIG. (9)

Figure (10) The volume fraction of γ' of a 5% Ti alloy at various ageing temperatures.

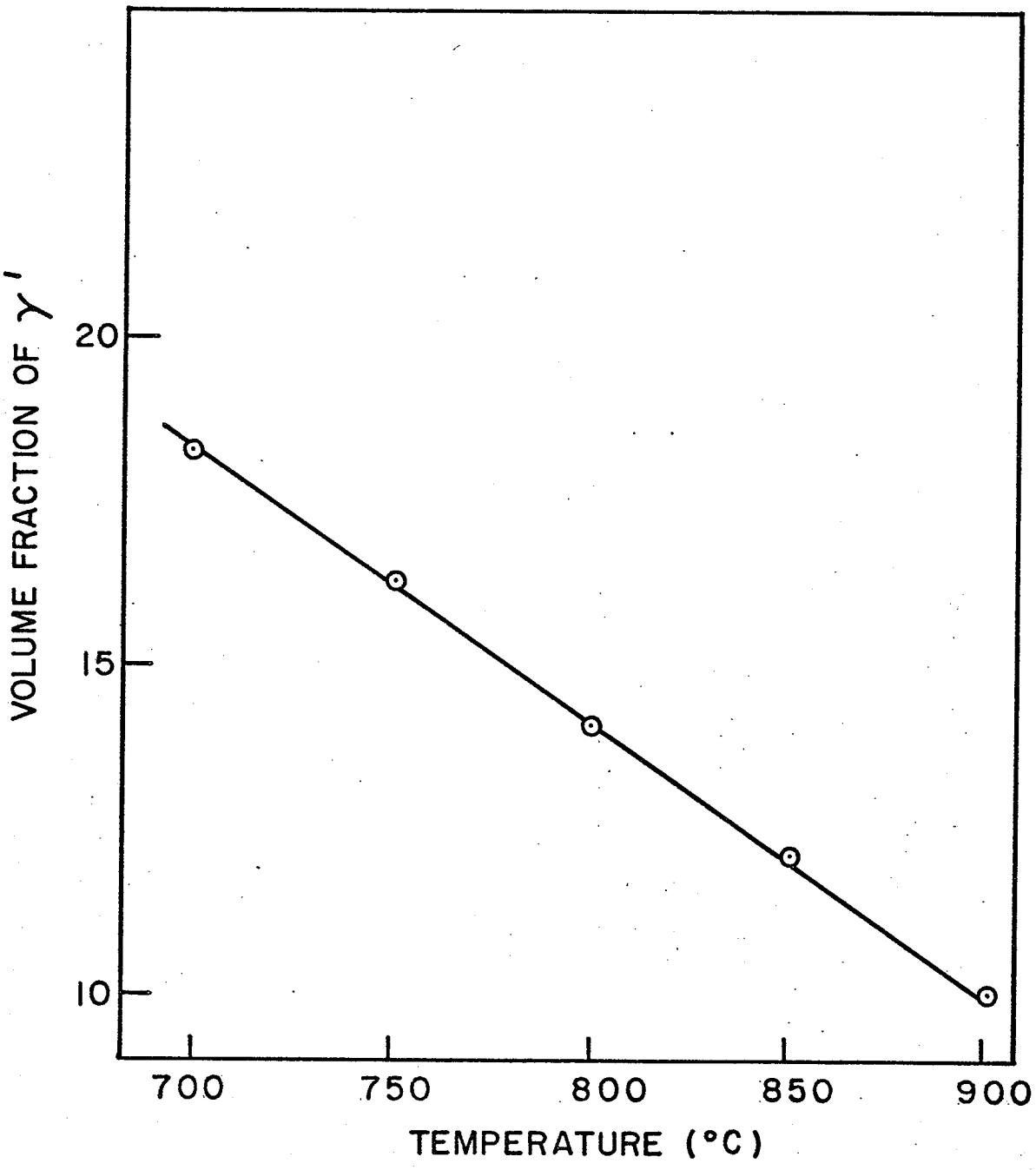
VOLUME FRACTION OF γ'
20
15
10
700
750
800
850
900
TEMPERATURE (°C)

FIG. (10)

Figure (11) The variation of volume fraction of γ' with three Ti compositions after ageing at 800° C and 900° C.

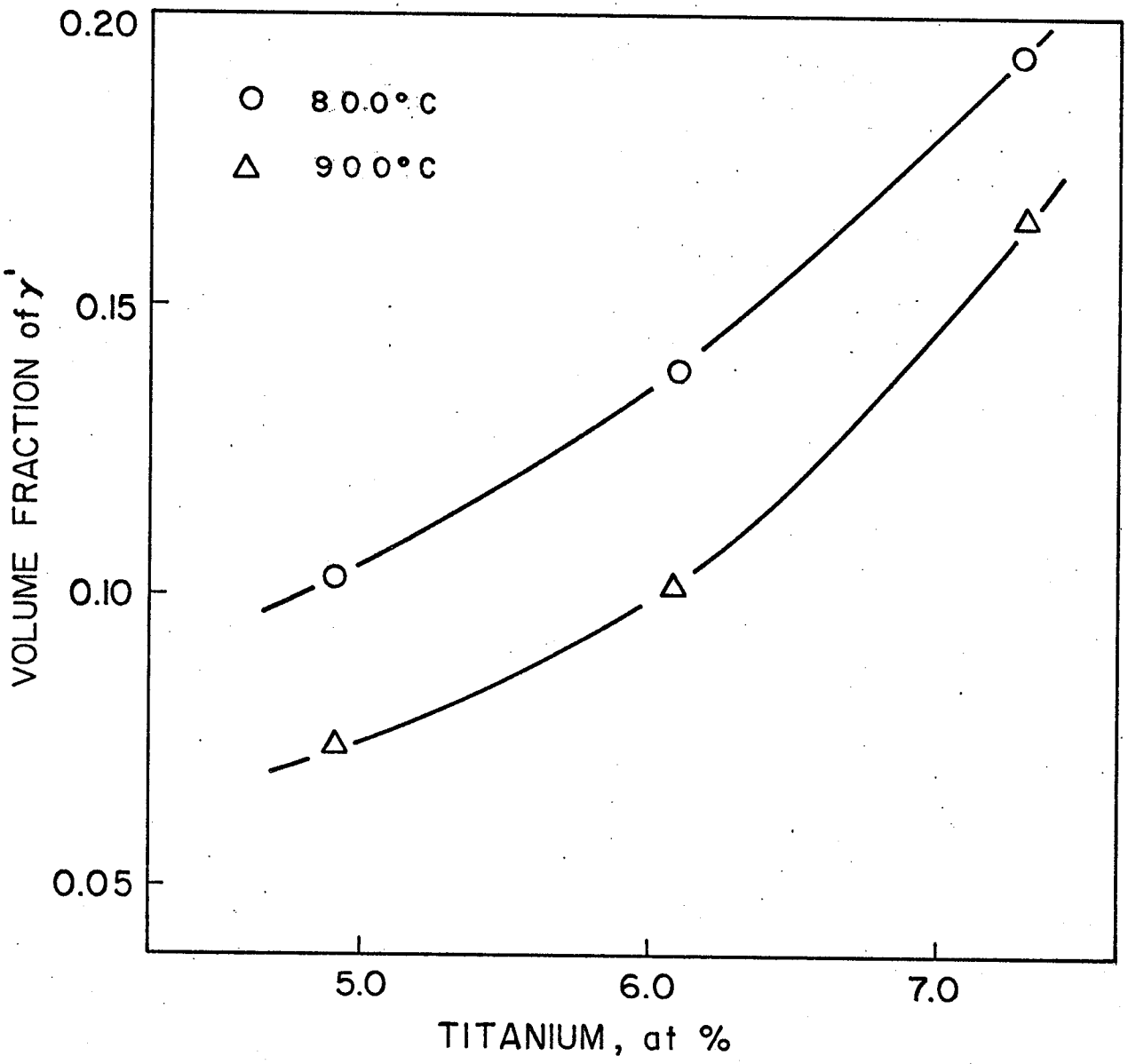
0.20
0.15
0.10
0.05
VOLUME FRACTION of γ'
800°C
900°C
5.0
6.0
7.0
TITANIUM, at %

FIG. (11)

Figure (12) γ - γ' Pseudo - Binary phase diagram.

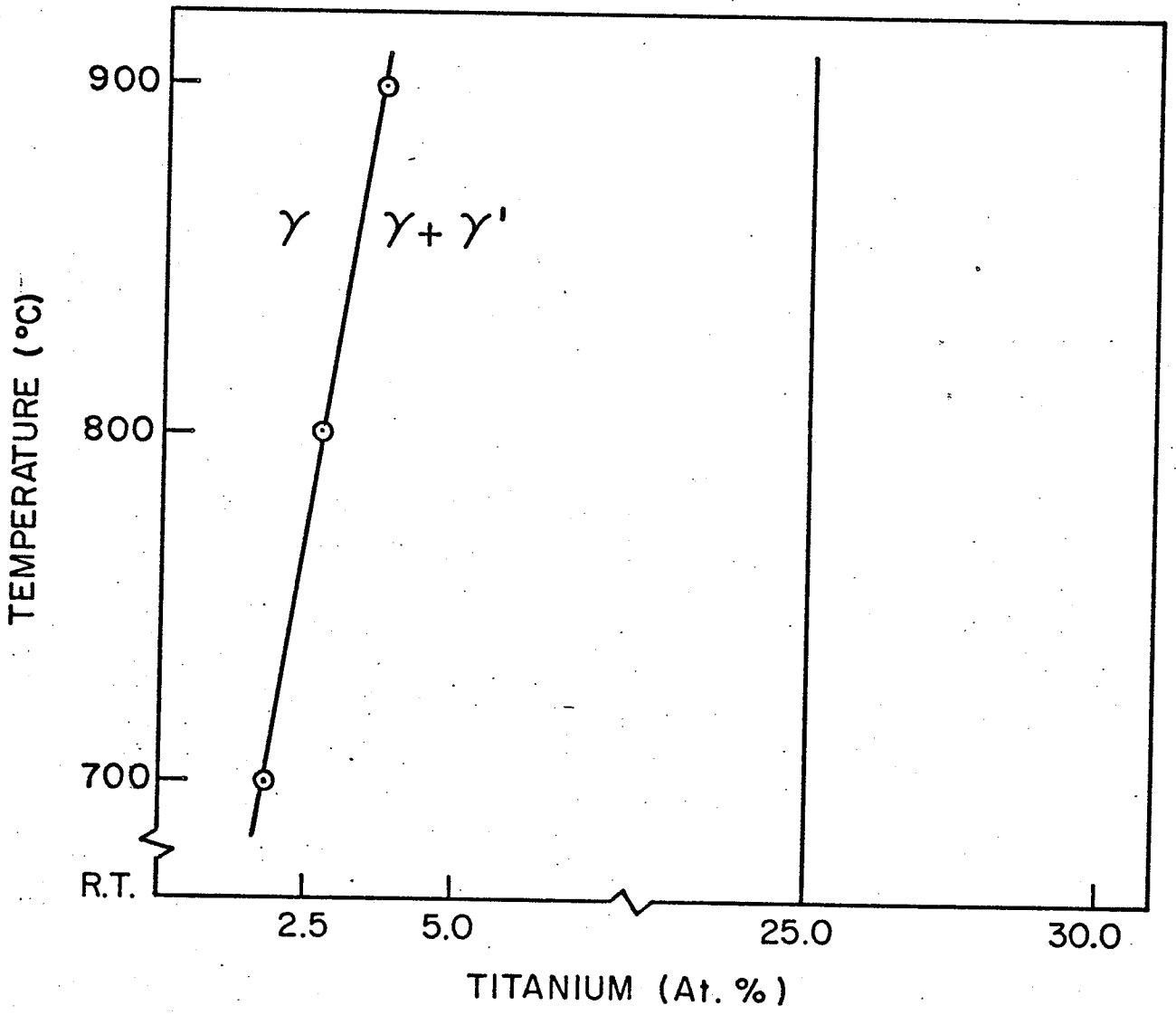

FIG. (12)

Table 3

Data for the Determination of the activation energy, Q, with rate constant, K', and volume fraction of γ'.

Temperature °K	Ti % (wt)	Volume fraction (f_v)	rate constant K' (A^3/sec)	C_e (At %)	$K'T/C_e$ (A^3. °K/sec)
973	5	0.174	2.755	1.78	1.505×10^5
1073	4	0.103	$(1.411 \pm 0.059) \times 10^2$	2.70	5.606×10^6
1073	5	0.140	$(1.410 \pm 0.042) \times 10^2$	2.70	5.603×10^6
1073	6	0.196	$(1.458 \pm 0.108) \times 10^2$	2.70	5.792×10^6
1173	4	0.075	$(2.726 \pm 0.118) \times 10^3$	3.73	8.573×10^7
1173	5	0.100	$(2.590 \pm 0.054) \times 10^3$	3.73	8.145×10^7
1173	6	0.167	$(2.737 \pm 0.051) \times 10^3$	3.73	8.607×10^7

2. The Coarsening Behavior.

2.1 Growth kinetics of γ'.

When the growth of particles in a matrix is diffusion controlled, it follows the LSW theory of coarsening (see Chapter II). According to this theory the radius of a spherical particle, r(t) after growth time t, is given by the following expression:

$$\bar{r}_{(t)}^3 - \bar{r}_{(o)}^3 = \frac{8\,\gamma_s\, D\, C_e\, \Omega^2\, t}{9RT} = Kt$$

as discussed in Chapter II. This relationship applies to the growth of spherical particles. For cuboid particles, however, this relationship has been modified[5] by substituting, half the mean edge length ($\bar{a}/2$) for the radius term, $\bar{r}$. Thus the LSW theory for cuboids becomes

$$\bar{a}_{(t)}^{3} - \bar{a}_{(o)}^{3} = \frac{64\ \gamma_s\ D\ C_e\ \Omega^2\ t}{9RT} = K't \qquad \ldots\ (37)$$

In order to evaluate the coarsening kinetics of γ' phase in the present alloy, $\bar{a}$ was plotted as a function of ageing time, at various temperature, as shown in Fig. (13). It is seen that at all the three temperatures of ageing the (particle size)^3 varies linearly with ageing time which suggests that the growth of γ' phase follows LSW theory of diffusion controlled growth. It is also observed that at $t = 0$, the extrapolated lines pass through a point close to the origin suggesting thereby that the values of $\bar{a}_{(o)} \simeq 0$. The applicability of LSW theory was further confirmed by plotting log ($\bar{a}/2$) against log t at different ageing temperatures. This yielded straight lines with a slope of 1/3 at all the ageing temperatures as shown in Fig. (14).

2.2 The effect of volume fraction on the growth kinetics of γ'.

The basic expression of the LSW theory does not contain a volume fraction term. It was assumed that the volume fraction of particles should be sufficiently small during coarsening. Ardell[32] has modified the LSW theory to incorporate the volume fraction term, f_v, in the growth equation. According to this modified theory, (MLSW theory), the rate constant, K, should increase with increasing volume fraction as follows:

$$K = \frac{6\ \gamma_s\ D\ C_e\ \Omega^2\ \rho^3}{vRT} \qquad \ldots\ (38)$$

Figure (13) The variation in γ' (particle size)^3 with time at various temperatures of ageing.

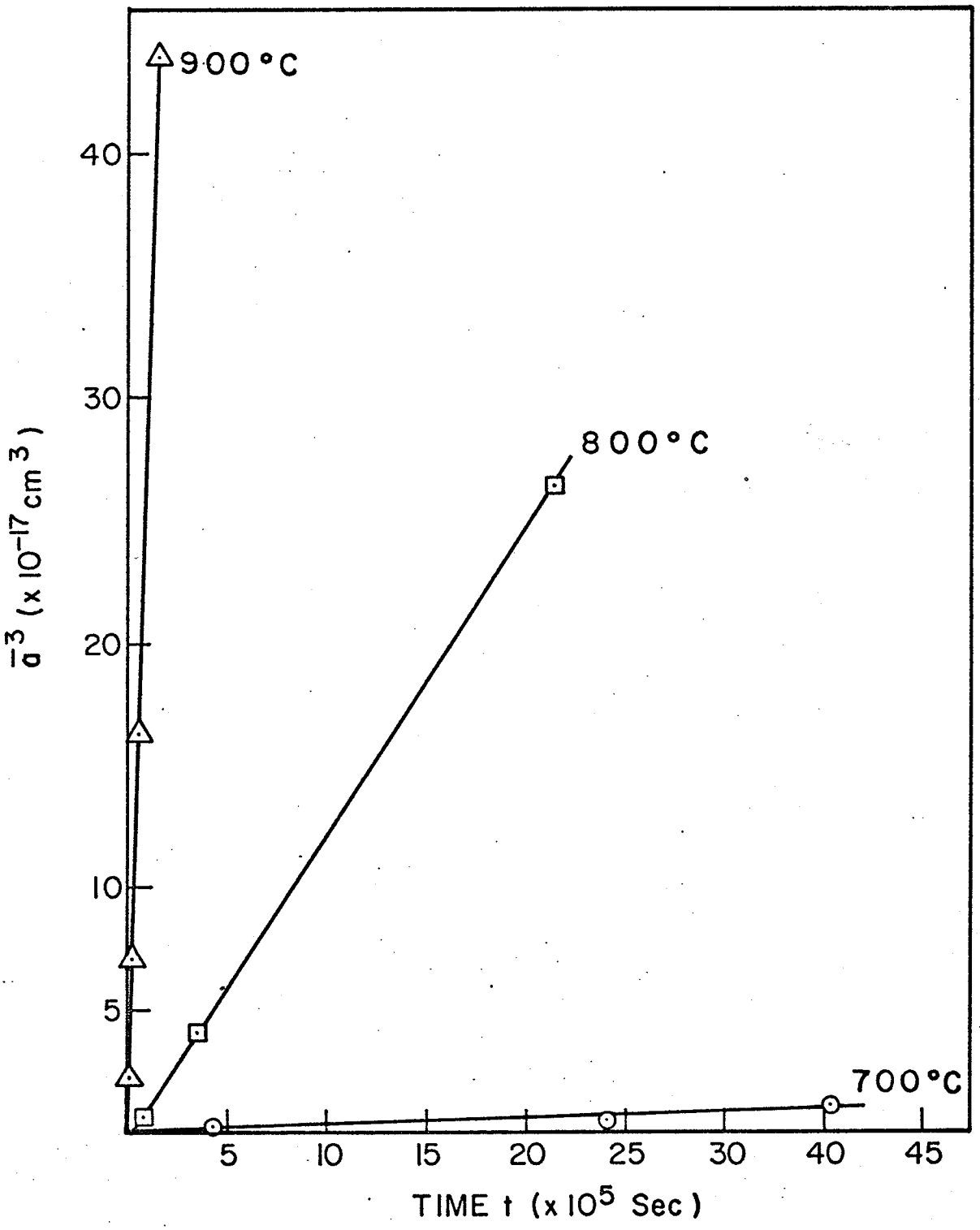
900 °C
800 °C
700 °C
40
30
20
10
5
$\bar{a}^3$ (x 10^{-17} cm^3)
5
10
15
20
25
30
40
45
TIME t (x 10^5 Sec)

FIG. (13)

Figure (14) Log plots of Half-Mean Edge Length of γ' against ageing time at different ageing temperatures.

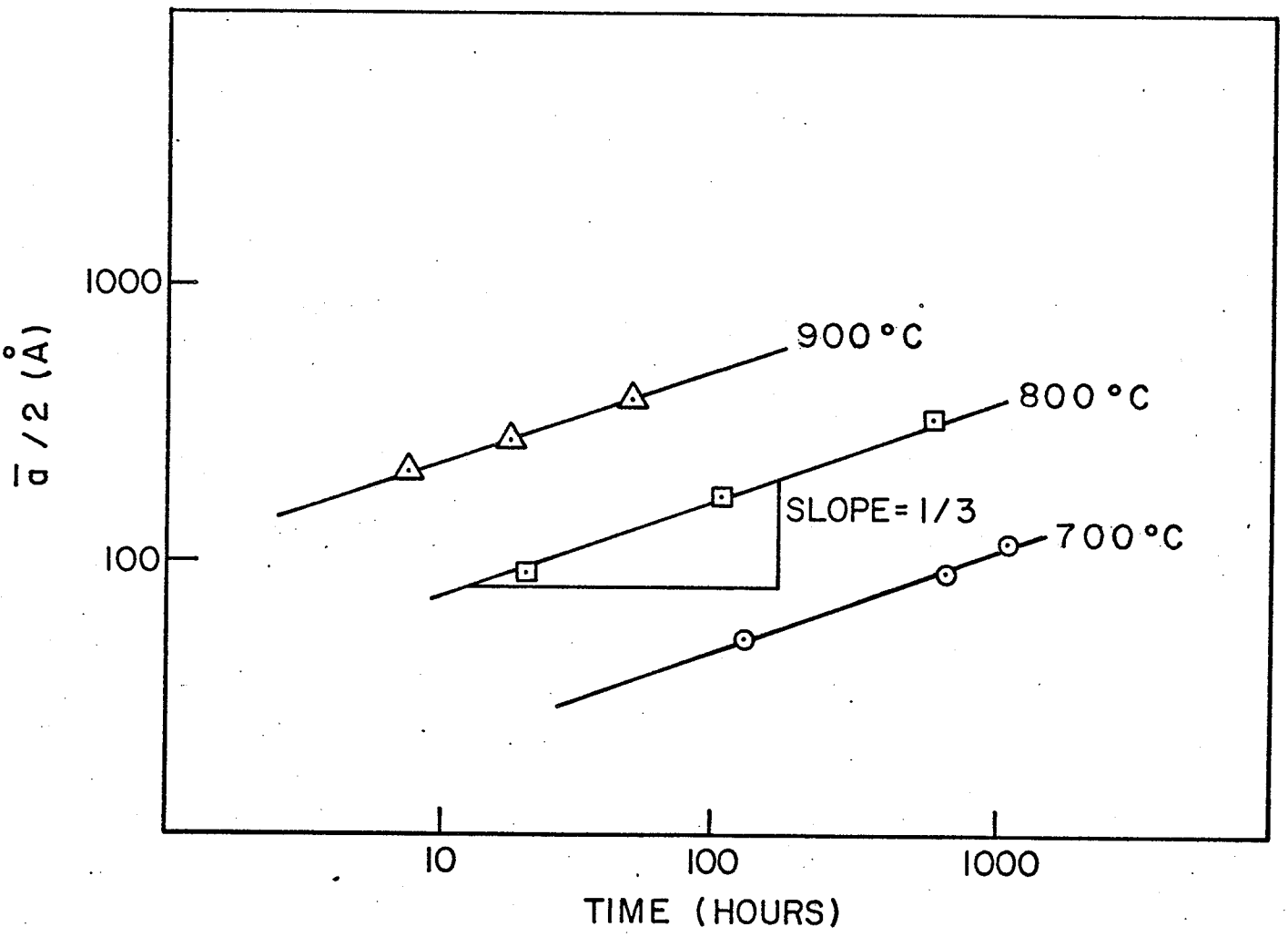
1000
100
$\bar{a}/2$ (Å)
900 °C
800 °C
700 °C
SLOPE = 1/3
10
100
1000
TIME (HOURS)

FIG. (14)

where

$$\rho = \frac{r}{r^*} \qquad V = \frac{3\,\rho_M^2}{1 + 2\beta'\rho_M - \beta'}$$

$$\beta' = \frac{6\,f_V^{1/3}}{e^{8f_V}\,\Gamma(f_V)} \qquad \rho_M = \frac{(\beta'^2 + \beta' + 1)^{1/2} - (1 - \beta')}{\beta'}$$

The additional symbols in the above equations are,

r^* - critical particle radius.

ρ_M - maximum reduced particle size of the theoretical distribution function.

$\Gamma(f_V)$ - a function of f_V.

The MLSW theory predicts that the basic growth kinetics remain the same as the LSW theory but the coarsening rates, values of the slope of $\bar{r}^3$ vs t plots should increase with the increasing volume fraction of the precipitate particles.

The effect of volume fraction on the growth kinetics in the present system was studied by plotting $\bar{a}^3$ against t for three different alloys with various Ti contents, at two temperatures. Fig. (15) and Fig. (16) show these results at 800 and 900° C, respectively. It should be noted that at both the ageing temperature, for all the three alloys, $(\text{particles size})^3$ varies linearly with ageing time, and the extrapolated values of $a_{(o)}$ at t = 0 lies close to zero as observed in 5% Ti alloy. These results suggest that the growth kinetics of the three alloys are identical and follow a diffusion controlled mechanism.

The applicability of LSW or MLSW theory was confirmed by the log $(\bar{a}/2)$ vs log t plot. As shown in Fig. (17), these plots are

Figure (15) The variation in γ' (particle size)^3 with time at 800° C for 4, 5, and 6% Ti alloys.

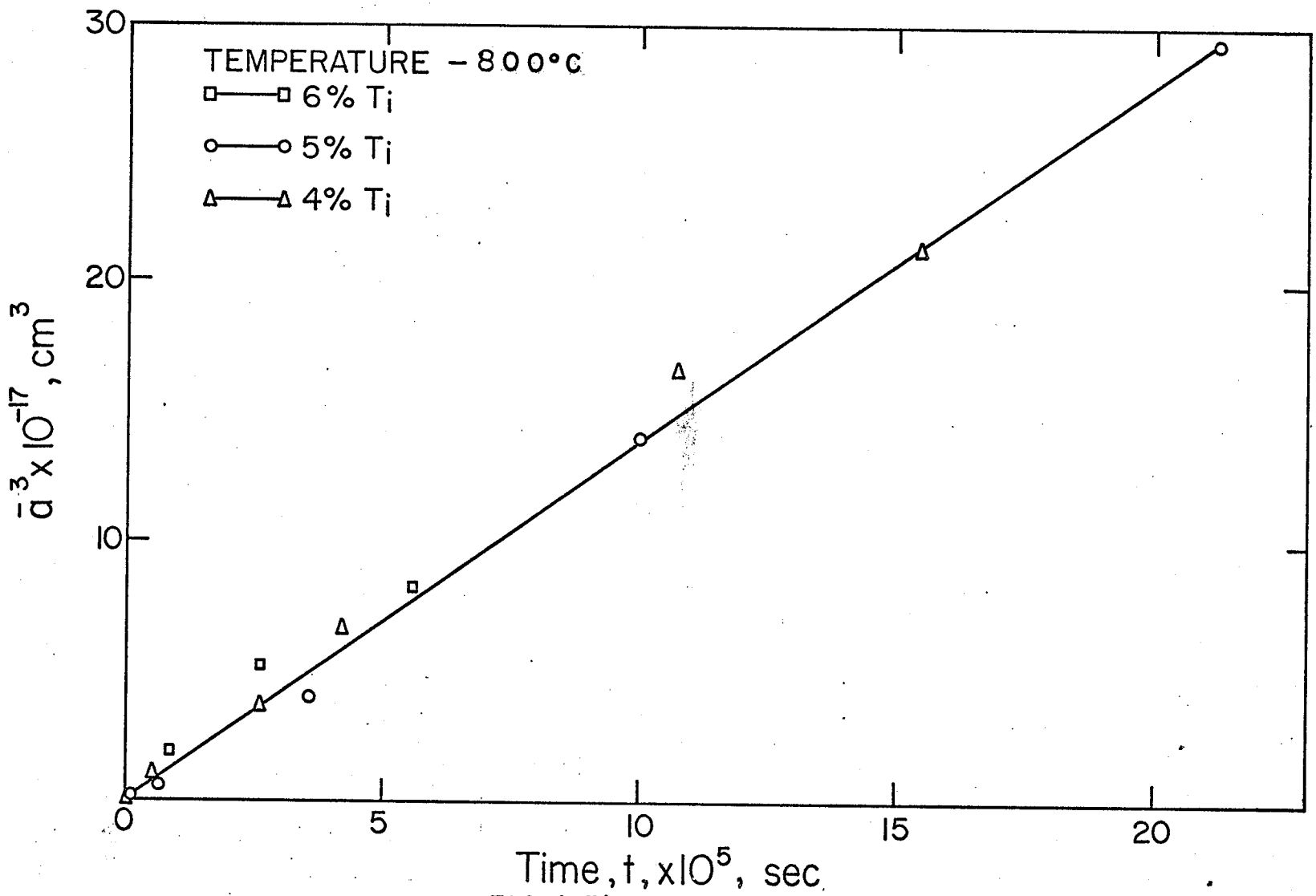
TEMPERATURE – 800°C
6% Ti
5% Ti
4% Ti
30
20
10
0
5
10
15
20
$\bar{a}^3 \times 10^{-17}$, cm^3
Time, t, x10^5, sec

FIG. (15)

Figure (16) The variation in γ' (particle size)^3 with time at 900° C for 4, 5, and 6% Ti alloys.

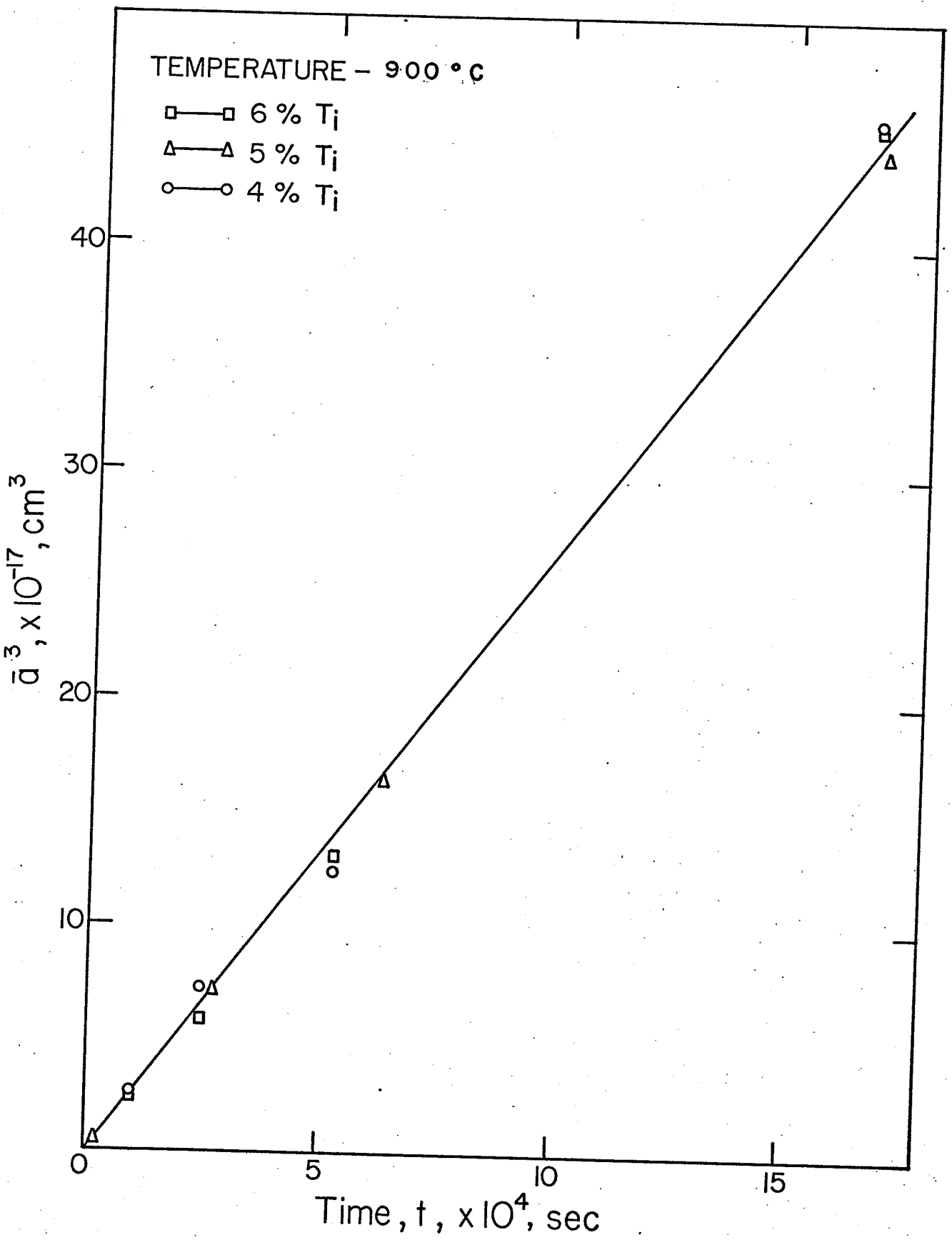
TEMPERATURE – 900 °C
6 % Ti
5 % Ti
4 % Ti
40
30
20
10
0
5
10
15
$\bar{a}^3$, x 10^{-17}, cm^3
Time, t, x 10^4, sec

FIG. (16)

Figure (17) Log - log plots of Half Mean Edge Length of γ' against ageing time for 4, 5, and 6% Ti alloys at 800 and 900° C.

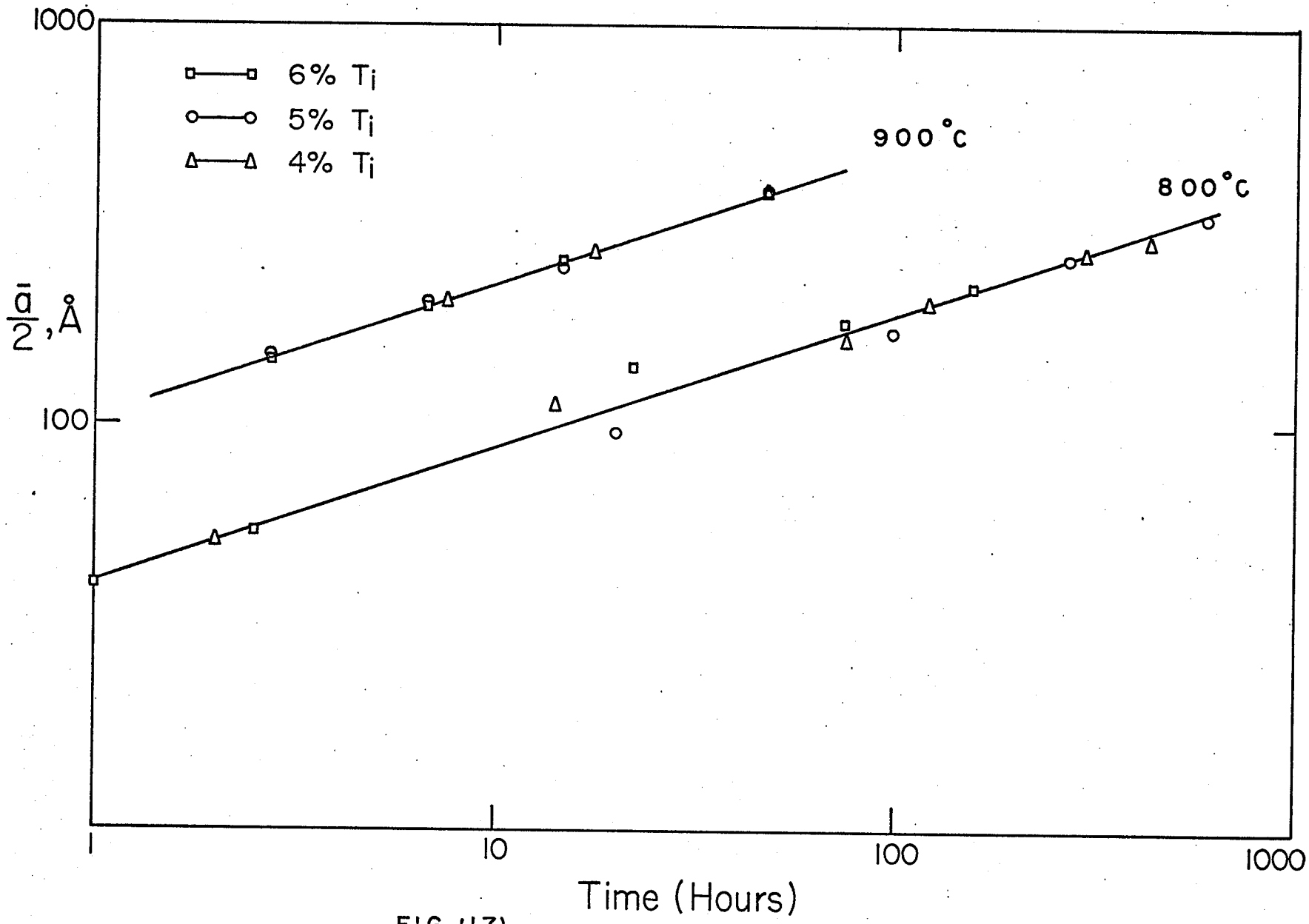
1000
100
6% Ti
5% Ti
4% Ti
900°C
800°C
$\frac{a}{2}$, Å
1
10
100
1000
Time (Hours)

FIG. (17)

straight lines with a slope of 1/3. The rate constants, K', calculated from these plots are given in Table (3) along with the volume fraction of γ' in all the three alloys at various temperatures. It is observed that although the volume fraction of γ' at 900° C varies from 7% to 16%, the value of K' is constant within the experimental limits. Similarly at 800° C, the value of f_v varies from 10% in 4% Ti alloy to 20% in 6% Ti alloy, the value of K' remains constant.

2.3 Activation energy for the growth of the γ' particles.

The activation energy for the growth of the precipitate particles can be found from the diffusion coefficient, D, in the growth equation, as defined by $D = D_o \exp(-Q/RT)$, where D_o is the pre-exponential coefficient, Q is the activation energy and R, T have their usual meaning. Since, in the equation of growth kinetics, K', C_e and T are the only temperature dependent terms and γ_s, Ω are constant for a given phase system, the rate constant K' may be expressed as:

$$K' = \frac{\overline{A}.C_e \cdot f(\overline{r},\overline{f}_v)}{T} \exp\left(\frac{-Q}{RT}\right) \qquad \ldots\ldots \quad (39)$$

where $\overline{A}$ is a constant. Therefore if a function $f(\overline{r},f_v)$ is known at various temperatures, the activation energy, Q, can be easily determined from the slope of the $\ln(K'T/C_e)$ vs $\frac{1}{T}$ plot.

The values of various parameters for this plot are given in Table (3) along with the calculated values of C_e and K' for ageing time, for all the three alloys. Fig. (18) shows the $\ln(TK'/C_e)$ vs $\frac{1}{T}$ Arrheneous plot. It is seen that for the 5% Ti alloy this plot, as determined by

Figure (18) Arrhenius plot for the determination of the activation energy for coarsening of γ'.

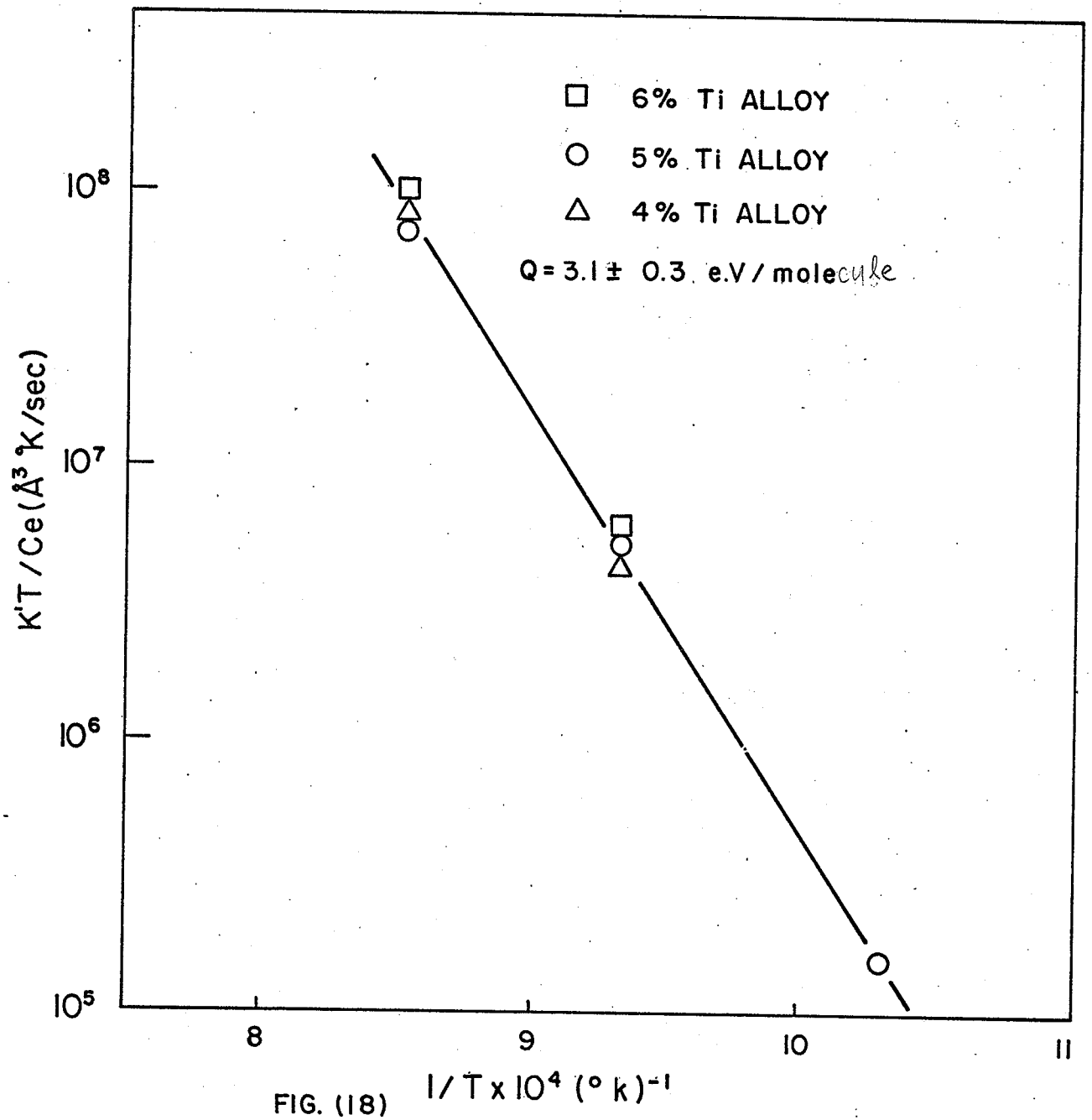
6% Ti ALLOY
5% Ti ALLOY
4% Ti ALLOY
Q = 3.1 ± 0.3 e.V / molecule
10^8
10^7
10^6
10^5
K'T / Ce (Å³ °K/sec)
8
9
10
11
1/T x 10^4 (° k)$^{-1}$

FIG. (18)

the "least square fit" method, is a straight line. The activation energy, Q, for the growth of γ' particles, from this plot was calculated to be 3.1 $\pm$ 0.3 e.V./molecule. Unfortunately, at 700° C data for only the 5% Ti alloy are available. However, it is seen that the two points for the 4% and 6% Ti alloys, at 800 and 900° C, lie on the straight line obtained for the 5% Ti alloy. Furthermore, it is observed that the value of $(K'T/C_e)$ for all the three alloys are the same within the temperature range of ageing. These observations suggest that the activation energy for the growth process of γ' is the same for all the three alloys, despite a significant change in the volume fraction of γ'.

2.4 Distribution of particle size of γ'.

The distribution of γ' particles, in the 5% Ti alloy after various stages of growth at different temperatures, was examined by placing the various sizes of γ' in histograms at suitable particle size intervals. The histograms were normalized in accordance with the previous procedure, discussed in Chapter II, and plotted against the reduced particle size $\rho = a/\bar{a}$ for comparison with the theoretical distribution predicted by the LSW theory. Fig. (19) shows these histograms at various stages of ageing along with the theoretical distribution. It is seen that the distribution of γ' particles in the present system is much broader during the early stage of ageing and becomes narrower as ageing is continued, but is never less than the theoretical curves. The cut-off values are also always greater than

the theoretical value of $\rho_c = 1.5$. The closest they come to the theoretical value are 1.8 at 900° C after 17.5 hours, 1.7 at 800° C after 100 hours, and 2.0 at 700° C after 1124 hours. The maximam are also never as large as the theoretical value, although they seem to occur around the same value of ρ as the theoretical maximum. Unfortunately, the size distribution of γ' particles in the other two alloys could not be investigated due to a lack of time. Therefore, the effect of the volume fraction of γ' phase on its size distribution could not be established.

3. Deformation behavior.

The deformation behavior of these alloys was studied by tensile testing in an Instron machine. The structure of the deformed specimens was also examined to correlate it with the deformation behavior of the alloys. The results of these studies are presented in the following two main sections.

1) Yielding Behavior

2) Serrated Yielding Behavior

3.1 Yielding behavior.

The 0.2% offset yeild stress and ductility, as determined by % elongation, for all the three alloys aged at 800° C, for various times, was evaluated. The variation in these with ageing time is shown in figure 20. It is seen that the yield stress and ductility in all the three alloys follow the classical pattern of age hardenable

Figure (19) Observed and theoretical distribution of γ' particle size in 5% Ti alloy.

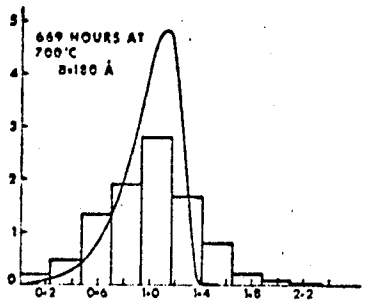
669 HOURS AT
700°C
δ=180 Å

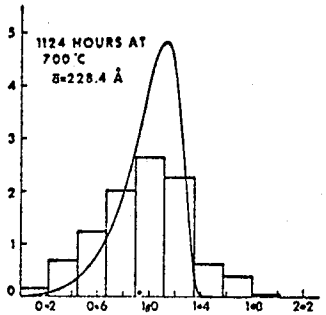
1124 HOURS AT
700°C
δ=228.4 Å

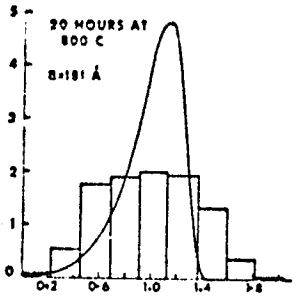
20 HOURS AT
800°C
δ=181 Å

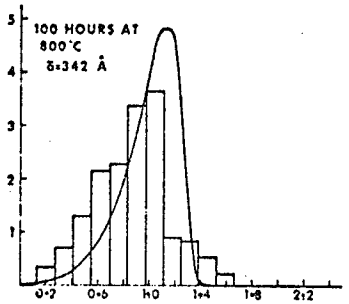
100 HOURS AT
800°C
δ=342 Å

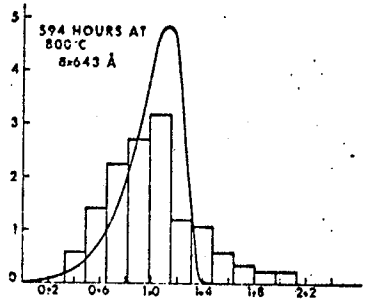
594 HOURS AT
800°C
δ=643 Å

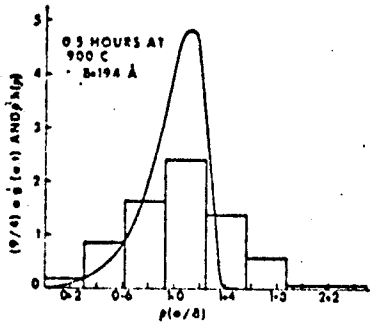
0.5 HOURS AT
900°C
δ=194 Å

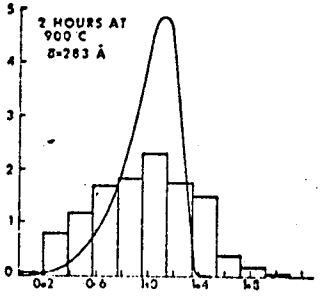
2 HOURS AT
900°C
δ=263 Å

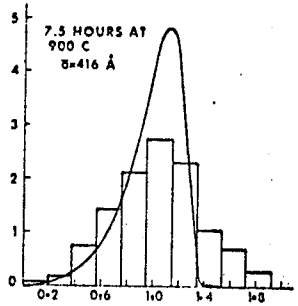
7.5 HOURS AT
900°C
δ=416 Å

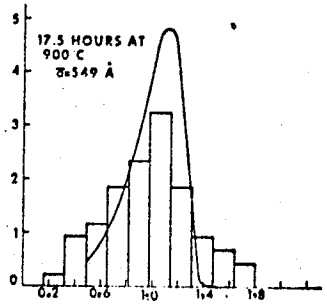
17.5 HOURS AT
900°C
δ=549 Å

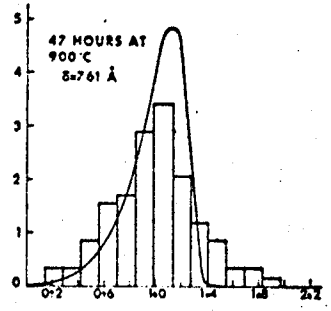
47 HOURS AT
900°C
δ=761 Å

FIG. (19)

Figure (20) The effect of ageing at 800° C on 0.2% offset yield stresses and elongations for 4%, 5%, and 6% Ti alloys.

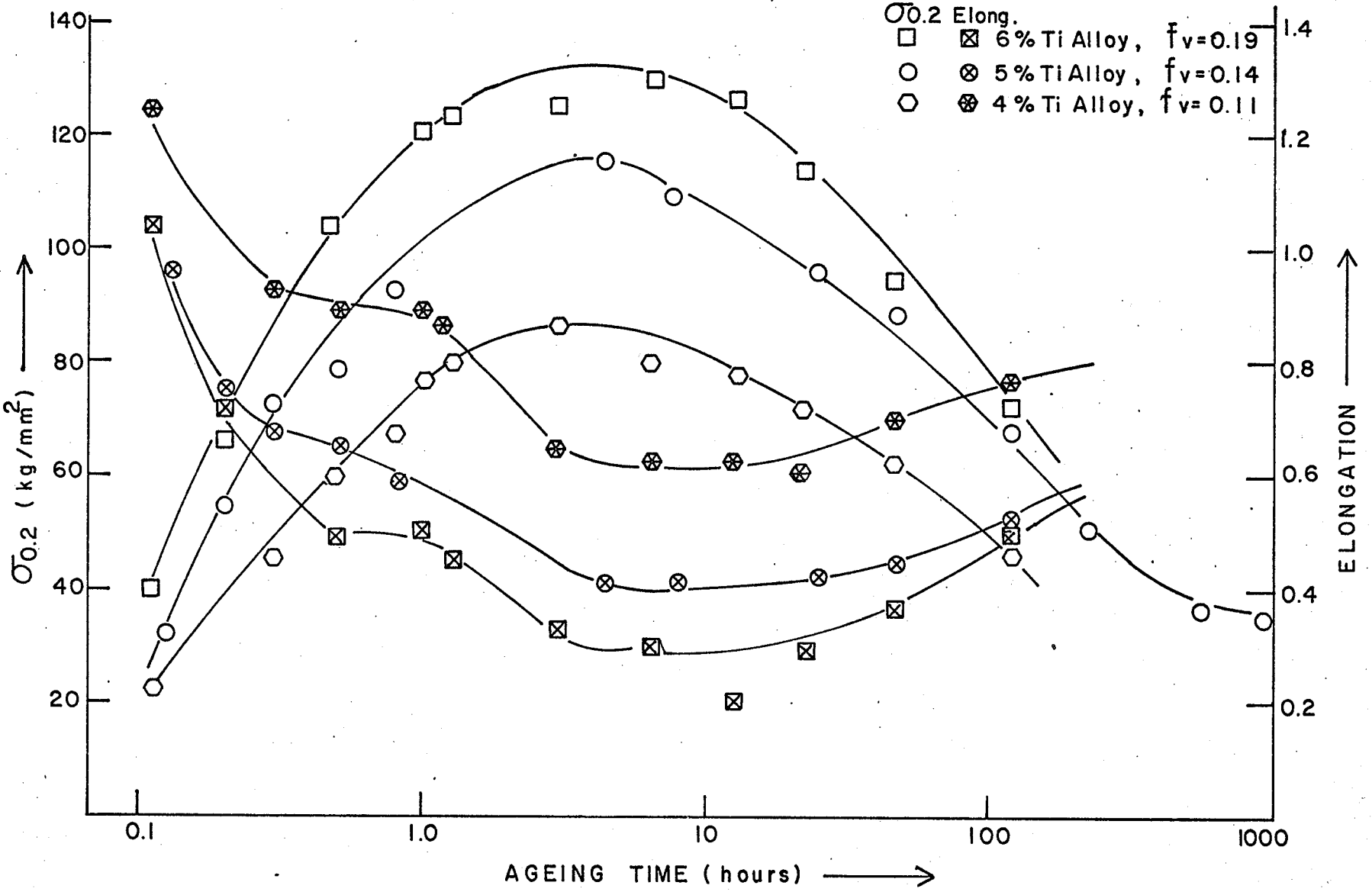
σ0.2 Elong.
6% Ti Alloy, fv=0.19
5% Ti Alloy, fv=0.14
4% Ti Alloy, fv=0.11
σ0.2 (kg/mm2)
ELONGATION
AGEING TIME (hours)
140
120
100
80
60
40
20
1.4
1.2
1.0
0.8
0.6
0.4
0.2
0.1
1.0
10
100
1000

FIG. (20)

alloys i.e. with ageing yield stress is first increased and then decreased, also, the ductility is reduced as the strength is increased and vice-versa. It should also be noted that the peak strength in all the three alloys occurs after about the same ageing time. Figure 21, shows the variation in the 0.2% offset yeild strength with the γ' precipitate particle size for all the three alloys. It is seen that, in all the three alloys, as the particle size is increased the strength first increases, attains a peak value and then decreases. It is also observed that in all the three alloys the peak strength occurs at about the same γ' particle size, i.e., 50-60 $\overset{o}{A}$. The contribution of the precipitate particles to the 0.2% yeild strength was determined by the expression $(\sigma_y - \sigma_o)$ where σ_y is the 0.2% yield strength of the aged alloy and σ_o is the .2% yield strength of the solution treated and quenched alloy. This is considered to be a reasonable assumption since the solution strengthening by 2.70 wt. % Ti in this alloy is not expected to be significant. Various precipitation strengthening mechanism, discussed in Chapter II, consider only single crystals. Therefore, to evaluate their applicability to the present alloy system, the polycrystalline tensile test values were divided by a factor of 3, as has been suggested in the past[15]. The contribution of the precipitation hardening to the critical resolved shear $\Delta\tau$, was, therefore, calculated by the following expression:

$$\Delta\tau = \frac{\sigma_y - \sigma_o}{3}$$

Now, if the precipitation strengthening involves the shearing of the ordered particles by the glide dislocation the increase in strength may be given by the following two expressions, as discussed Chapter II (equations 12 and 17).

$$\Delta\tau = \frac{\gamma_{APB}}{2b}\left[\left(\frac{4\gamma_{APB}\, f_v r_s}{\pi T^*}\right)^{1/2} - f_v\right] \quad \ldots\ldots \quad (12)$$

$$\Delta\tau = 3G\varepsilon^{3/2}\left(\frac{r_s\, f_v}{b}\right)^{1/2} \quad \ldots\ldots \quad (17)$$

According to these equations a plot of $\Delta\tau$ against $(r_s)^{1/2}$, at a constant volume fraction of the precipitate phase, should be a straight line. Therefore, $\Delta\tau$ was plotted against $(r_s)^{1/2}$ for all the three alloys. As shown in figure 21 this yielded a straight line, for all the three alloys, in the particle size range of 10-50 $\mathring{A}$. The straight line component of these curves can be represented by the expression,

$$\Delta\tau = B\, r_s^{1/2} - \delta$$

Beyond the particle size range of 10-50 $\mathring{A}$ the $\Delta\tau$ - $r_s^{1/2}$ curve shows an inflexion point and the value of $\Delta\tau$ begins to drop with increasing particle size.

When the particle size is large the precipitation strengthening mechanism usually involves Orowan looping process. The increase in strength by this process, as already discussed in Chapter II, is given by the following expression (Equation 23)

$$\Delta\tau = \frac{0.81\ Gb}{2\pi\ L_o(1-\nu)^{1/2}} \ln\left(\frac{2r_s}{r_o}\right) \quad \ldots\ldots \quad (23)$$

Figure (21) The relationship between mean planar particle size of γ' and shear stress increases.

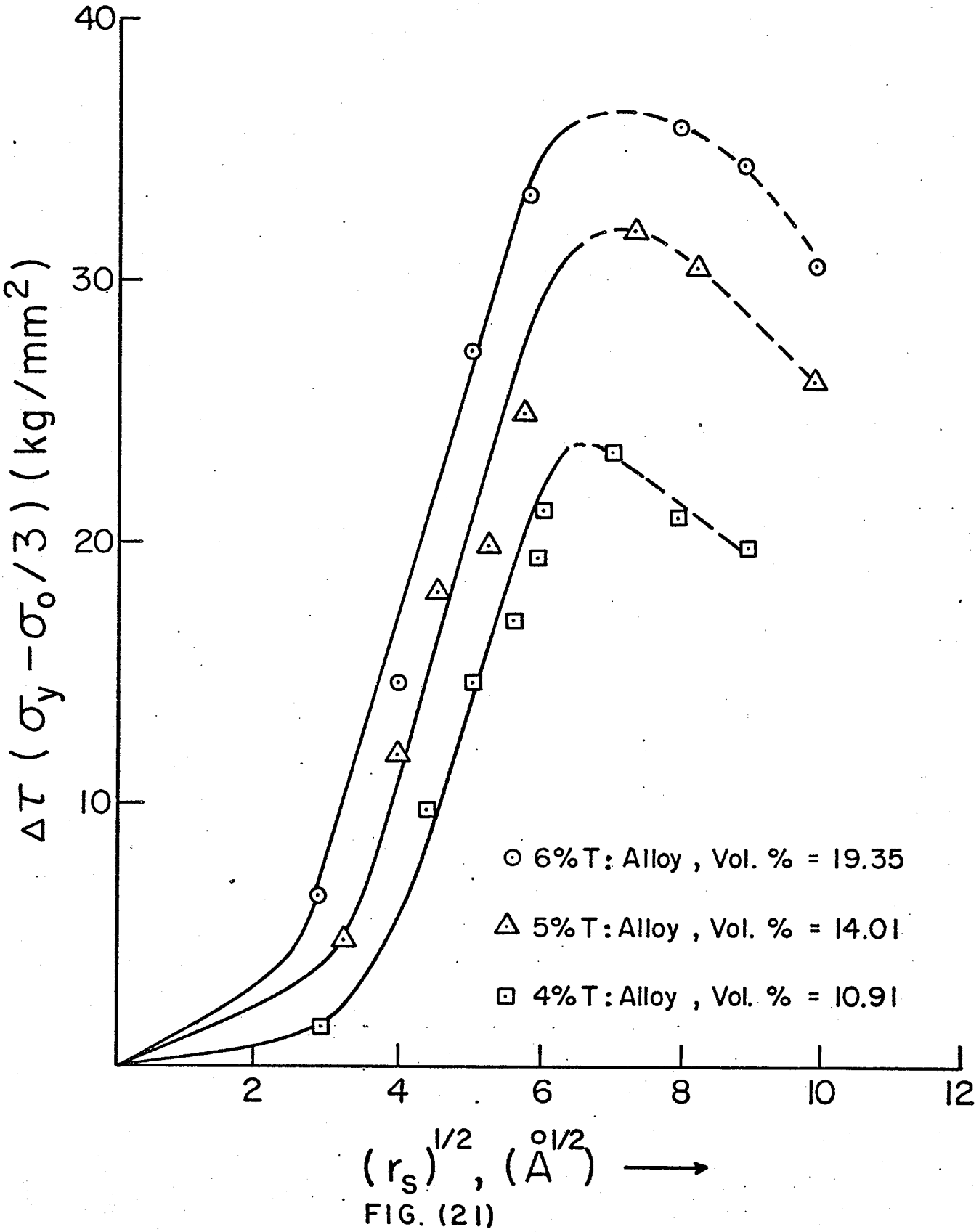
40
30
20
10
$\Delta\tau\ (\sigma_y - \sigma_o/3)\ (kg/mm^2)$
2
4
6
8
10
12
$(r_s)^{1/2}, (\mathring{A}^{1/2})$ ⟶
⊙ 6% T: Alloy , Vol. % = 19.35
△ 5% T: Alloy , Vol. % = 14.01
⊡ 4% T: Alloy , Vol. % = 10.91

FIG. (21)

This expression suggest that a plot of $\Delta\tau$ against $\frac{1}{L} \ln \frac{2r_s}{r_o}$ should be a straight line. Figure 22 shows that this plot for all the three alloys is not only a straight line, but all the points fall on the same straight line.

3.1.1 Dislocation structures.

In order to study the dislocation interaction with γ' precipitates, thin foils after 1-4% tensile deformation at room temperature, were examined. The solid solution treated and 3.5% deformed specimens show a typical dislocation structure of cold worked F.C.C. metals with a high stacking fault energy, i.e., little evidence of dissociated dislocations, and dislocation tangle, as shown in Figure 23. The 5% Ti alloy specimen aged for 10 minutes at 800° C and deformed 2% (Figure 24) shows a marked change in dislocation structure through the formation of the paired dislocations. At this stage the γ' precipitate particles are not clearly visible but their presence is suggested by the mottled appearance of the matrix. The 4% Ti alloy specimen aged for 30 minutes exhibits well defined dislocation loops confined to their slip planes (Figure 25). In addition to the dislocation loops, few paired dislocations are also present. On further ageing (1.5 hours at 800° C) the number of pinched off loops is significantly increased with a decrease in the number of paired dislocation, as shown in Figure 26. The specimen aged for 11 hours, (Figure 27) retains a large number of loops associated with particles along the broad slip band. Figure 28 and 29 show the bright and dark field microstructures of a specimen

Figure (22) The relation between the increments of the shear stresses and the interparticle spacing of γ'.

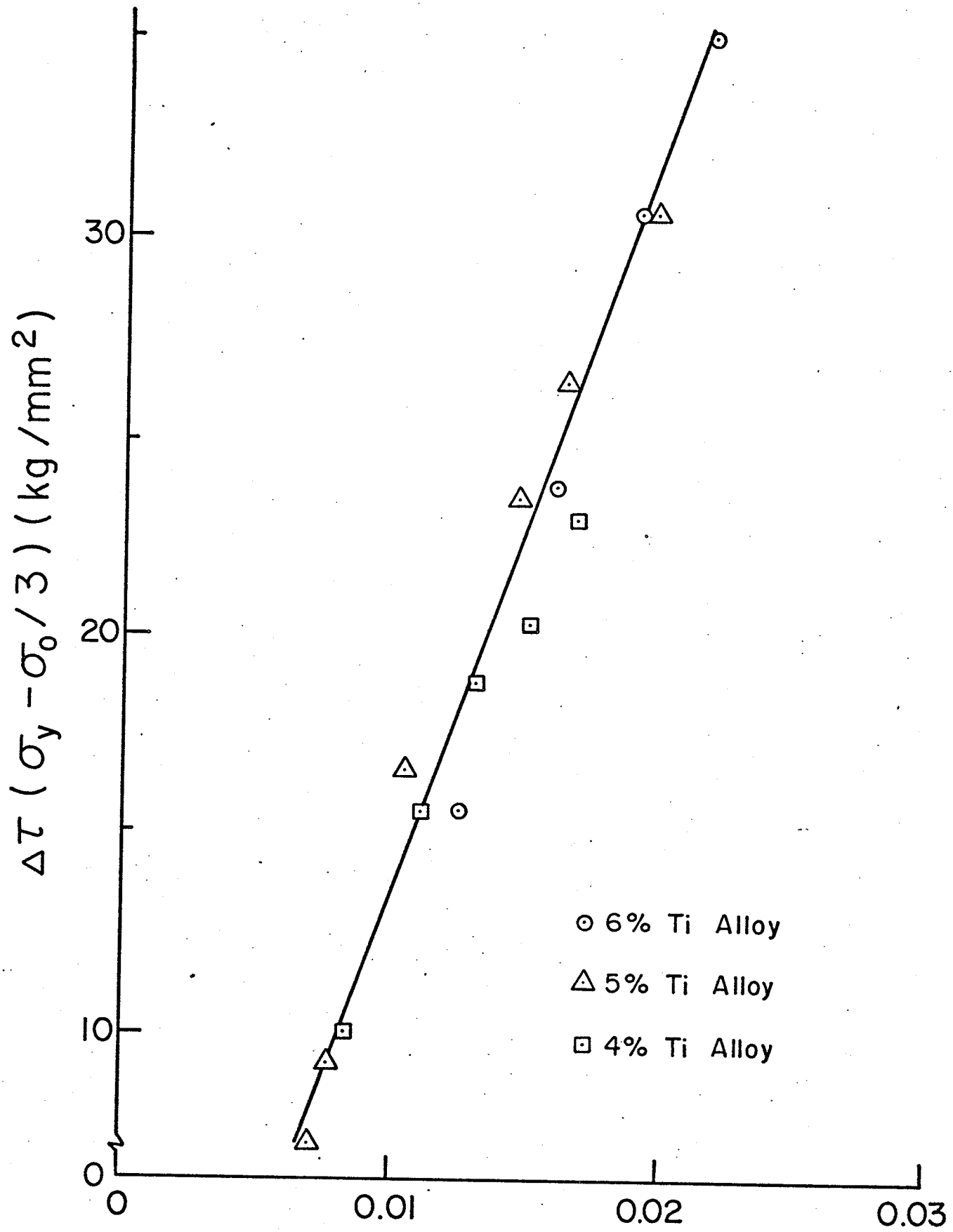
30
20
10
0
0
0.01
0.02
0.03
$\Delta\tau\,(\sigma_y - \sigma_0/3)\,(kg/mm^2)$
$\frac{1}{L}\ln\frac{2r_s}{b}\ (Å^{-1})$
⊙ 6% Ti Alloy
△ 5% Ti Alloy
⊡ 4% Ti Alloy

FIG. (22).

aged for 12 hours at 800° C and 3.5% deformed. The dark field micrograph, taken with the help of a (100) superlattice reflection due to γ', indicates no evidence of particle shearing by paired dislocations. As ageing proceeds, the loops were more uniformly distributed throughout specimen and little evidence of localized slip band was found. This is shown in Figure 30 which is the microstructure of 4% Ti alloy aged for 120 hours at 800° C and 4% deformed.

The above observations indicate that in these alloys during the early stages of ageing, when the γ' particles are small, the dislocation-precipitate interaction results in the shearing of the γ' particles by paired dislocations. Whereas, when the particle size is large the precipitate-dislocation interaction results in the formation of well defined dislocation loops, which are stoppedprimarily at the γ/γ' interface (Figure 31).

3.1.2 Determination of anti phase boundary energy.

In the past, several techniques have been used by different investigators to determine the anti phase boundary energies. Raynor and Silcock[15] by using "Minimum Orowan-loop size" and "Dislocation pair spacing" methods concluded that the former gave a much higher value than the latter. Singhal[111] has, however, pointed out that this may be due to the presence of coherency strains around the precipitate particles, which will tend to stabilize small loops. By equating the forces that result from the self stress of the loop, externally applied shear stress, misfit, and antiphase boundary energy he obtained the following expression for the determination of A.P.B. energy:

$$\gamma_{APB} = \frac{Gb^2}{8\pi\, r_\theta} \frac{2-\nu}{1-\nu} \frac{\ln 8\, r_\theta}{b} + \tau_{A.P.} b - 2Gb\frac{(a_p - a_m)}{a_m} \quad \ldots\ (40)$$

Figure (23) The dislocation structure of 5% Ti alloy solution treated at 1250° C and deformed 3.5% at room temperature.

Figure (24) The dislocation structure of 5% Ti alloy aged 10 minutes at 800° C and deformed 2% at room temperature.

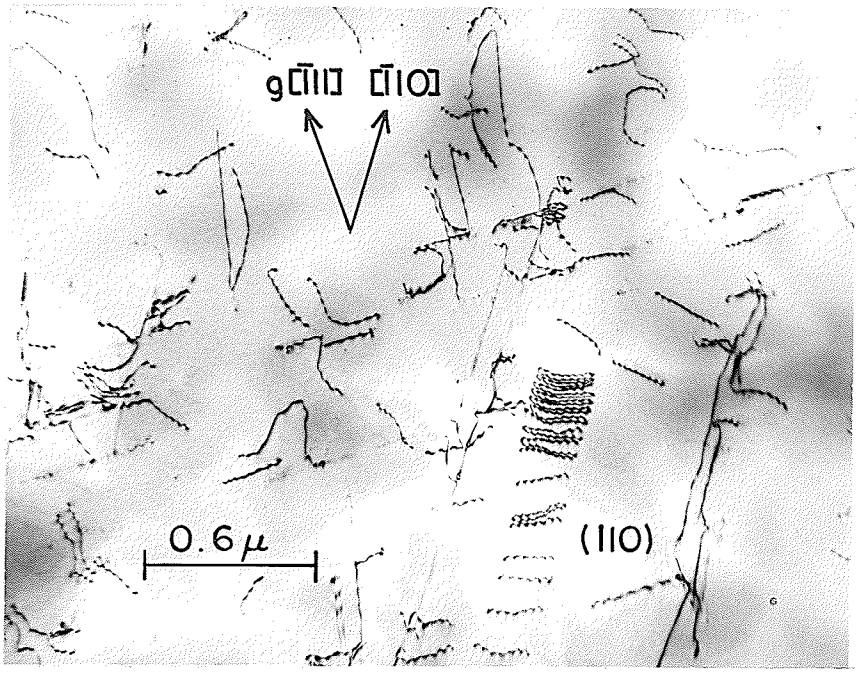

FIG. 23

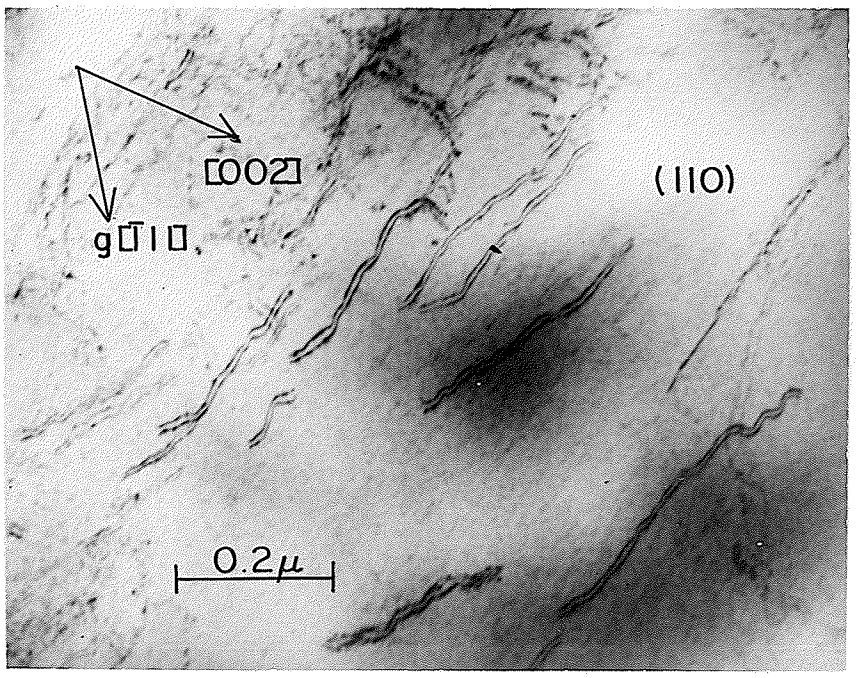

FIG. 24

Figure (25) The dislocation structure of 4% Ti alloy aged 30 minutes at 800° C and deformed 2% at room temperature.

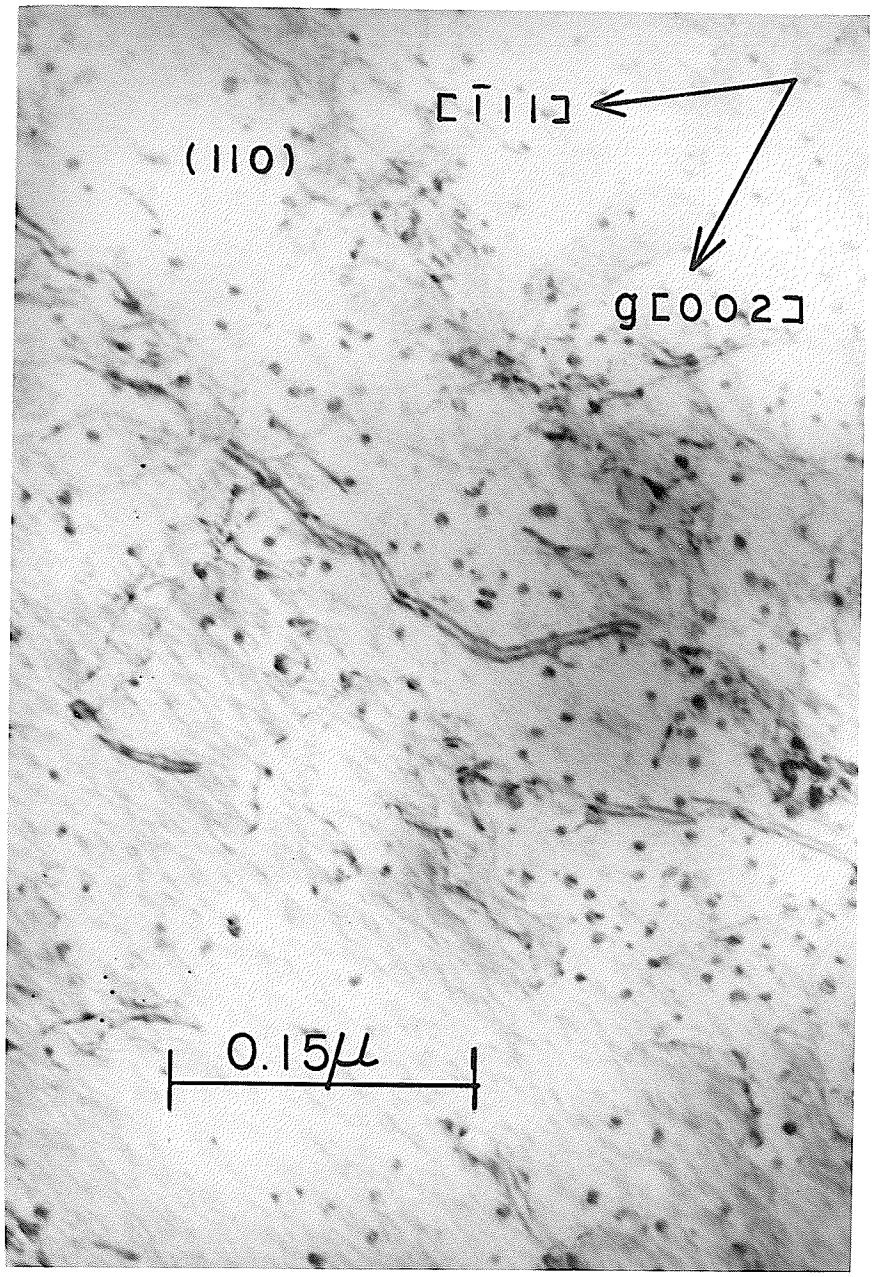

FIG. 25

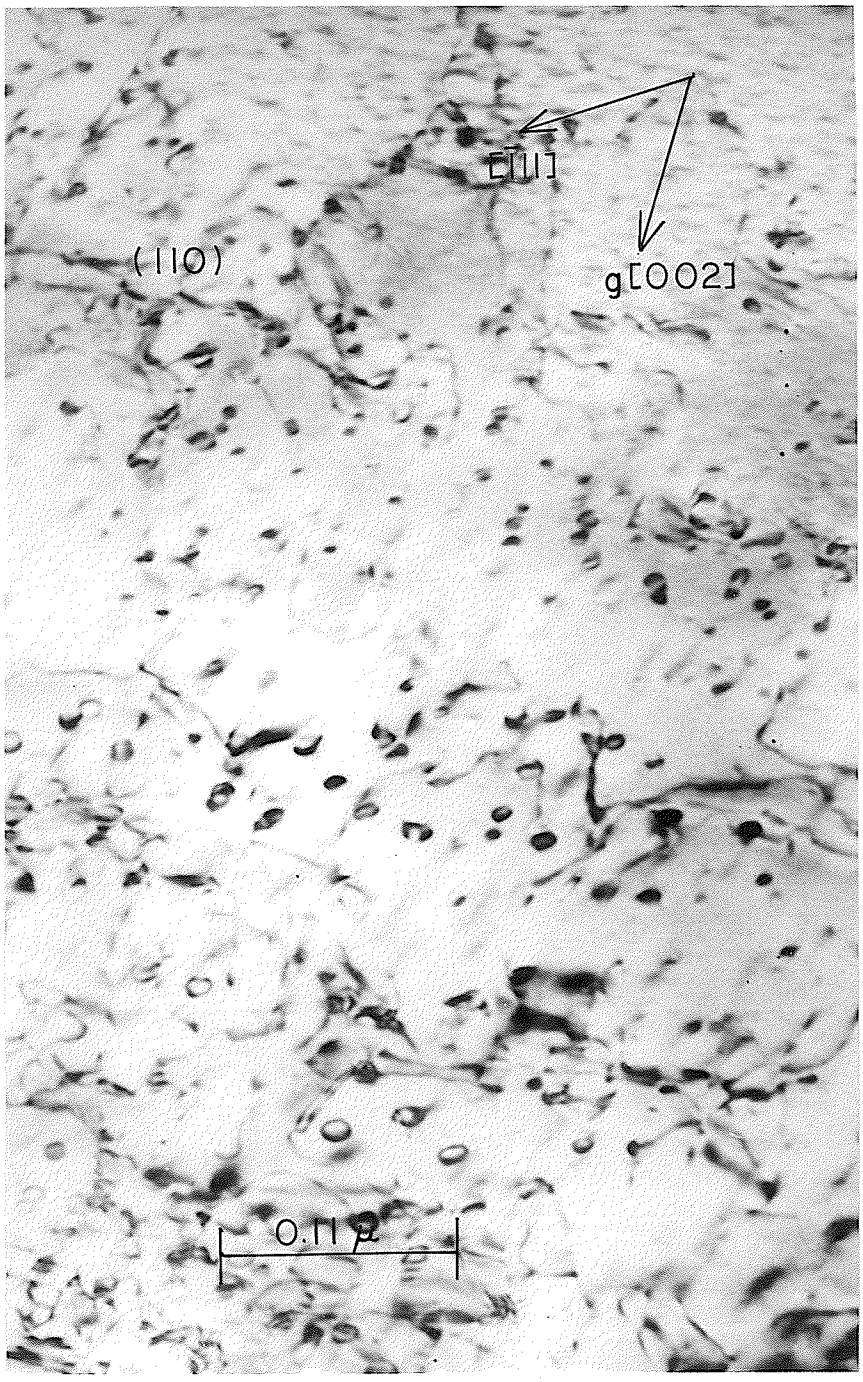

FIG. 26

Figure (27) The dislocation structure of 4% Ti alloy aged 11 hours at 800° C and defomred 4% at room temperature.

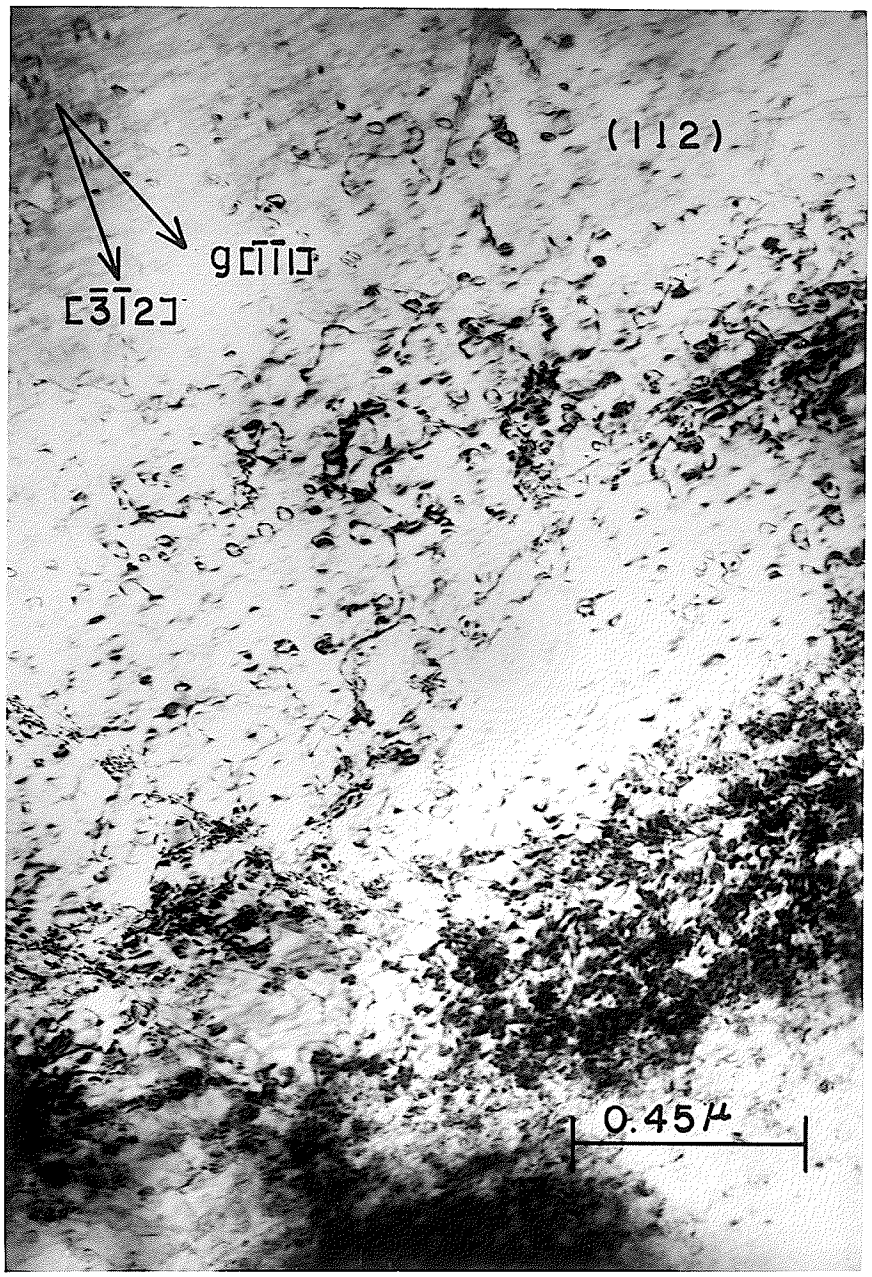

FIG. 27

Figure (28) The dislocation structure on (111) plane after 3.5% strain at room temperature in a specimen of 5% Ti alloy aged 12 hours at 800° C.

Figure (29) Dark-field of Figure (28) using (001) superlattice reflection, in specimen aged 12 hours at 800° C and strained 3.5% (5% Ti alloy).

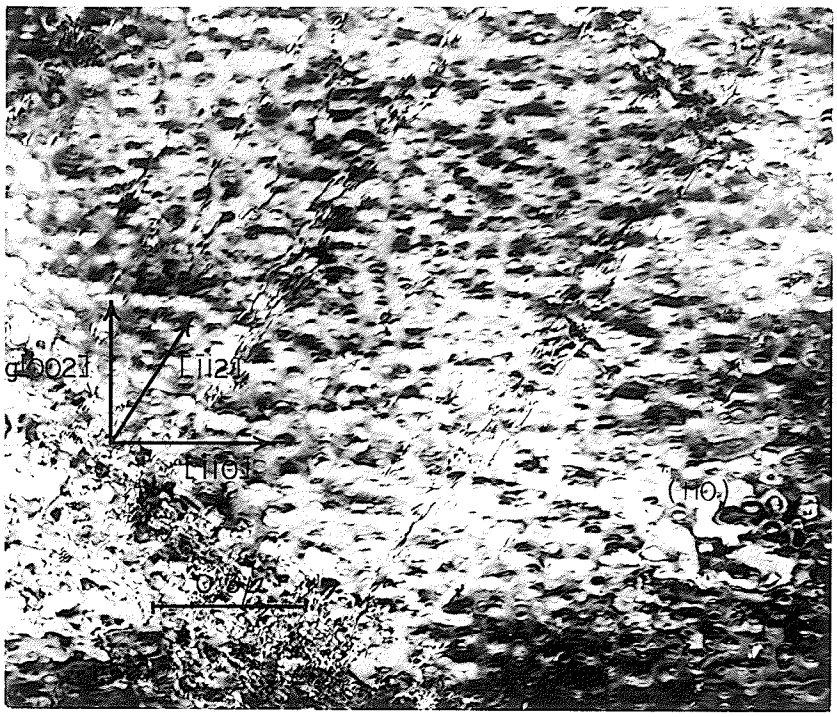

FIG. 28

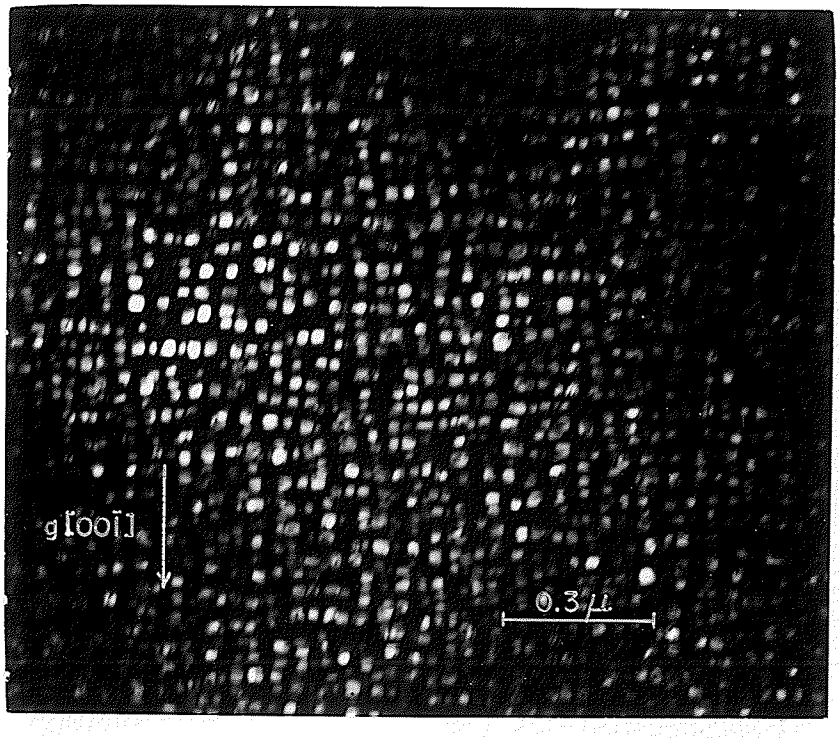

FIG. 29

Figure (30) Dislocation structure of 4% Ti alloy aged 96 hours at 800° C and strained 4% at room temperature.

Figure (31) Dislocation structure of specimen aged 96 hours at 800° C and deformed 2% at room temperature (6% Ti alloy).

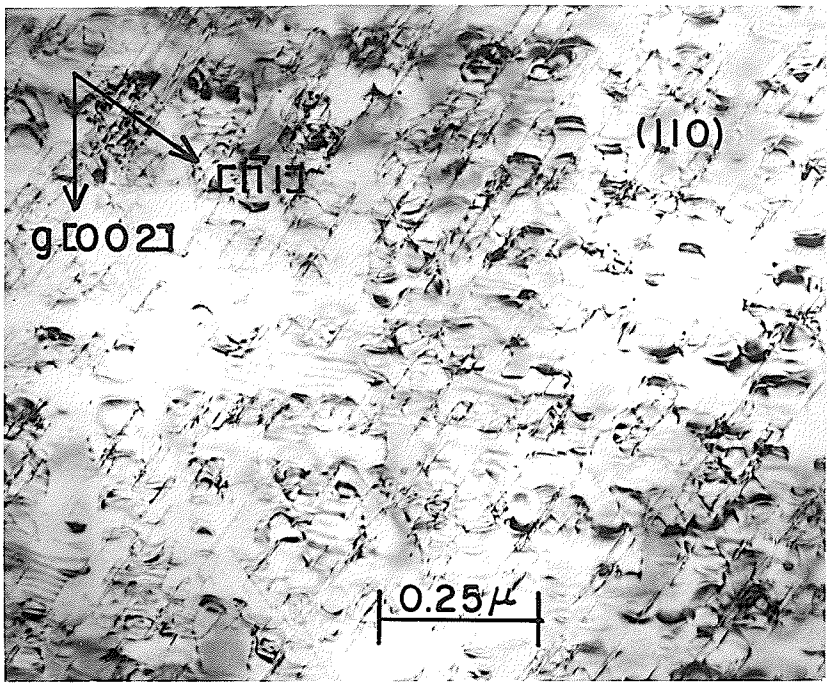

FIG. 30

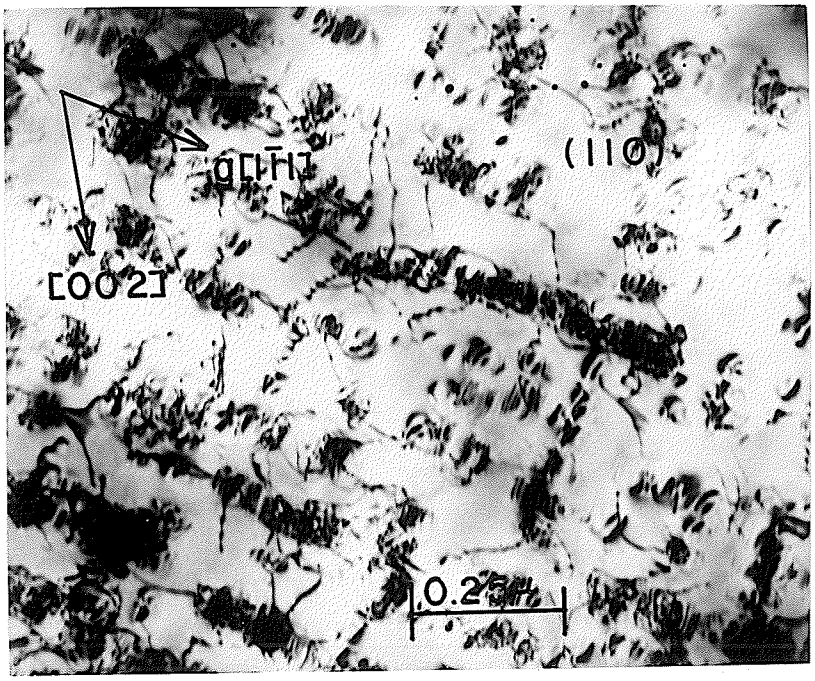

FIG. 31

where G is shear modulus, r_θ, the smallest loop radius, b, Burgers vector, ν, poisson's ratio, a_p, the lattice parameter of the particle, a_m, the lattice parameter of the matrix, and τ_{AP}, applied shear stress.

This expression was used in the present investigation to determine the A.P.B. energy. The smallest loop was first observed in specimen aged for 30 minutes at 800° C when the mean particle radius was 33.5 $\overset{o}{A}$. The minimum loop was measured to have a radius of 57 $\overset{o}{A}$. Thus, taking $\nu = 1/3$, $\tau_{ap} = 37.5$ kg/mm^2 and $\varepsilon = (a_p - a_m)/a_m = 1.3\%$ we obtain $\gamma_{APB} = 193$ ergs/cm^2.

Flinn[63] has estimated A.P.B. Energy for LI_2 type superlattices theoretically. He found that the total energy/unit area associated with a $(\frac{a}{2})$ <110> type A.P.B. is given by:

$$\gamma_{APB} = \frac{2\, V_{LI2}}{a_p^2} \frac{h}{(N_{h.k.\ell})^{1/2}} \qquad \ldots . \qquad (41)$$

where $N = h^2 + k^2 + \ell^2$, $V_{LI_2} = \dfrac{\kappa T_c^{(112)}}{2F_A F_B Z_{AB}}$,

κ, Boltzman constant, T_c, the critical ordering temperature, F_A, F_B, the atomic fraction of A and B atoms, and Z_{AB}, the number of first nearest neighbor atoms.

It has been suggested[113] that the above expression for V for LI_2 type superlattice gives a considerably lower value than that which is based on more accurate quasi chemical treatments,

$$V_{LI_2} = \frac{\kappa T_c}{0.82} \qquad \ldots . \qquad (42)$$

Taking T_c = 1000° C[62] and a = 3.56 Å γ_{APB} was found to be 196 erg/cm^2. This is in good agreement with value obtained by the "minimum loop size" method.

3.2 Serrated yielding behavior.

In the present experiments the serrated yielding of the austenitic superalloys has been considered in terms of the previous models. The alloys of Co - Ni - Cr - Ti system are convenient for investigating these models from several points of view:

(a) In the quenched solid solution condition they are a normal f.c.c. substitutional solid solution and should behave in a comparable manner to other f.c.c. alloys, eg. Au - Cu.

(b) On ageing at 800° C they precipitate the γ' $(Co, Ni, Cr)_3$ Ti phase. Hence the influence of concentration of solute atoms should be apparent from a comparison between the solid solution and the aged material.

(c) After 118 hours at 800° C the particles have coarsened and the material is in the overaged condition. The volume fraction of precipitate is constant after 5 hours of ageing at 800° C and hence the influence of particle size and particle spacing on serrated yielding should be apparant.

(d) The deformation of the aged alloys, when the particle size was larger than 56 Å was observed to be by the Orowan looping process. Therefore, by selecting proper ageing treatments complications due to the particle shearing process can be eliminated.

(e) The volume fraction of γ' phase with different amounts of Ti did not influence the growth rate of γ' particles. This means that one can obtain a similar particle size at various volume fraction and interparticle spacing of γ'. Therefore the influence of various particle distribution on the serrated yielding should be relevant for the direct comparison.

3.2.1 The characteristics of serrated yielding.

Three different types of serrated yielding were observed in the present alloy system, named A, B and C respectively. The type A shows periodic regular serrations which rise above the general level of the stress-strain curves and usually appear at high strain rate. The type B, called a fine serration, appear at relatively high strains, and are superimposed on the serrations of the type A; they essentially show an irregular and rapid oscillation about the general level of the stress-strain curves. Fig. (32) and (33) show the type A and B, respectively, which are similar to those first reported by Russell in Cu - Sn alloys[84].

The type C are characterized by an abrupt load drop below the general level of the curve as shown in Fig. (34), and are observed at relatively high temperatures and when the serrations are about to disappear. This is identical to those reported by Soler - Gomex and Tegart[83].

Each of these types of serrations were observed in both the aged and unaged alloys under various experimental conditions, ie. ageing

treatments and alloy composition. However, the major consideration is given to type A serrations since these were present at the onset of the serrated yielding (ε_c). In addition to the critical strain, ε_c, the type A serrations are also characterized by an yield drop, $\Delta\sigma$, and a delay strain, ε_s, between consecutive serrations, as indicated in the inset of Fig. (32).

Figs. (35) and (36) show the variation of $\Delta\sigma$ with strain for unaged and aged alloys, respectively. The yield drop, $\Delta\sigma$, for each periodic serrations is also consistent with two components; the discontinuous increase in flow stress prior to the yield drop, $\Delta\sigma_f$, and the displacement of the level of the force-elongation curve, $\Delta\sigma_d$. The increase in $\Delta\sigma$ with increasing strain is mainly due to the increase in $\Delta\sigma_d$. Whereas, the discontinuous flow stress rise, $\Delta\sigma_f$, is not found to increase significantly with strain after the first few serrations, it decreases gradually at large strains.

The strain between serrations, ε_s, also increases linearly with strain. This is illustrated in figure 37 which shows ε_s vs ε plots for the 5% Ti alloy, in the solid solution condition, at various testing temperatures. This is very similar to that reported for type A serrations in Cu - Sn alloys[84]. It is also seen that the slope of the ε_s vs ε plots also increase with the increasing temperature and this is similar to the trend observed in Al - Mg - Si[114], Au - In[83], and Cu - Sn[84] alloys. But, the delay strain, ε_s, is unaffected by the specimen gauge length as shown in Fig. (38) which is similar to the observation of Al - Mg - Si[114] alloys.

Figure (32) Load-Elongation Curve exhibiting locking serrations ($\dot{\varepsilon} = 3.28 \times 10^{-4}$/sec, at 300° C).

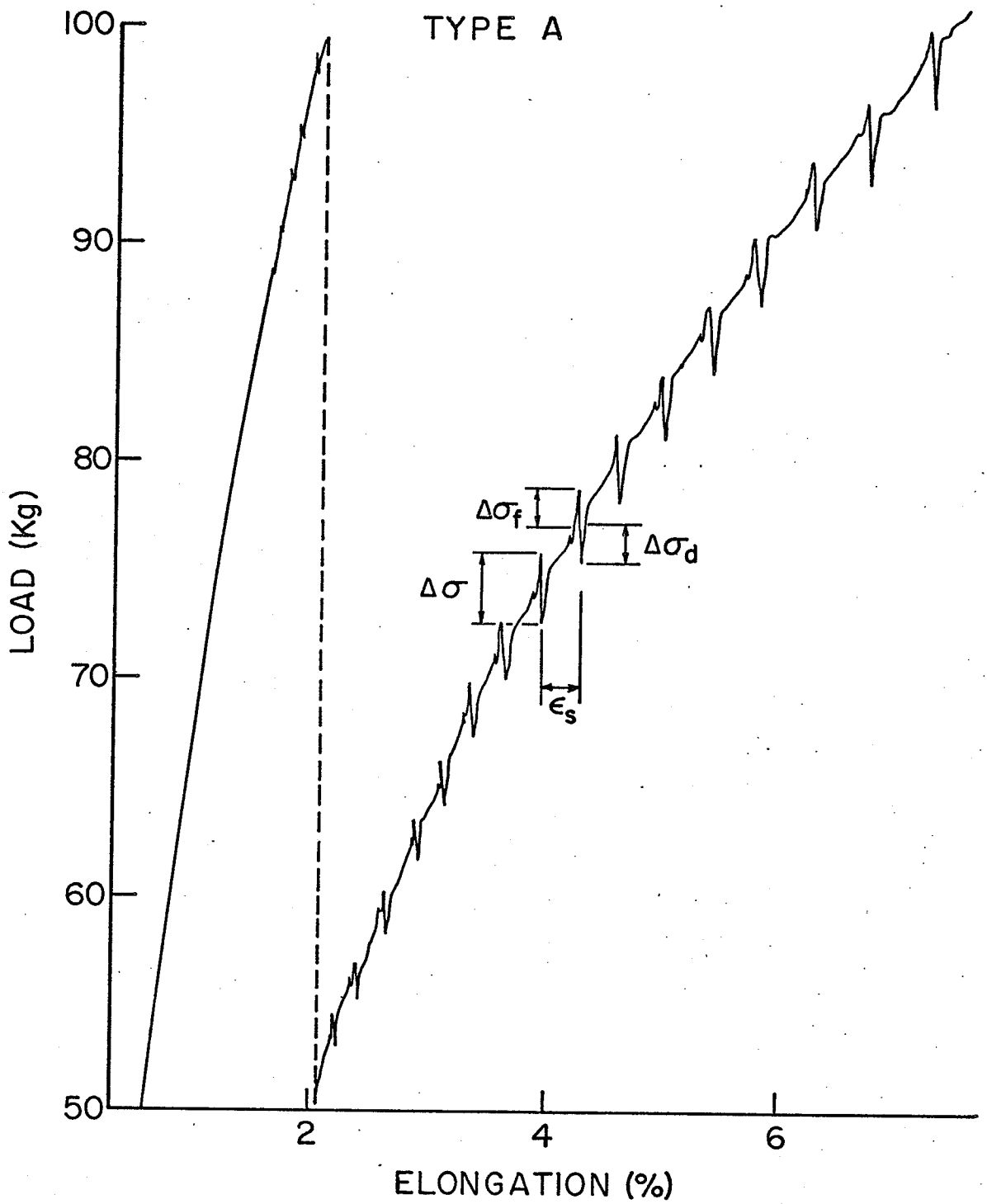
TYPE A
100
90
80
70
60
50
LOAD (Kg)
2
4
6
ELONGATION (%)
$\Delta\sigma_f$
$\Delta\sigma_d$
$\Delta\sigma$
ϵ_s

FIG. (32)

Figure (33) Load-Elongation Curve exhibiting irregular locking plus unlocking serrations.
($\dot{\varepsilon} = 1.31 \times 10^{-4}$/sec, at 400° C).

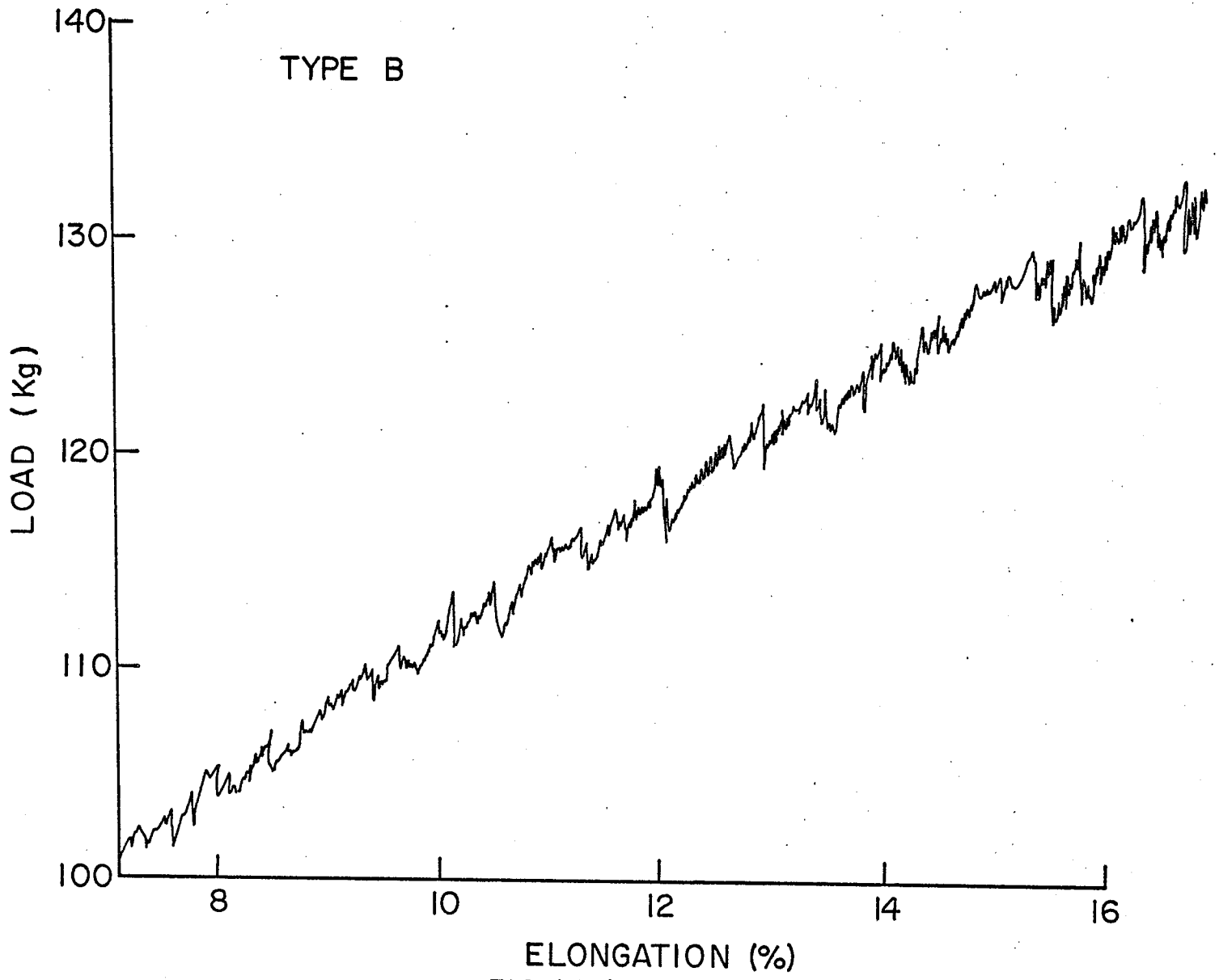

FIG. (33)

Figure (34) Load-Elongation curve exhibiting unlocking serrations ($\dot{\varepsilon} = 3.28 \times 10^{-5}$/sec., at 500° C).

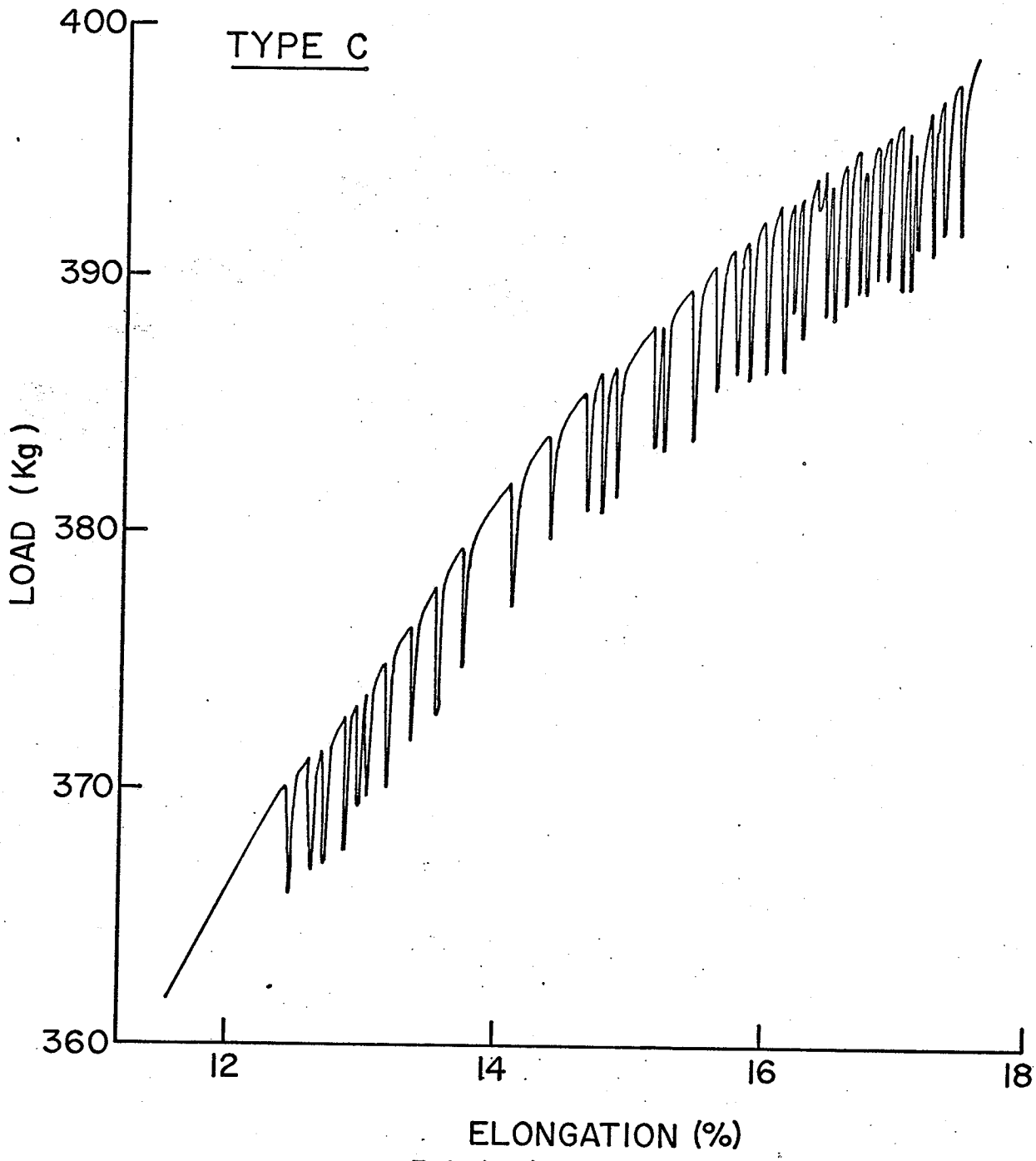

FIG. (34)

The tensile test results were also examined to determine the effect of the temperature of testing on the flow stress of the solution treated and aged alloys. In figure 39 the 0.2% flow stress of the three alloys, after various heat-treatments, is plotted against the testing temperature. It is seen that after an initial drop the 0.2% flow stress remains essentially constant between 400 - 700° C and in some cases it even increases slightly. The plateau in the flow stress-temperature curve corresponds to the serrated yielding region. As the testing temperature in increased beyond 700° C a significant decrease in the flow stress of all the three alloys occurs.

3.2.2 Critical strain-temperature relationship.

Fig. (40) shows the critical strain, ε_c, against temperature relationship for the three heat treatments of 5% Ti alloy. It is apparent that as the ageing time increases the critical strain to serrations decreases, regardless of whether the specimen has been heat treated beyond the peak strength or not. According to the following two equations, which were discussed in Chapter II, a plot of log ε_c against $\frac{1}{T}$ is expected to be linear with a gradient proportional to the vacancy migration energy.

$$\dot{\varepsilon} = \frac{4b\ \rho_m\ D_o\ C_V}{\ell} \exp\left(\frac{-Q_m}{\kappa T}\right) \quad \ldots\ (27)$$

$$\dot{\varepsilon} = \left(\frac{\alpha C_o}{C_1}\right)^{3/2} 3L\ \rho_m\ C_V\ U_m\ D_o \exp\left(\frac{-Q_m}{\kappa T}\right) \quad \ldots\ (34)$$

Fig. (41) shows that the plots are only linear for the aged specimens at higher temperatures.

Figure (35) The effect of strain and temperature on the serration magnitude for solid solution treated alloys.

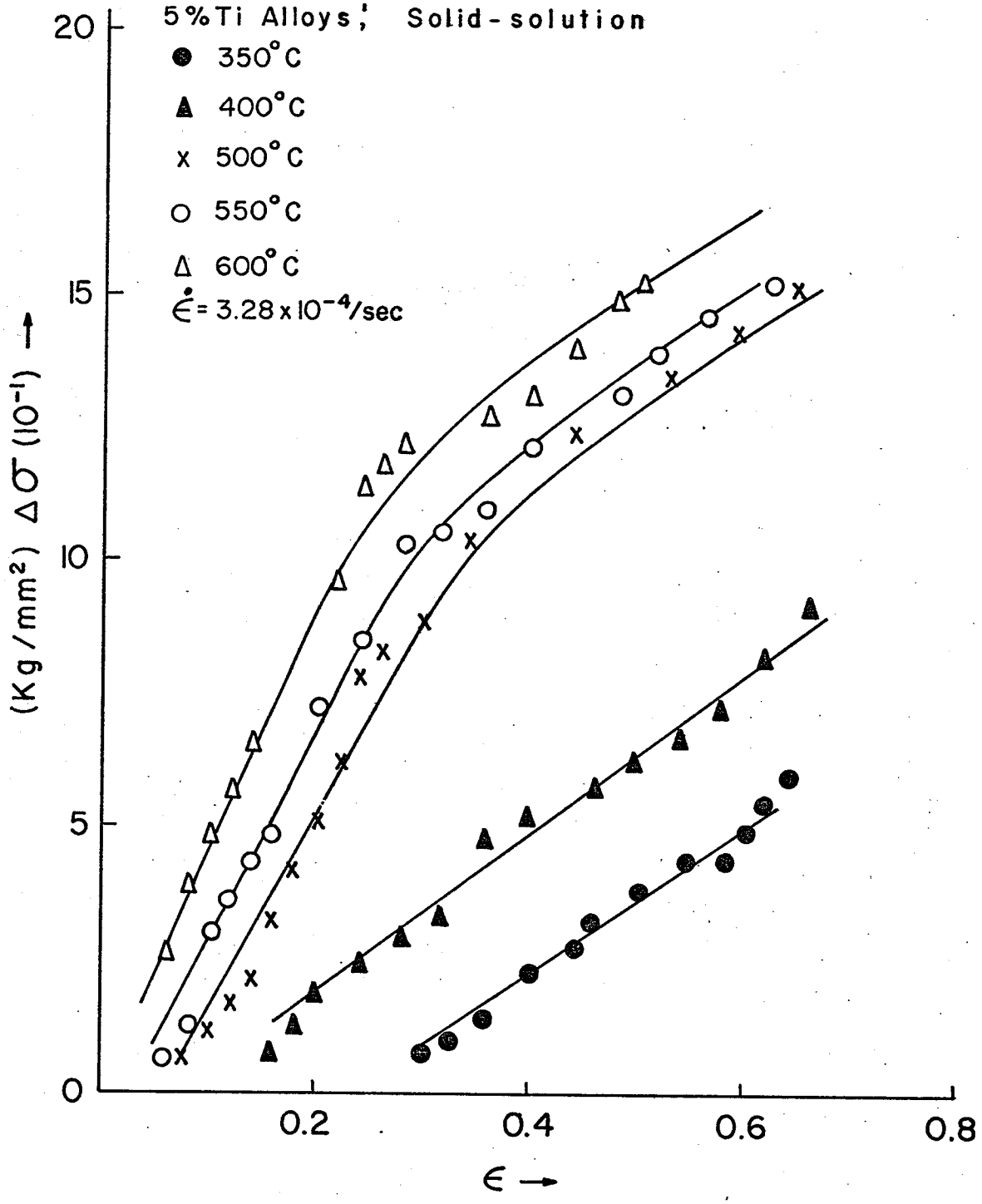
5% Ti Alloys; Solid-solution
350°C
400°C
x 500°C
550°C
600°C
$\dot{\epsilon} = 3.28 \times 10^{-4}$/sec
20
15
10
5
0
0.2
0.4
0.6
0.8
$\epsilon \rightarrow$
(Kg/mm²) $\Delta\sigma$ (10^{-1}) →

FIG. (35)

Figure (36) The effect of strain and temperature on the serration magnitude for aged alloys.

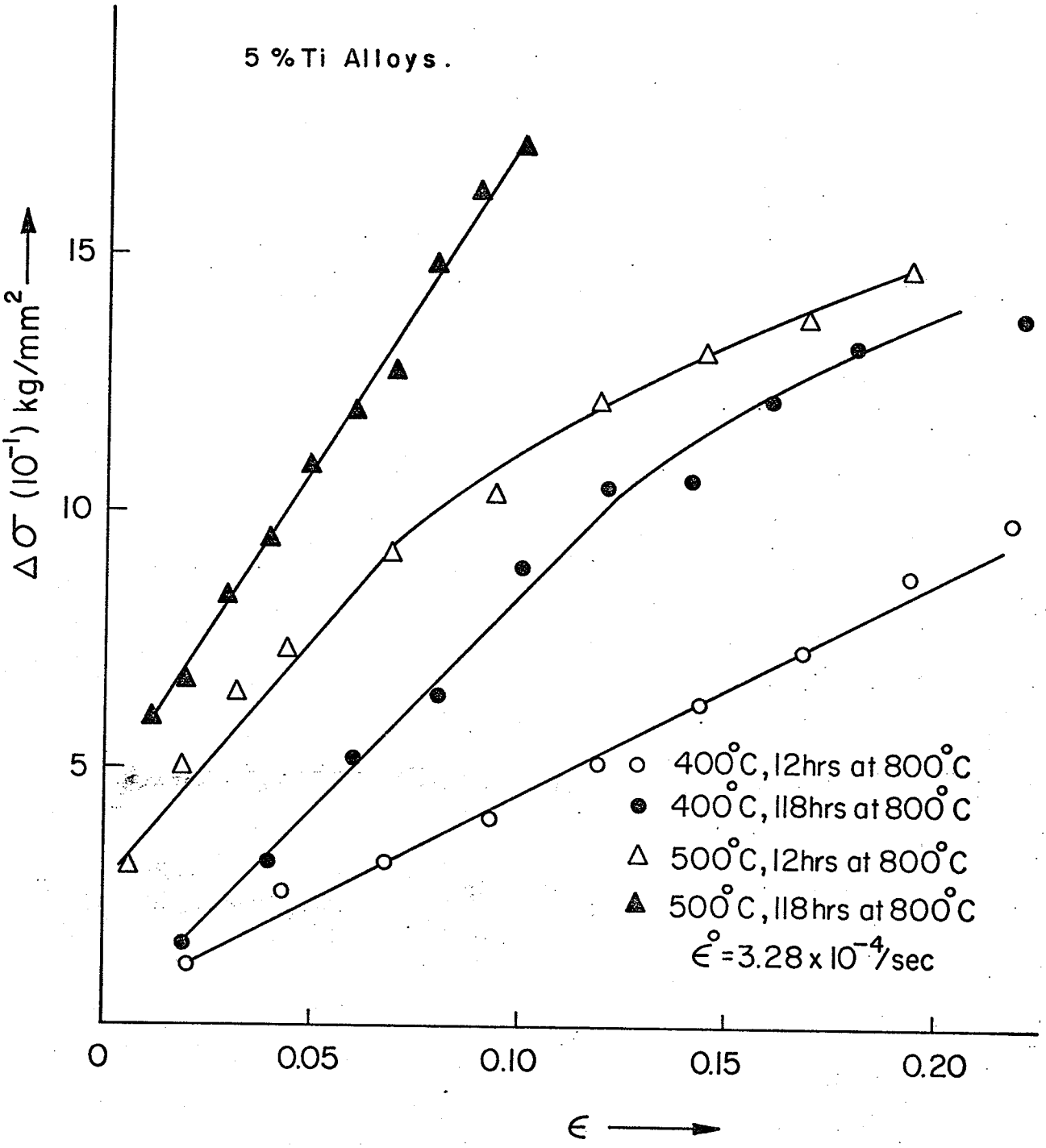
5 % Ti Alloys.
Δσ (10⁻¹) kg/mm²
15
10
5
0
0.05
0.10
0.15
0.20
ε
400°C, 12hrs at 800°C
400°C, 118hrs at 800°C
500°C, 12hrs at 800°C
500°C, 118hrs at 800°C
ε° = 3.28 x 10⁻⁴/sec

FIG. (36)

Figure (37) The effect of temperature on the strain between successive periodic locking serrations, ε_s, for 5% Ti solid-solution treated alloy.

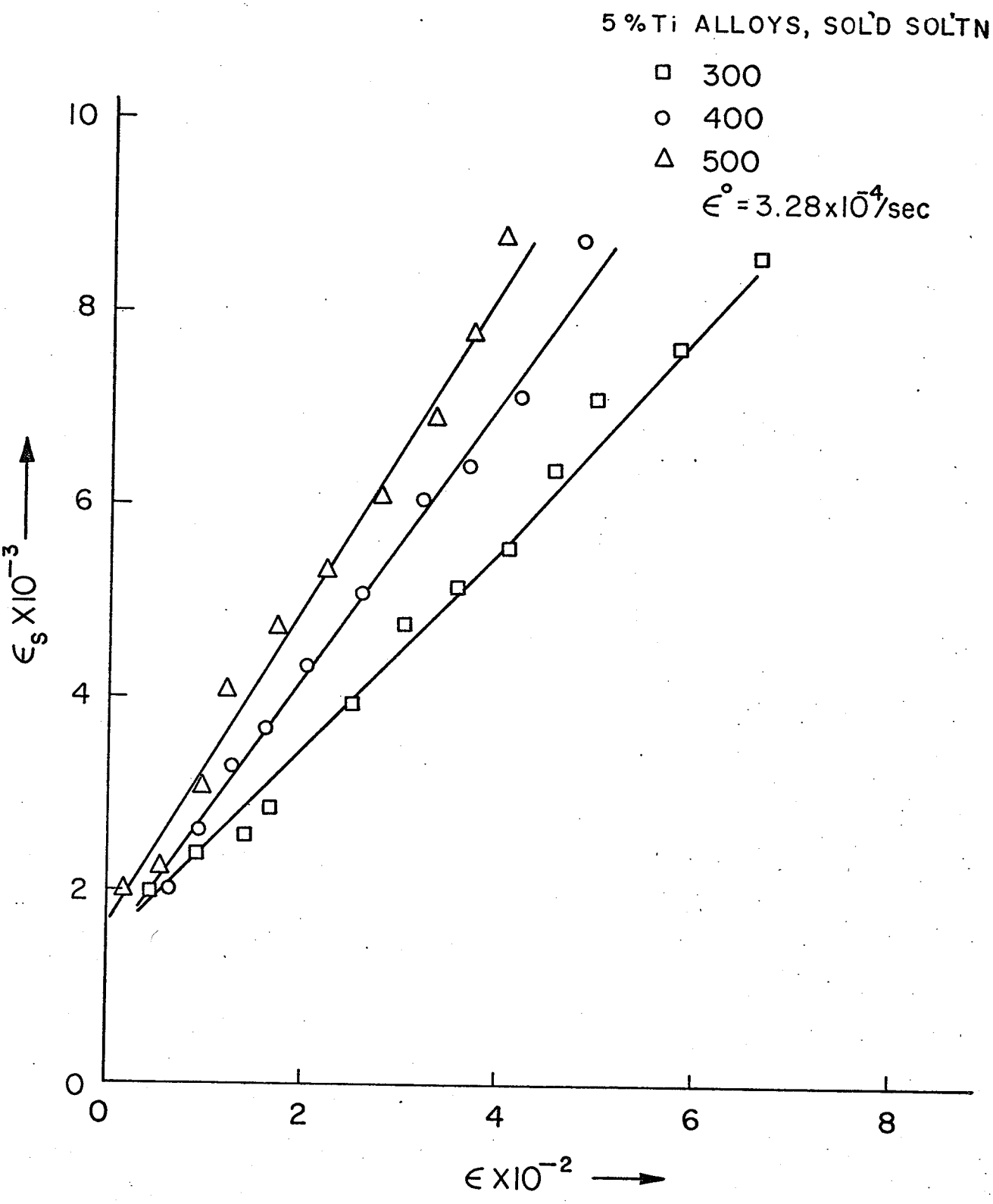
5 % Ti ALLOYS, SOL'D SOL'TN
300
400
500
$\dot{\epsilon}^{\circ} = 3.28 \times 10^{-4}$/sec
$\epsilon_s \times 10^{-3}$
$\epsilon \times 10^{-2}$
0
2
4
6
8
10

FIG. (37)

Figure (38) The effect of strain and gauge length on the strain between successive periodic locking serrations, ε_s , in solution treated 5% Ti alloys.

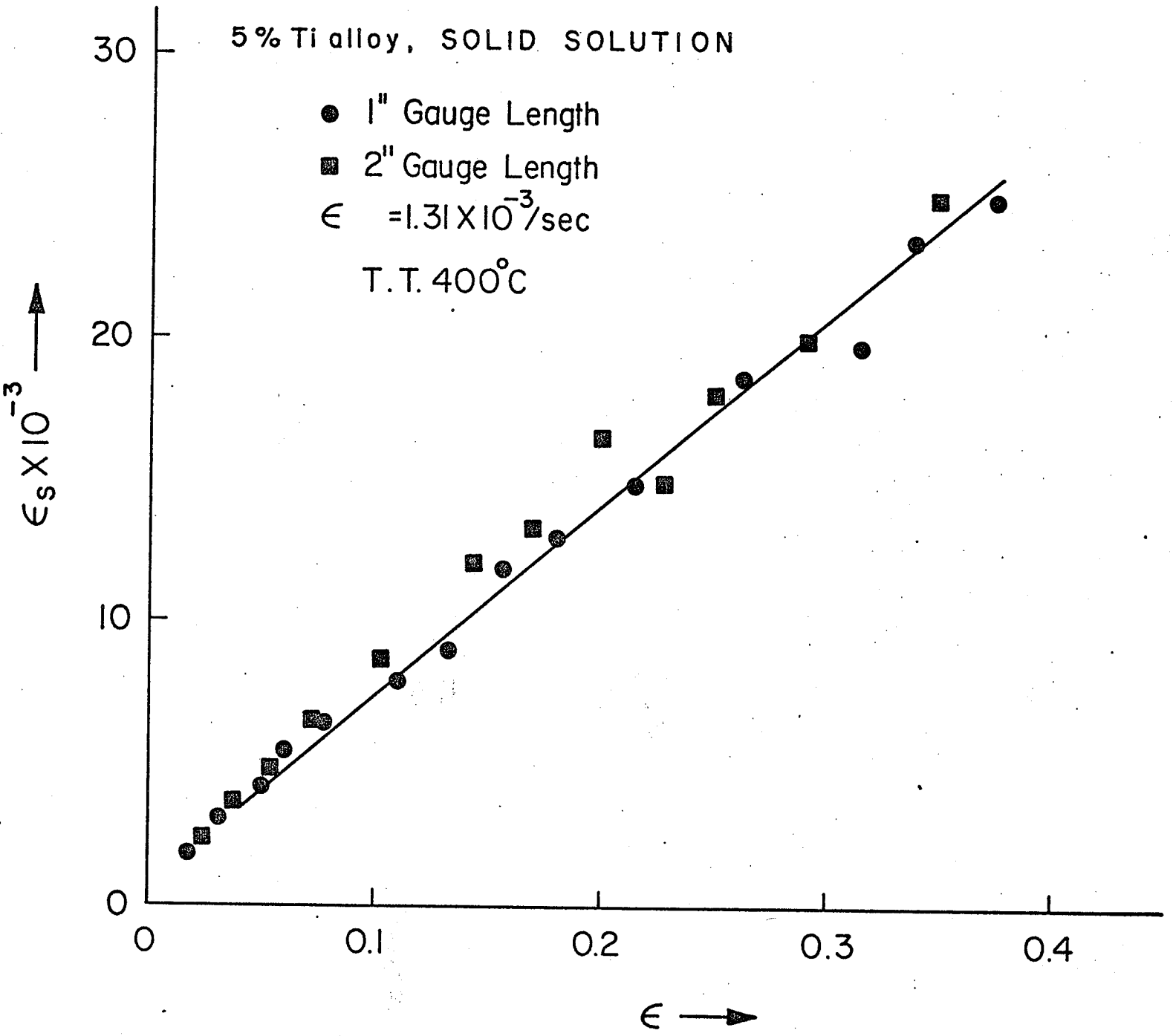
5% Ti alloy, SOLID SOLUTION
1" Gauge Length
2" Gauge Length
ϵ =1.31 X 10⁻³/sec
T.T. 400°C
30
20
10
0
0
0.1
0.2
0.3
0.4
ϵs X 10⁻³
ϵ

FIG. (38)

Figure (39) The temperature dependence of 0.2% offset yield stresses of the three alloys after various ageing treatments.

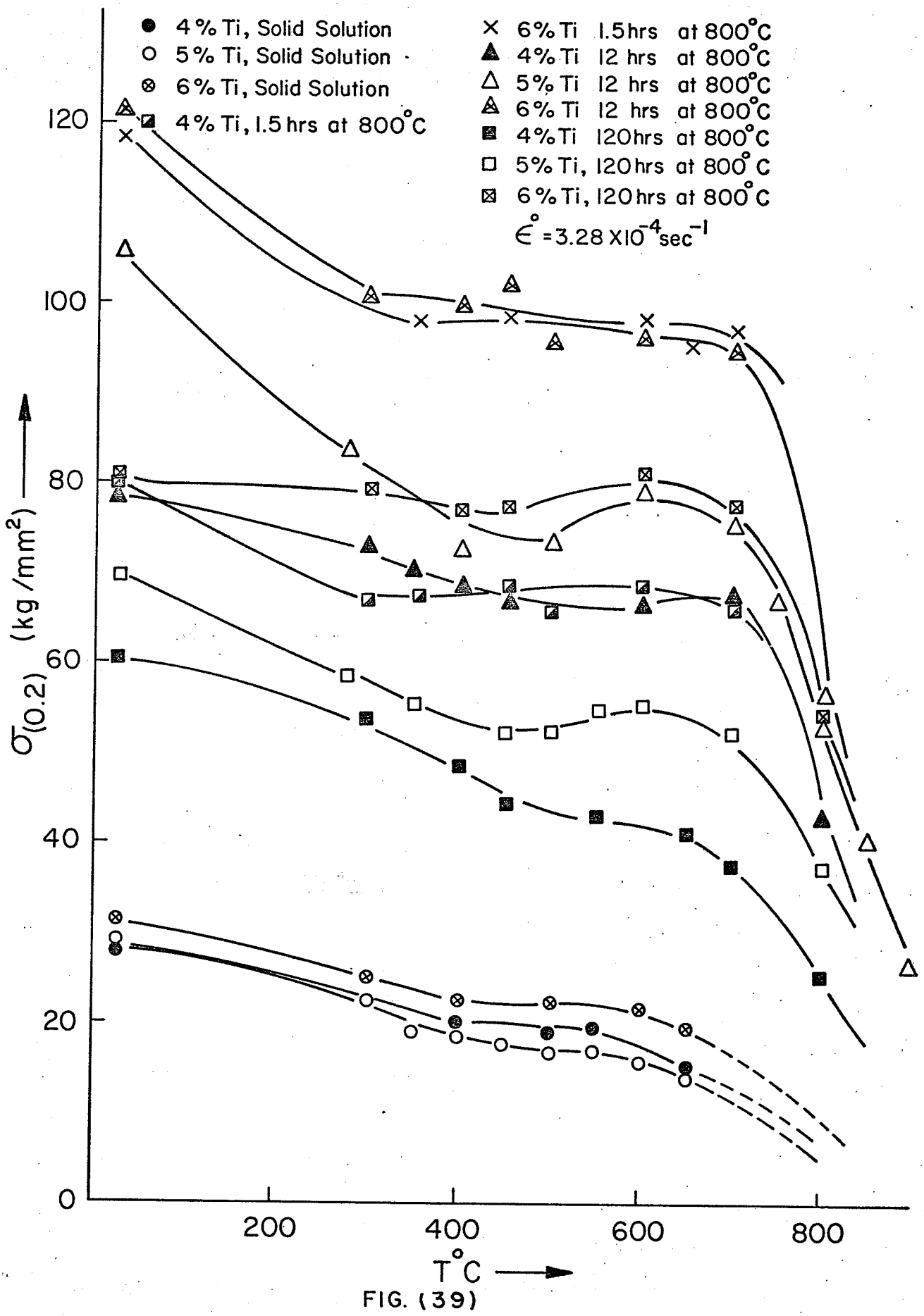
4% Ti, Solid Solution
5% Ti, Solid Solution
6% Ti, Solid Solution
4% Ti, 1.5 hrs at 800°C
6% Ti 1.5hrs at 800°C
4% Ti 12 hrs at 800°C
5% Ti 12 hrs at 800°C
6% Ti 12 hrs at 800°C
4% Ti 120hrs at 800°C
5% Ti, 120hrs at 800°C
6% Ti, 120hrs at 800°C
$\dot{\epsilon}^{\circ} = 3.28 \times 10^{-4} sec^{-1}$
$\sigma_{(0.2)}$ (kg/mm^2)
0
20
40
60
80
100
120
200
400
600
800
T°C

FIG. (39)

Figure (40) The temperature dependence of the critical strain ε_c, for serrations in 5% Ti alloy.

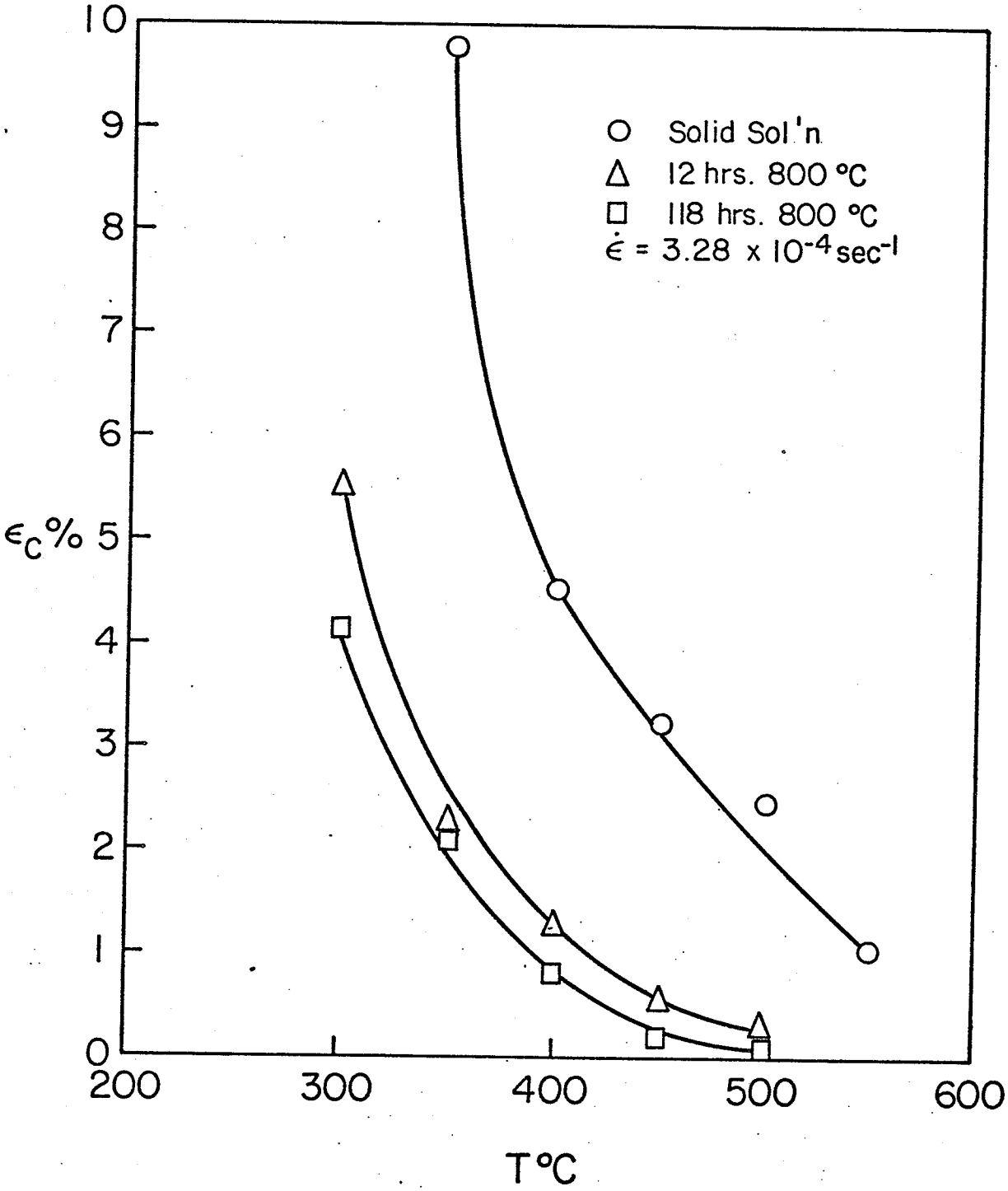
10
9
8
7
6
5
4
3
2
1
0
ϵ_c%
200
300
400
500
600
T°C
Solid Sol'n
12 hrs. 800 °C
118 hrs. 800 °C
$\dot{\epsilon}$ = 3.28 x 10^{-4} sec^{-1}

FIG. (40)

Figure (41) A plot of log ε_c against 1/T for the three heat treatments in 5% Ti alloy.

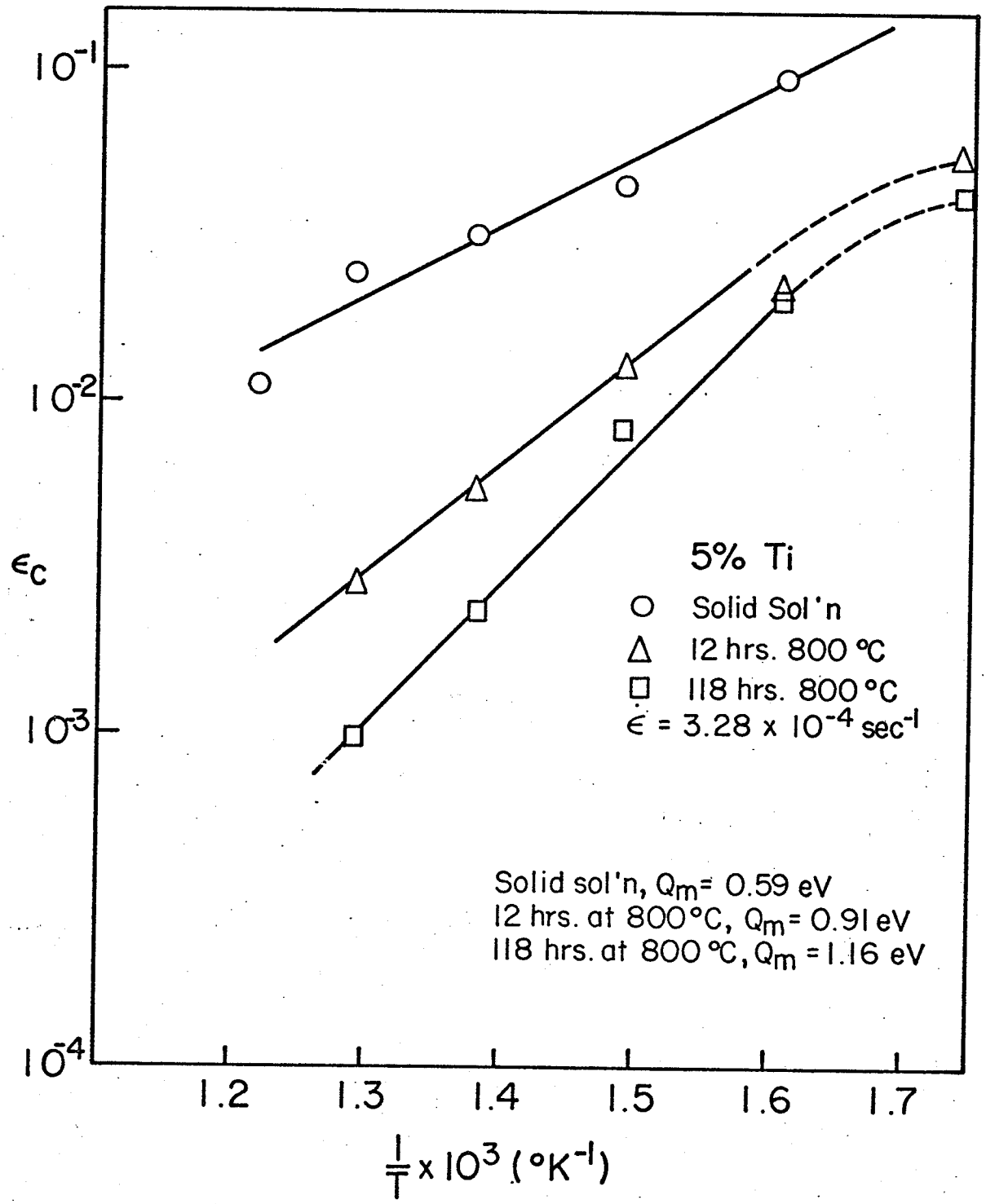
10^{-1}
10^{-2}
10^{-3}
10^{-4}
ϵ_c
5% Ti
Solid Sol'n
12 hrs. 800 °C
118 hrs. 800 °C
$\dot{\epsilon} = 3.28 \times 10^{-4}$ sec^{-1}
Solid sol'n, Q_m= 0.59 eV
12 hrs. at 800°C, Q_m= 0.91 eV
118 hrs. at 800 °C, Q_m = 1.16 eV
1.2
1.3
1.4
1.5
1.6
1.7
$\frac{1}{T} \times 10^3$ (°K^{-1})

FIG. (41)

The effect of strain rate on the flow stress was studied only for 5% Ti alloy aged for 12 hours at 800° C which is in the region of the optimum strength at room temperature. Figure 42 shows the plots of the strain rate dependence of the flow stress in the temperature range of 400 to 900° C. Below 600° C the inverse strain rate effect upon the flow stress, due to strain ageing, is observed. Above 600° C a normal strain rate dependence of the flow stress is seen, i.e., as the strain rate is increased the flow stress is also increased. The flow stress temperature curve, at all the strain rates, shows a maximum which occurs in the region of 600° C - 700° C. This observation is similar to that reported in figure 39.

3.2.3 Critical strain-strain rate relationship.

The following two equations, which were also discussed in Chapter II,

$$\varepsilon_c^{m+\beta} = \frac{\ell\, \dot{\varepsilon}\, \exp(Q_m/\kappa T)}{4b\, D_o\, N\, A} \qquad \ldots\ldots \quad (30)$$

$$\varepsilon_c^{m+\beta} = \left(\frac{C_1}{\alpha C_o}\right)^{3/2} \frac{\dot{\varepsilon}\, \kappa T\, b\, \exp\left(\frac{Q_m}{\kappa T}\right)}{3L\, NA\, U_m\, D_o} \qquad \ldots\ldots \quad (35)$$

suggest that a plot of log ε_c against log $\dot{\varepsilon}$ at constant temperature should be linear with a gradient of $(m+\beta)$. Fig. (43) shows that a linear relationship is obtained at 400° C for all the three treatments, giving a constant value of $(m+\beta) = 1.4 \pm 0.1$. The solid solution tested at 550° C and the specimens aged for 118 hours at 800° C and tested at 350° C also gave $m+\beta = 1.4$. Thus in the temperature range of serrations for the 5% Ti alloy $(m+\beta)$ appears to be temperature independent.

Figure (42) The effect of temperature and strain rate upon the flow stress for 5% Ti alloy aged 12 hours at 800° C.

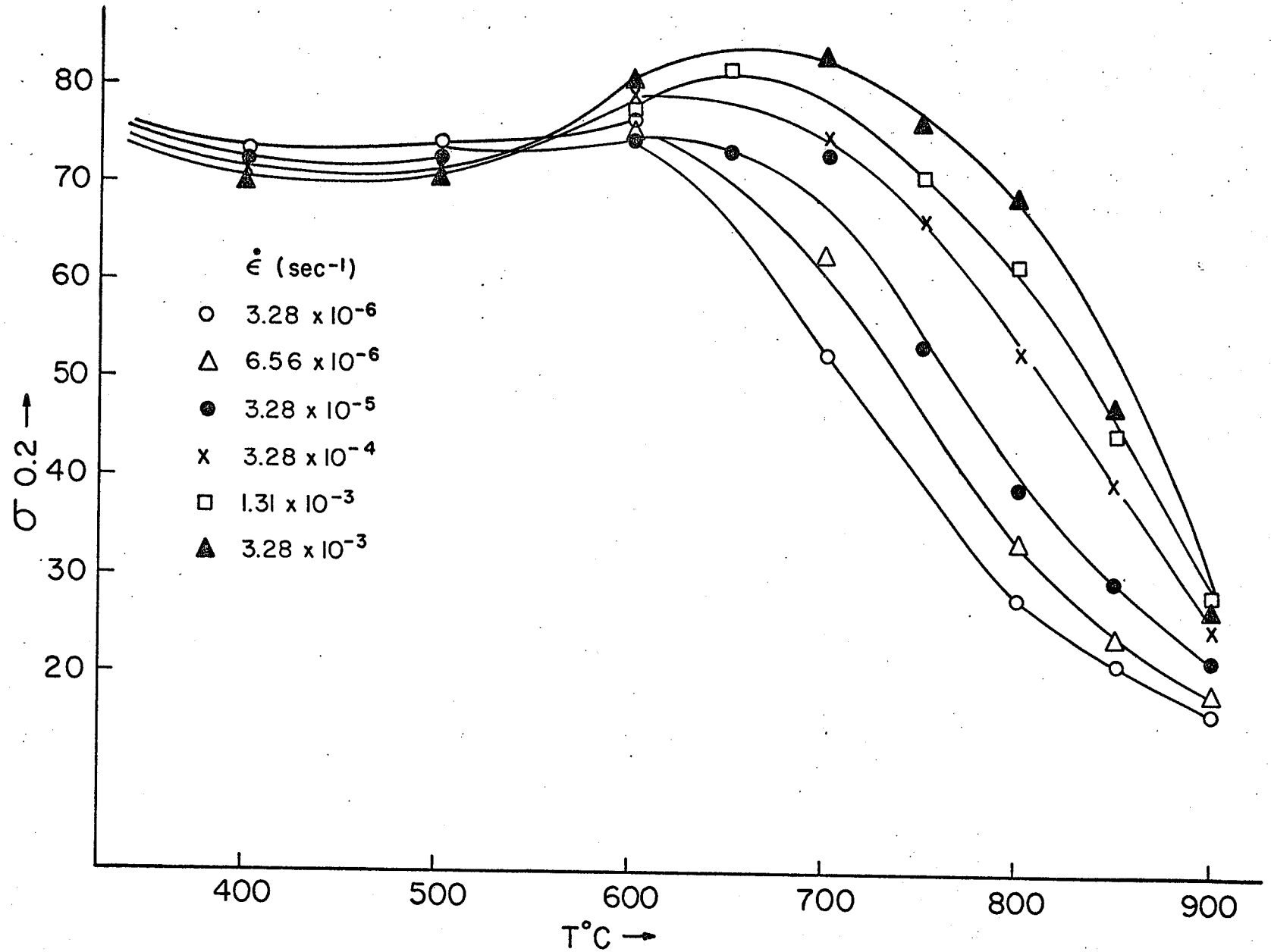
80
70
60
50
40
30
20
σ 0.2 →
$\dot{\epsilon}$ (sec⁻¹)
3.28 x 10⁻⁶
6.56 x 10⁻⁶
3.28 x 10⁻⁵
3.28 x 10⁻⁴
1.31 x 10⁻³
3.28 x 10⁻³
400
500
600
700
800
900
T°C →

FIG. (42)

Figure (43) A plot of log ε_c against log $\dot{\varepsilon}$ for the three heat treatments in 5% Ti alloys.

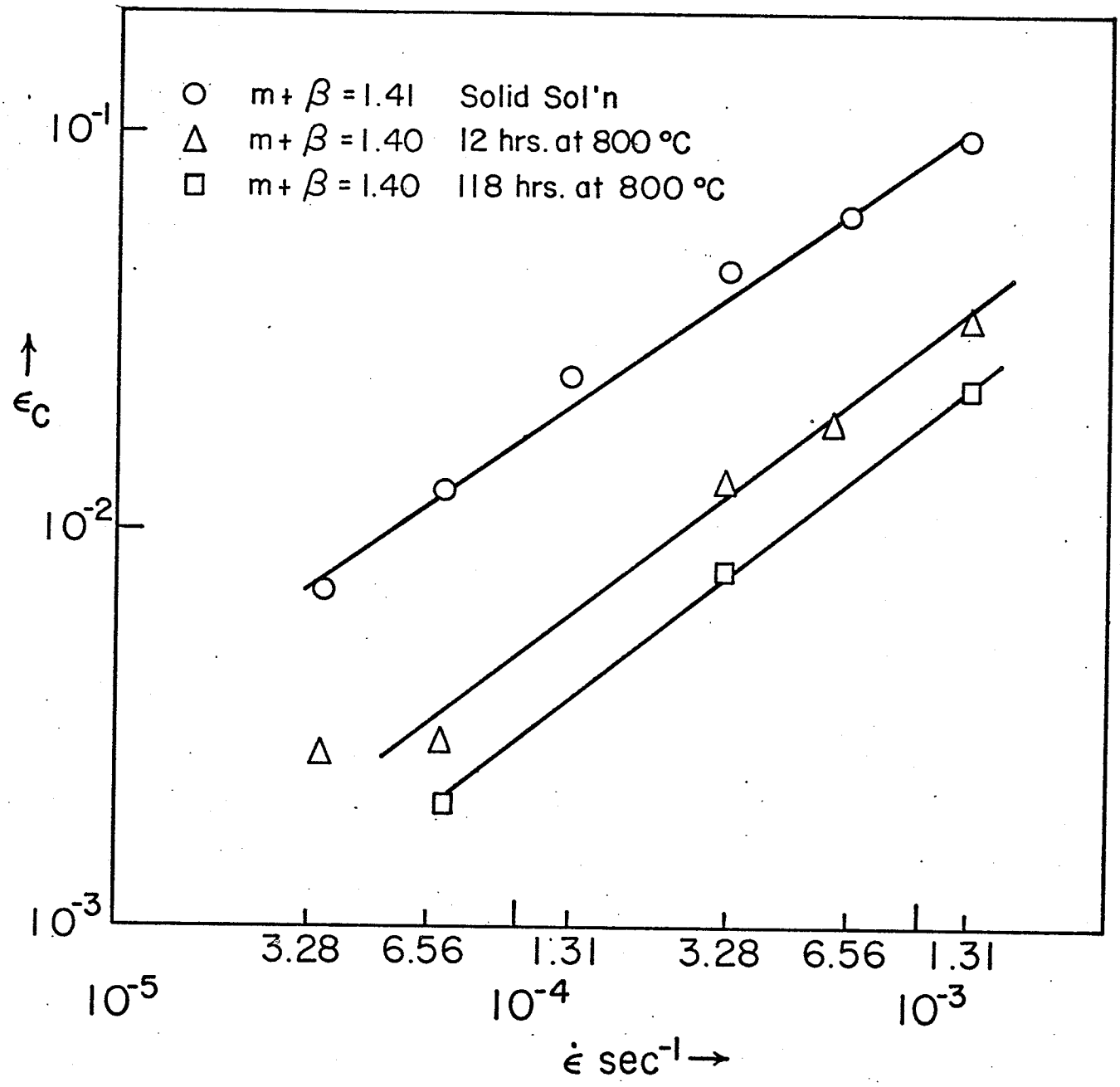
○ m+β=1.41 Solid Sol'n
△ m+β=1.40 12 hrs. at 800 °C
□ m+β=1.40 118 hrs. at 800 °C
10^{-1}
10^{-2}
10^{-3}
ϵ_c
3.28
6.56
1.31
3.28
6.56
1.31
10^{-5}
10^{-4}
10^{-3}
$\dot{\epsilon}$ sec^{-1} →

FIG. (43)

3.2.4 Determination of activation energy, Q_m.

Equation (30) and (35) show that a plot of log ε_c against 1/T for constant $\dot{\varepsilon}$, has a slope proportional to $Q_m/m+\beta$. Using a value of $m+\beta = 1.4$, the following activation energies are obtained from Fig. (41):

solid solution $Q_m = 0.59 \pm 0.05$ e.V.

12 hours at 800° C $Q_m = 0.91 \pm 0.1$ e.V.

118 hours at 800° C, $Q_m = 1.16 \pm 0.05$ e.V.

While this method of obtaining Q_m is customary in the literature, it ignores any temperature dependence of $m+\beta$ and ℓ where $\ell = U_m\, b/KT$. Any temperature dependence can be accounted for by plotting log $\dot{\varepsilon}T$ against 1/T for constant ε_c. Fig. (44) shows this relationship for some representative ε_c values. Considering an extensive range of ε_c values the following activation energies were obtained:

solid solution, $Q_m = 0.55 \pm 0.05$ e.V.

12 hours at 800° C, $Q_m = 1.47 \pm 0.15$ e.V.

118 hours at 800° C, $Q_m = 1.36 \pm 0.05$ e.V.

3.2.5 Development of m and β.

Cottrell[115] initially used the expression of Seitz[91] and Mott[92] for vacancy production

$$C_V = 10^{-4}\ \varepsilon$$

or the more general expression

$$C_V = A\ \varepsilon^m \qquad \ldots \qquad (43)$$

Figure (44) The variation of $\log \dot{\varepsilon} T$ with $1/T$.

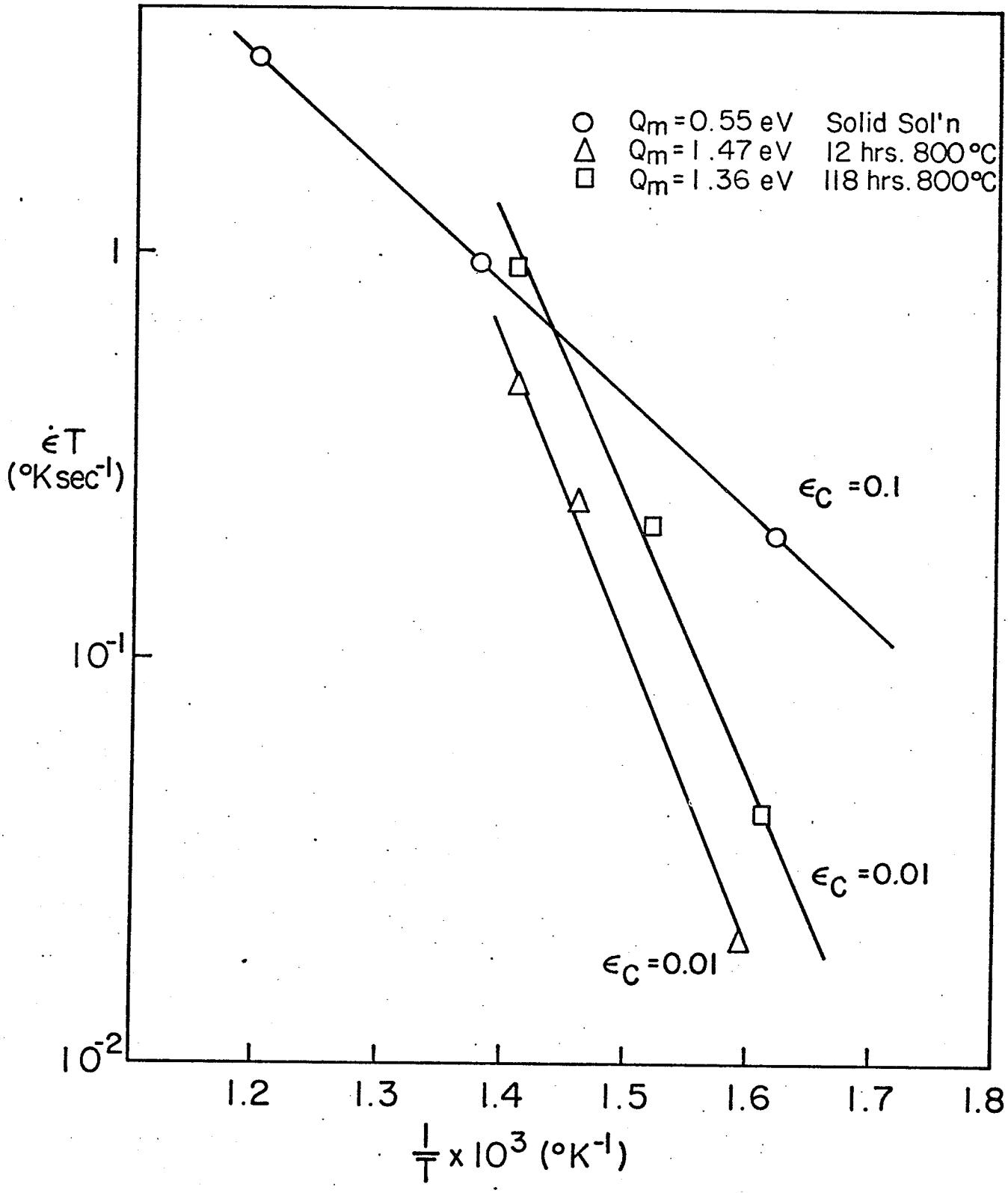
O Qm = 0.55 eV Solid Sol'n
Δ Qm = 1.47 eV 12 hrs. 800°C
□ Qm = 1.36 eV 118 hrs. 800°C
ϵC = 0.1
ϵC = 0.01
ϵC = 0.01
ϵ̇T (°K sec⁻¹)
1
10⁻¹
10⁻²
1.2
1.3
1.4
1.5
1.6
1.7
1.8
1/T x 10³ (°K⁻¹)

FIG. (44)

Van Bueren[78] has proposed a moving jog mechanism with m = 2 for multiple slip. An alternative mechanism is that due to Saada[96]. This model, which is based on the recombination of dislocations, predicts a vacancy concentration proportional to the strain energy

$$C_V = A_1 \int_o^\varepsilon \sigma \, d\varepsilon. \qquad .... \qquad (44)$$

As pointed out by Wijler et.al.[116], if the stress-strain curve is represented by

$$\sigma = A_2 \, \varepsilon^n \qquad .... \qquad (44a)$$

where σ is the true stress, ε is the true strain, and A_2 and n are constants, substitution of (44a) in (44) and integrating gives

$$C_V = B_1 \, \varepsilon^{n+1} \qquad .... \qquad (45)$$

From a comparison (43) and (45) we obtain

$$m = n + 1. \qquad .... \qquad (46)$$

However, experimental results of Basinski and Saimoto[117] on single crystals of Cu, and by Tseng[118] on polycrystalline Cu, indicate that vacancy accumulation is more rapid than Saada's theory predicts. They suggest the expression:

$$C_V = B_2 \int_o^\varepsilon \sigma^2 \, d\varepsilon. \qquad .... \qquad (47)$$

Using (44) one then obtains:

$$C_V = B_3 \, \varepsilon^{2n+1} \qquad .... \qquad (48)$$

and

$$m = 2n + 1 \qquad \ldots . \qquad (49)$$

From $\log \sigma$ - $\log \varepsilon$ plots at 400° C and considering only the smooth portion of the curves the work hardening exponent n, was constant at 0.36 ± 0.02 ie. $\sigma = A_2 \varepsilon^{0.36}$. Thus, from equation (46) $m = 1.36$ and from (49) $m = 1.72$. Fig. (43) gives values of $m+\beta = 1.4$ i.e. $m \leq 1.4$. Hence the Saada expression for the strain dependence of vacancy concentration gives the only reasonable value for m. Ham and Jaffrey[85] also introduced the concept that the mobile dislocation density was strain dependent via equation (29). The above considerations suggest that $\beta \simeq 0$ and that in the present alloy the mobile dislocation density is independent of strain.

3.2.6 The value of L.

In the static strain ageing expression (35) the value of the effective obstacle spacing, L, is critical. It has been assumed that L is independent of strain as has been shown to be the case in the Cu - Sn system[107]. Evidence was found to support this assumption in the present work, in that the flow stress increase on making a strain rate change, in the smooth region of the stress-strain curve, was constant. Fig. (45) shows the variation of $\Delta\sigma$ with ε for a strain rate change from 3.28×10^{-4}/sec to 1.3×10^{-3}/sec.

If dislocations were the major obstacles L would be strain dependent and $\Delta\sigma$ would increase with strain in a manner typified by

Figure (45) The stress increment ($\Delta\sigma$) for a strain rate change from $\dot{\varepsilon}_1$ to $\dot{\varepsilon}_2$ against plastic strain (ε_p).

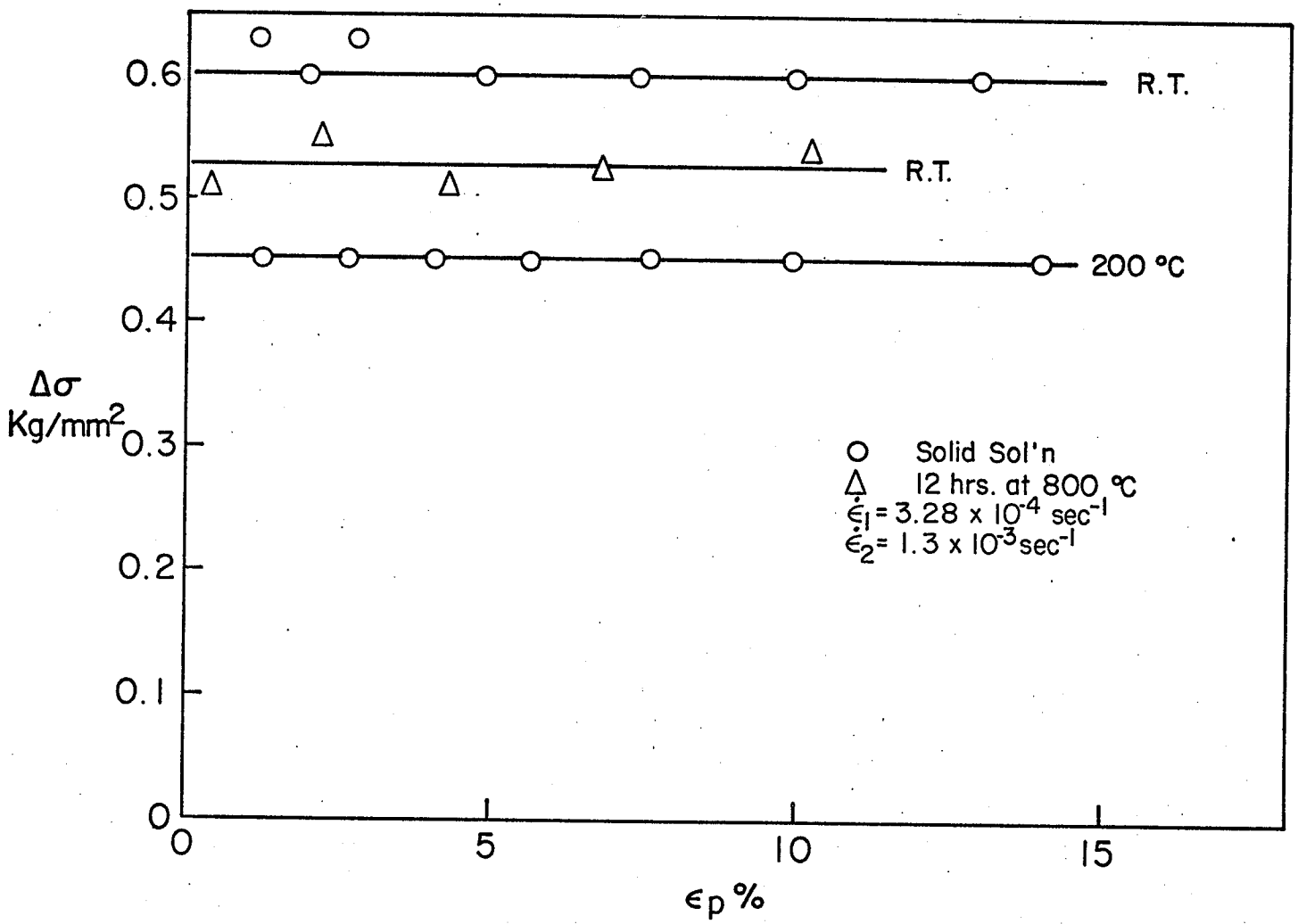
0.6
0.5
0.4
0.3
0.2
0.1
0
Δσ
Kg/mm²
0
5
10
15
εp %
R.T.
R.T.
200 °C
Solid Sol'n
12 hrs. at 800 °C
ε̇1 = 3.28 x 10⁻⁴ sec⁻¹
ε̇2 = 1.3 x 10⁻³ sec⁻¹

FIG. (45)

f.c.c. systems obeying the Cottrell - Stokes law. Since this is not the case in the present experiments the major obstacles are solute atoms or precipitate particles.

In the solid solution alloy atoms of Co, Ni and Cr, all with very similar atomic radii (1.252 Å, 1.244 Å and 1.267 Å respectively) are present together with Ti which has the much larger radius of 1.467 Å. Hence, dislocations are more likely to interact with Ti atoms than atoms of the other elements. Thus, following solution hardening theory one would have $L \sim C^{-1/2}$, where C is the concentration of Ti. This is almost certainly incorrect, since it suggests that the dislocations interact with individual solute atoms. The recent experiments of Basinski et. al.[119], indicate that the unit activation process involves the interaction between a dislocation and many solute atoms, implying an effective line length between obstacles much greater than the average distance between solute atoms. As a result there is unfortunately, no single relationship between the obstacles spacing and the solute concentration.

In the case of the aged alloys the major obstacles are expected to be the precipitate particles of γ'. There is some dispute as to the value of the obstacles spacing in precipitation hardening theory as discussed by Hilliard[120] and Kelley[121]. In the present investigation the suggestion of Brown and Ham[12] is followed. According to them, for particles undergoing Orowan looping, the obstacles spacing is given by;

$$L = \left[\left(\frac{\pi}{f_v}\right)^{1/2} - 2\right] r_s$$

where f_v is the volume fraction and $r_s = (\frac{2}{3})^{1/2} r$, r being the particle radius. In the present alloys the precipitate particles are cuboid and r is taken as equal to $\frac{d}{2}$ where d is the projected particle length on (111) planes. After 12 hours at 800° C the volume fraction of particle is 14.10% and $d/2 = r = 86.5$ Å. The volume fraction does not change with subsequent ageing, but after 118 hours at 800° C the particles have grown to $d/2 = r = 207.4$ Å. The resulting values of L from (35) are $L(12 \text{ hrs}) = 206.4$ Å and $L(118 \text{ hrs}) = 494.9$ Å. From (35) it is seen that, other factors remaining constant there should be a corresponding decrease in ε_c, and one can obtain

$$\left(\frac{\varepsilon_{12}}{\varepsilon_{118}}\right)^{m+\beta} = \frac{L_{118}}{L_{12}} = 2.4 \qquad \ldots \qquad (50)$$

where the subscript refer to the ageing treatment. Figure (46) is a plot of $(\varepsilon_{12})^{1.4}$ against $(\varepsilon_{118})^{1.4}$ and the resulting gradient is 1.5, i.e.

$$\left(\frac{L_{118}}{L_{12}}\right)_{exp.} = 1.5$$

Considering the assumptions involved in calculating L, such as uniform particle size, regular square array, etc. the agreement between the theory and experiment is quite reasonable.

3.2.7 Effect of C_o and L on ε_c, $m+\beta$, and Q_{in} value.

If dislocation network are the main obstacles to dislocation motion, L will be strain dependent. However, if solute atoms are the major barriers L will be independent of strain but dependent on solute

Figure (46) A plot of critical strain to serrations for 5% Ti alloy specimens aged 12 hours (ε_{12}) against the critical strain for specimens aged 118 hours (ε_{118}).

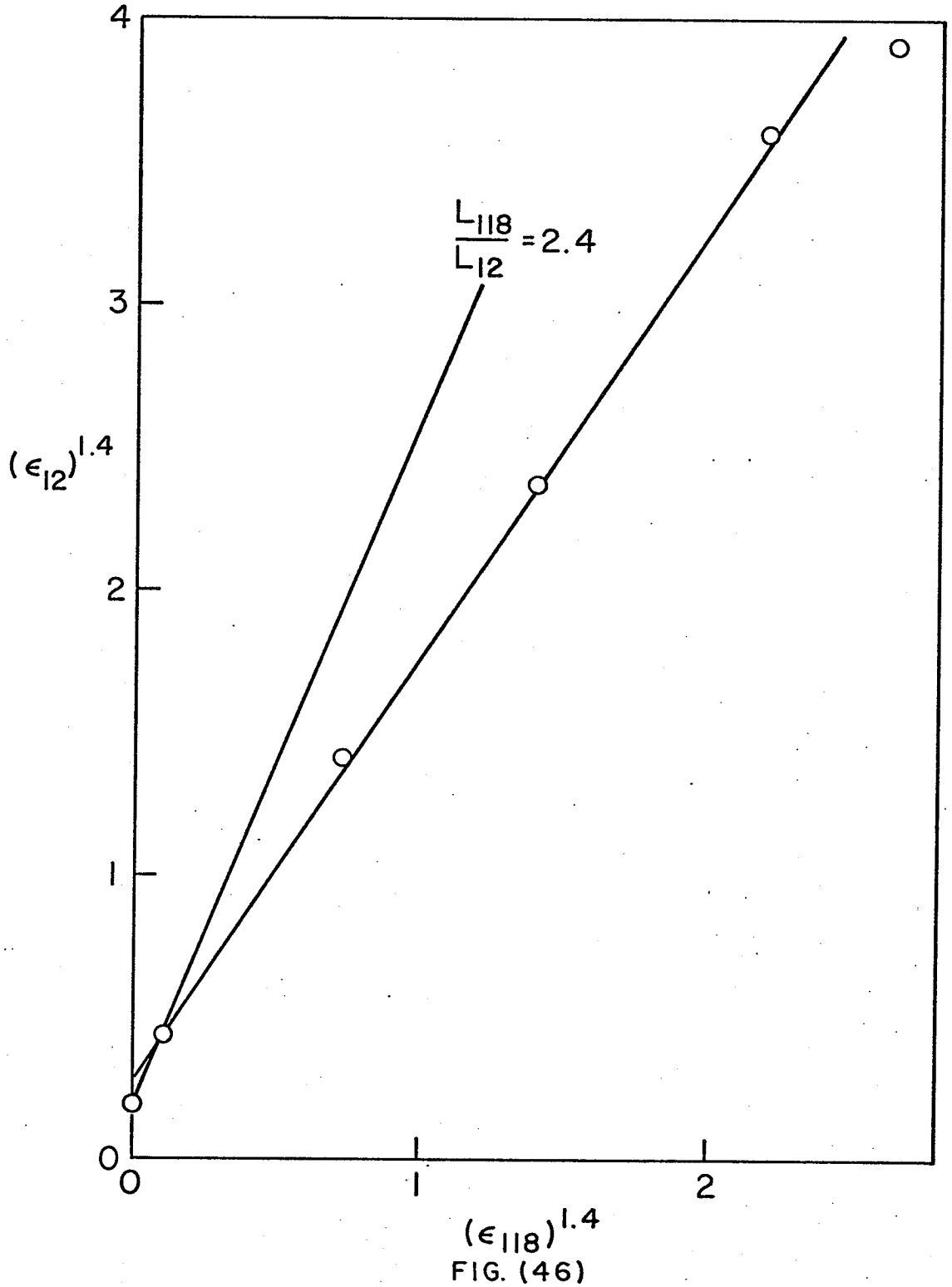

FIG. (46)

concentration, i.e. $L \propto C_o^{\alpha_1}$, where α_1 is a constant $\simeq -\frac{1}{2}$ in many solution hardening theories. Assuming that the mobile dislocation density, activation energy, etc., are independent of solute concentration, equation (35) yields

$$\varepsilon^{(m+\beta)} \propto C_o^{(\alpha_1 - 3/2)} \quad \ldots\ldots \quad (51)$$

Alternatively if particles are the major barriers L should be related to the interparticle spacing of the precipitate, $\bar{L}$, i.e. again assuming ρ_m, Q_m etc. independent of ageing time

$$\varepsilon^{(m+\beta)} \propto \frac{1}{L} \propto \frac{1}{\bar{L}} \quad \ldots\ldots \quad (52)$$

It, thus, follows from the above treatments that, if the solute atoms are main obstacles for the onset of serrated yielding, then:

$$\varepsilon^{m+\beta} = A_s C_o^{(\alpha_1 - 3/2)} \dot{\varepsilon} T \exp\left(\frac{Q_m}{\kappa T}\right) \quad \ldots\ldots \quad (53)$$

and if the precipitate particles are the main barriers, then

$$\varepsilon^{m+\beta} = A_p \frac{\dot{\varepsilon} T}{\bar{L}} \exp\left(\frac{Q_m}{\kappa T}\right) \quad \ldots\ldots \quad (54)$$

where A_s and A_p are constant for the solution treated and aged conditions respectively.

The effect of the barriers in terms of static strain ageing model can therefore be checked via the above equations and by varying the solute content and particle spacing in a series of similar alloys. Therefore, serrated yielding was also examined in 4.0% and 6.0% Ti alloys.

From equation (35), a plot of log ε_c against log $\dot{\varepsilon}$ at constant temperature should be linear with a gradient of $m+\beta$. Fig. (47) shows that a linear relationship is obtained at 400° C, in the solution treated condition, with $(m+\beta) = 1.41$.

Similar results were obtained at 300° C and 500° C with $m+\beta = 1.4$ and therefore $m+\beta$ is independent of temperature and solute content. It should be noted, however, that $\varepsilon_{\dot{c}}$ is dependent on temperature and solute content.

Fig. (48) shows similar plots for the aged alloys and again the relationship is linear with $(m+\beta) = 1.4$. Hence, $(m+\beta)$ is also independent of particle spacing. These results are in agreement with the previous results presented in section (3.2.3).

From equation (35) a plot of log ε_c against 1/T will provide a value for the activation energy for serrated yielding. Figures (41) and (49) (a) and (b) are plots for the three alloys. Using $m+\beta = 1.4$ the activation energies given in Table (4) are obtained. However, using the plots in Figures (41) and (49) (a) and (b) to obtain Q_m assumes $(m+\beta)$ and $\ell = U_m\, b/KT$ are independent of temperature. Experimentally it is observed that $(m+\beta)$ is temperature independent and any temperature dependence of ℓ can be accounted for by plotting log $\varepsilon^{(m+\beta)}/T$ against 1/T. Using $(m+\beta) = 1.4$, these plots are given in Figures (50) (a), (b) and (c) and the resulting Q_m values in Table (4). The second estimates for the activation energy in terms of C_o and $\bar{L}$ have also been considered, as shown in Figures (51) and (52), respectively, both approaches give a similar result in the present alloys.

Figure (47) A plots of log ε_c against log $\dot{\varepsilon}$ for the solution treated 4%, 5% and 6% Ti alloys.

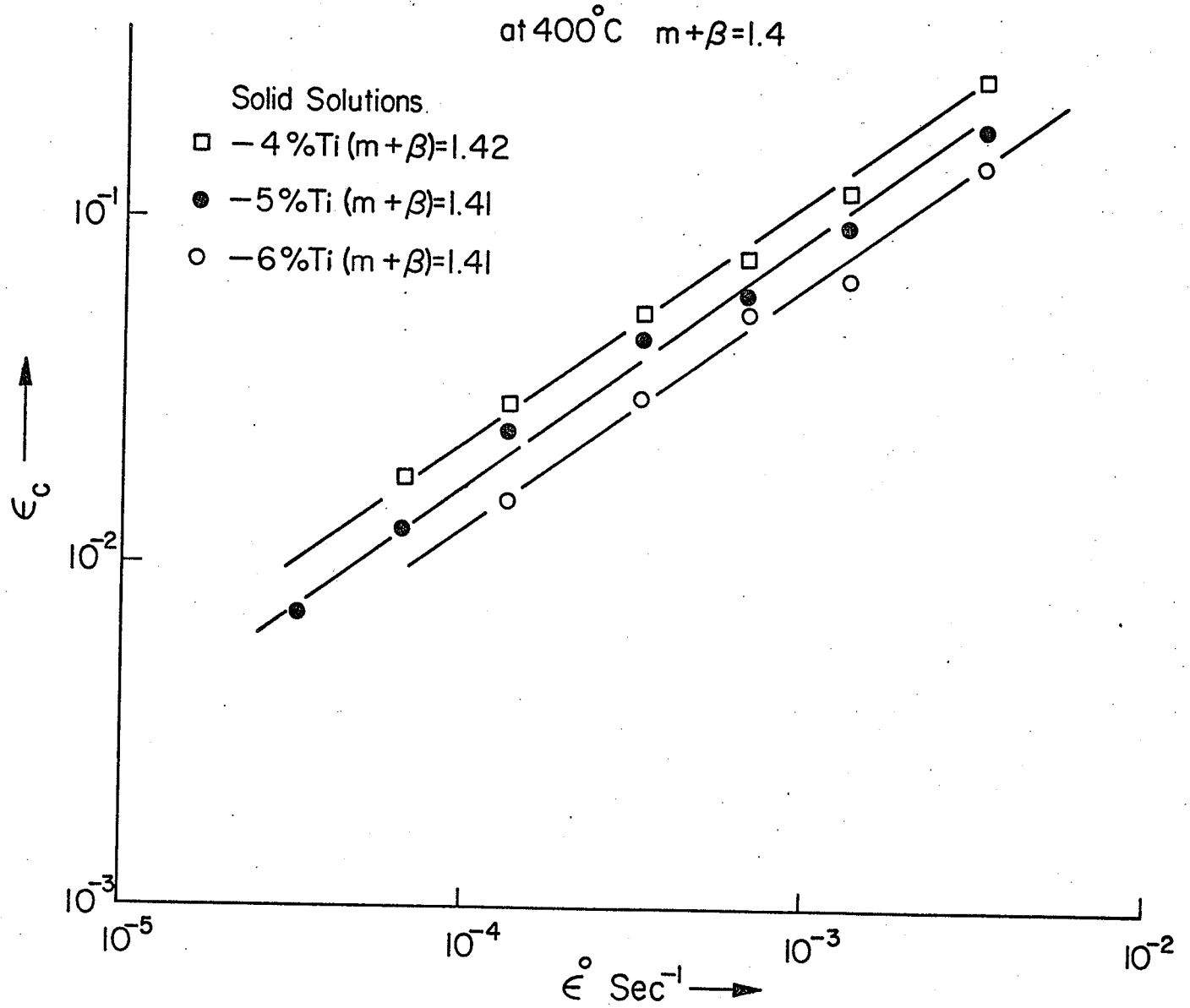
at 400°C m+β=1.4
Solid Solutions
□ −4%Ti (m+β)=1.42
● −5%Ti (m+β)=1.41
○ −6%Ti (m+β)=1.41
ϵ_c
10^{-1}
10^{-2}
10^{-3}
10^{-5}
10^{-4}
10^{-3}
10^{-2}
$\dot{\epsilon}$ Sec^{-1}

FIG. (47)

Figure (48) Plots of log ε_c against log $\dot{\varepsilon}$ for various alloys aged at 800° C and serrated at 400° C.

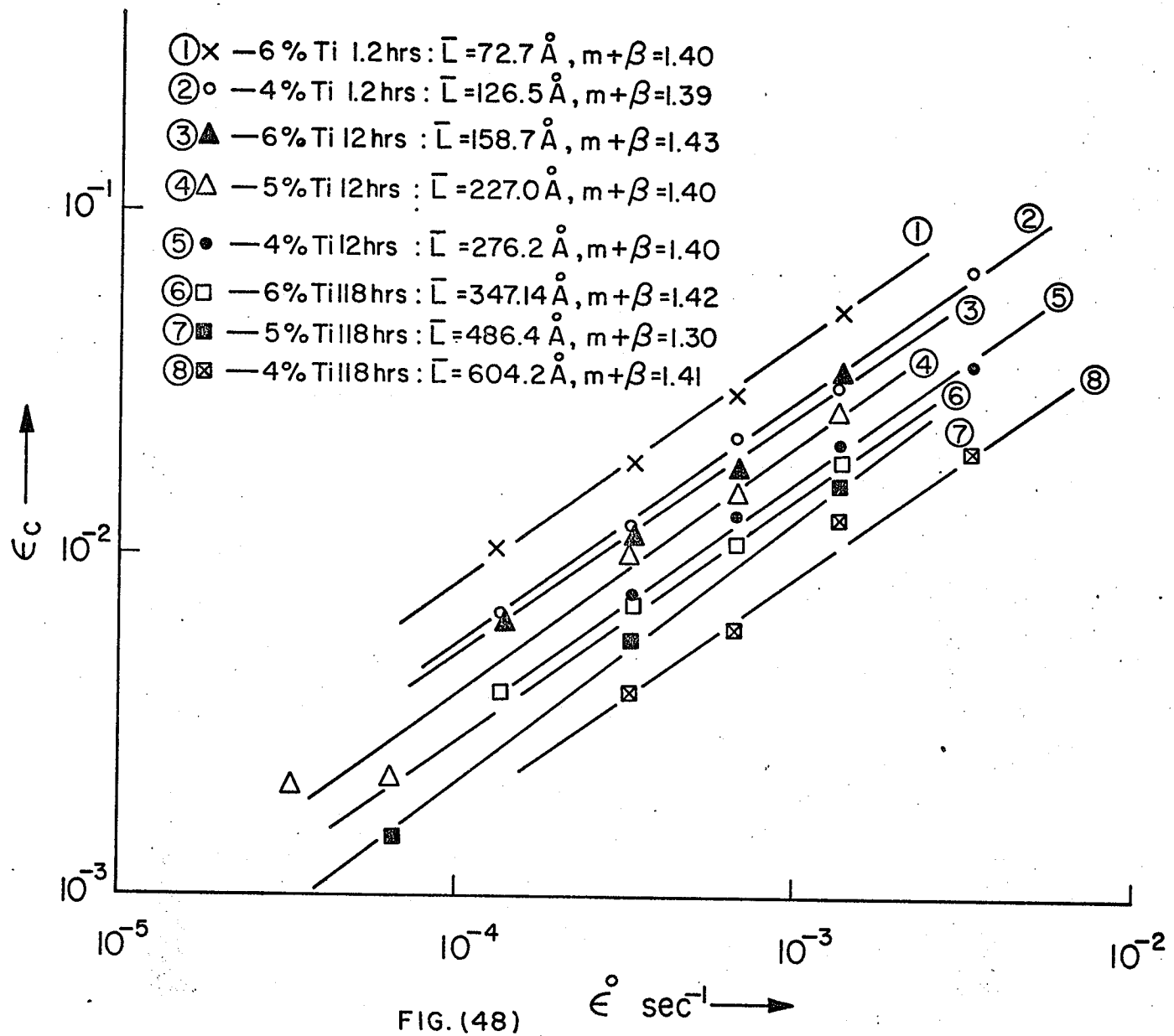
①× —6% Ti 1.2hrs : $\bar{L}$ =72.7 Å , m+β=1.40
②○ —4% Ti 1.2hrs : $\bar{L}$ =126.5 Å, m+β=1.39
③▲ —6% Ti 12hrs : $\bar{L}$ =158.7 Å , m+β=1.43
④△ —5% Ti 12hrs : $\bar{L}$ =227.0 Å, m+β=1.40
⑤● —4% Ti 12hrs : $\bar{L}$ =276.2 Å, m+β=1.40
⑥□ —6% Ti 118hrs : $\bar{L}$ =347.14 Å, m+β=1.42
⑦■ —5% Ti 118hrs : $\bar{L}$ =486.4 Å, m+β=1.30
⑧⊠ —4% Ti 118hrs : $\bar{L}$ = 604.2 Å, m+β=1.41
ϵ_c
10^{-1}
10^{-2}
10^{-3}
10^{-5}
10^{-4}
10^{-3}
10^{-2}
$\dot{\epsilon}$ sec^{-1}

FIG. (48)

Figure (49)(a) Plots of log ε_c against 1/T for the various heat treatments in 4% Ti alloys.

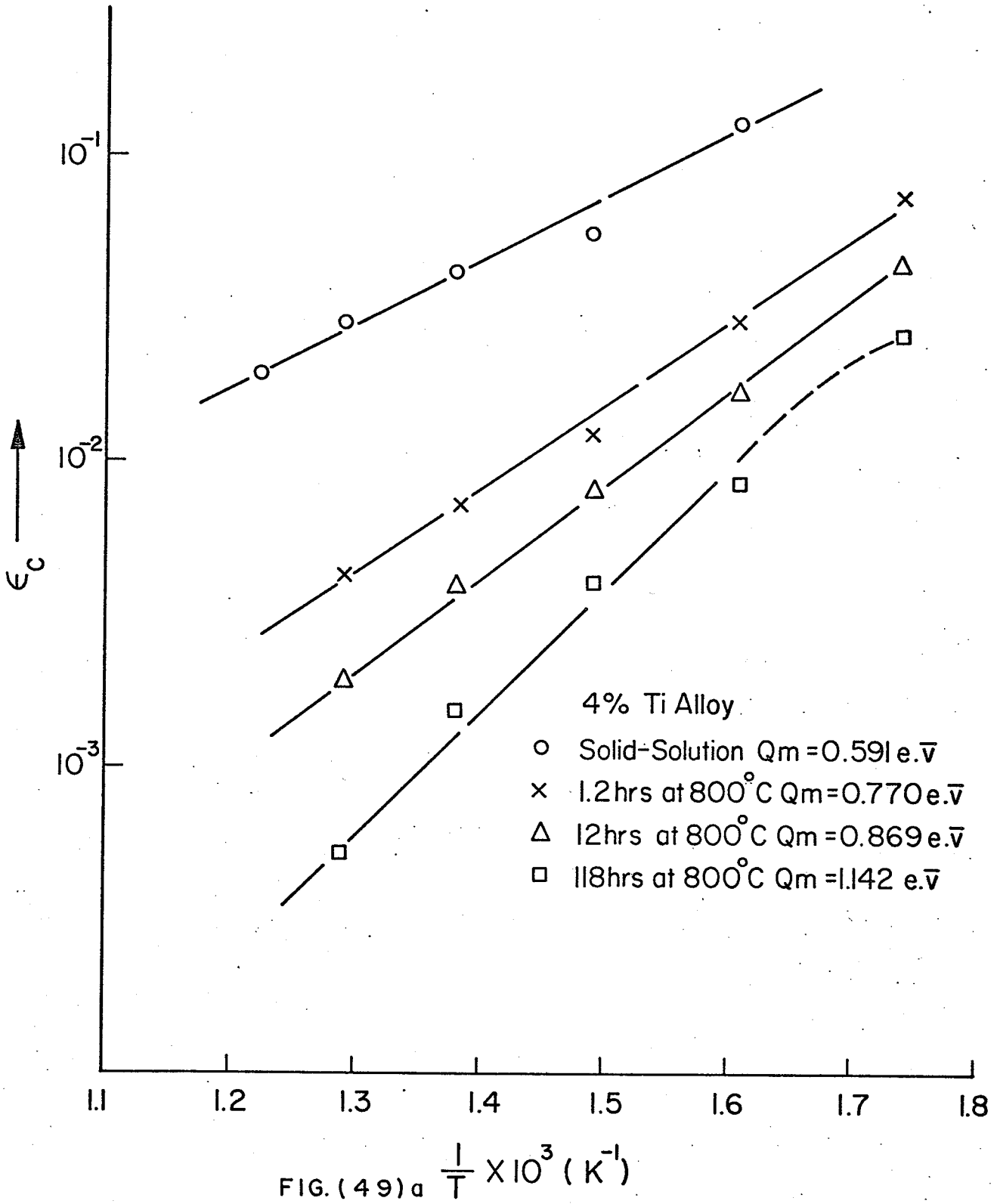
10^{-1}
10^{-2}
10^{-3}
ϵ_c
1.1
1.2
1.3
1.4
1.5
1.6
1.7
1.8
$\frac{1}{T} \times 10^3 (K^{-1})$
4% Ti Alloy
Solid-Solution Qm = 0.591 e.v
1.2 hrs at 800°C Qm = 0.770 e.v
12 hrs at 800°C Qm = 0.869 e.v
118 hrs at 800°C Qm = 1.142 e.v

FIG. (49) a

Figure (49)(b) Plots of log ε_c against 1/T for the various heat treatments in 6% Ti alloys.

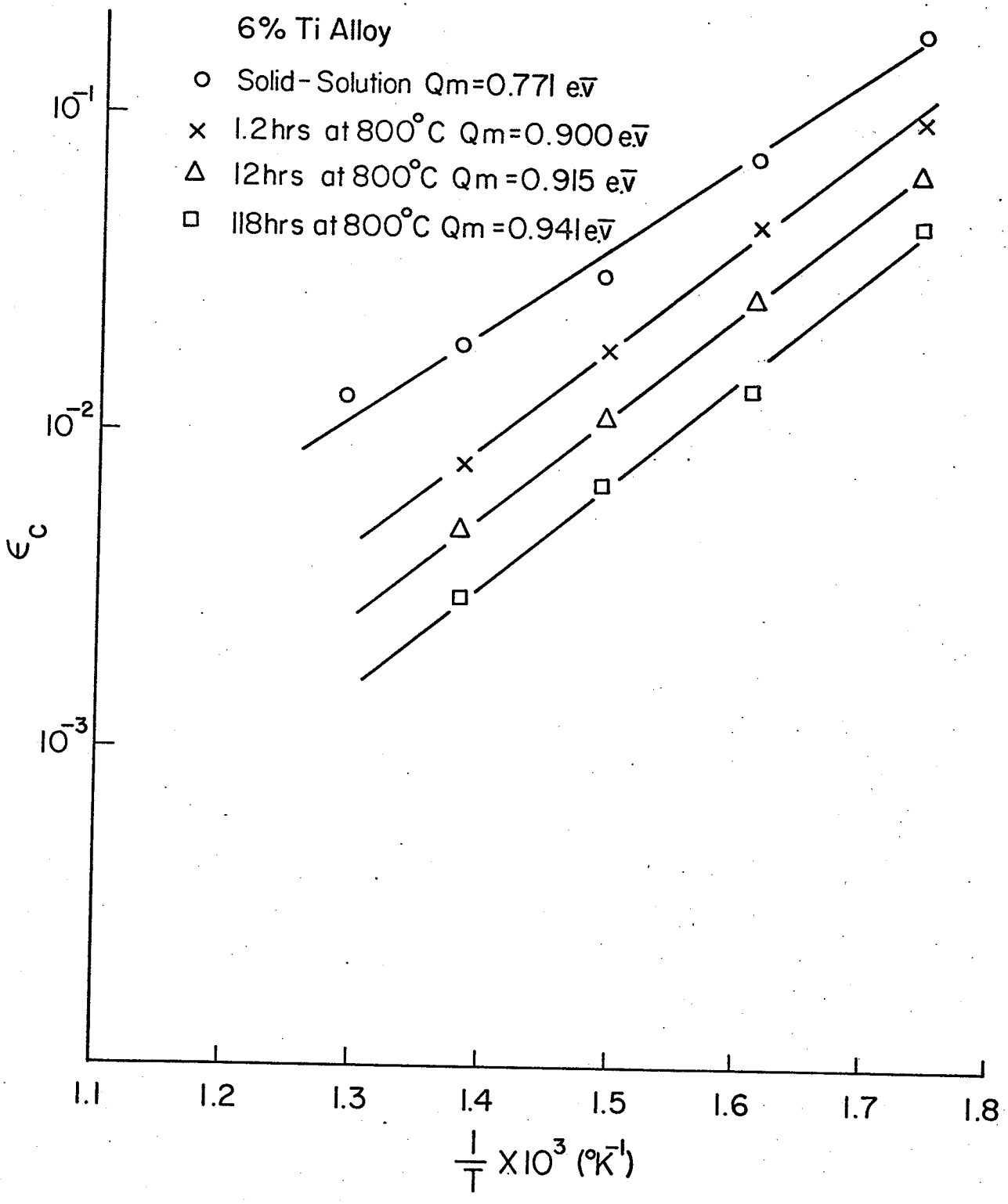
6% Ti Alloy
o Solid-Solution Qm=0.771 e.v
× 1.2hrs at 800°C Qm=0.900 e.v
Δ 12hrs at 800°C Qm=0.915 e.v
□ 118hrs at 800°C Qm=0.941 e.v
10^{-1}
10^{-2}
10^{-3}
ϵ_c
1.1
1.2
1.3
1.4
1.5
1.6
1.7
1.8
$\frac{1}{T} \times 10^3$ (°K^{-1})

FIG. (49)$_b$

Figure (50)(a) The variation of log $\varepsilon_c^{1.4}/T$ with 1/T for 4% Ti alloy.

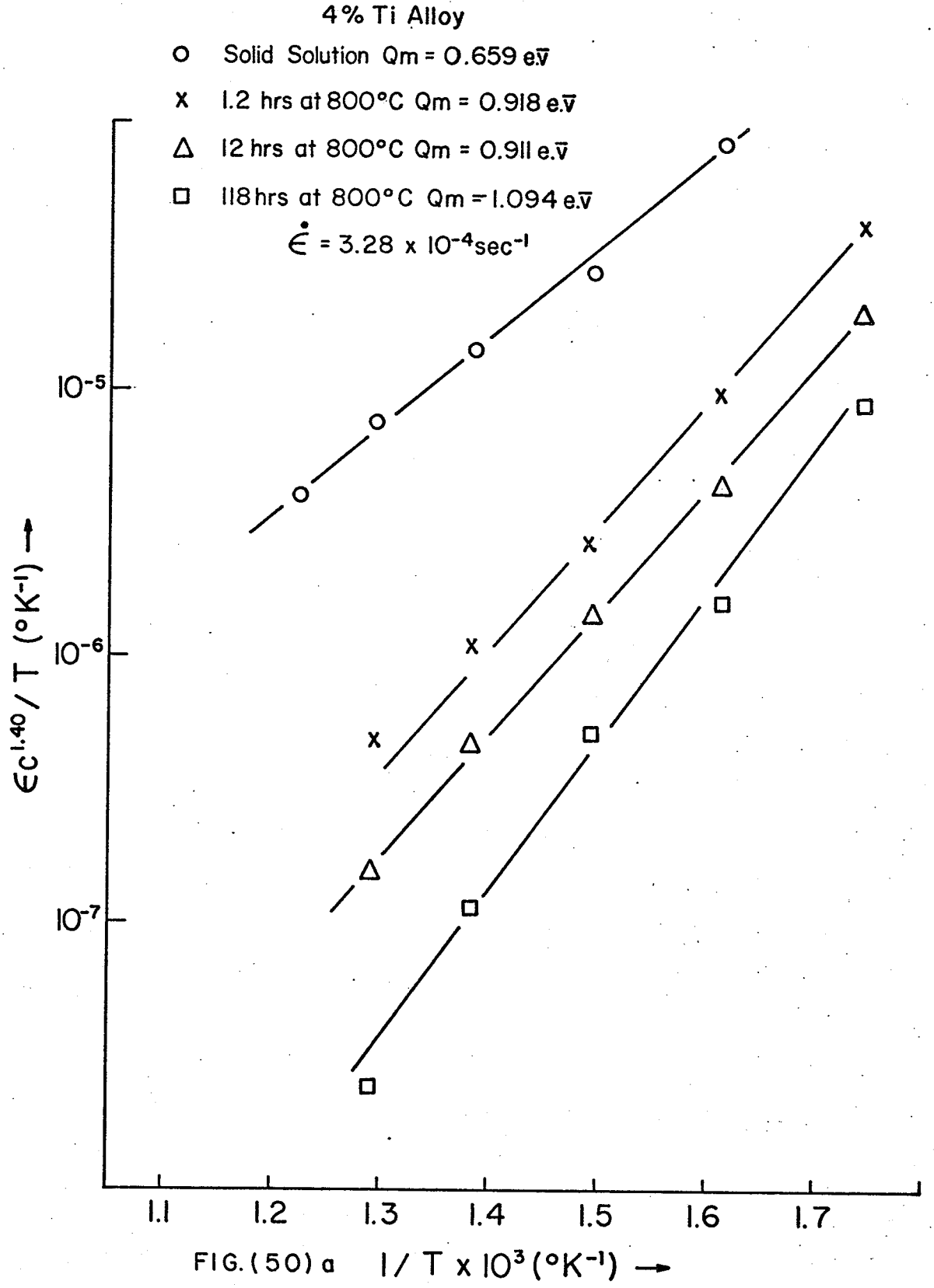
4% Ti Alloy
O Solid Solution Qm = 0.659 e.v
X 1.2 hrs at 800°C Qm = 0.918 e.v
Δ 12 hrs at 800°C Qm = 0.911 e.v
□ 118 hrs at 800°C Qm = 1.094 e.v
$\dot{\epsilon}$ = 3.28 x 10^{-4} sec^{-1}
10^{-5}
10^{-6}
10^{-7}
$\epsilon_c^{1.40} / T$ ($°K^{-1}$) →
1.1
1.2
1.3
1.4
1.5
1.6
1.7
1/ T x 10^3 ($°K^{-1}$) →

FIG. (50) a

Figure (50)(b) The variation of log $\varepsilon_c^{1.4}/T$ with 1/T for 5% Ti alloys.

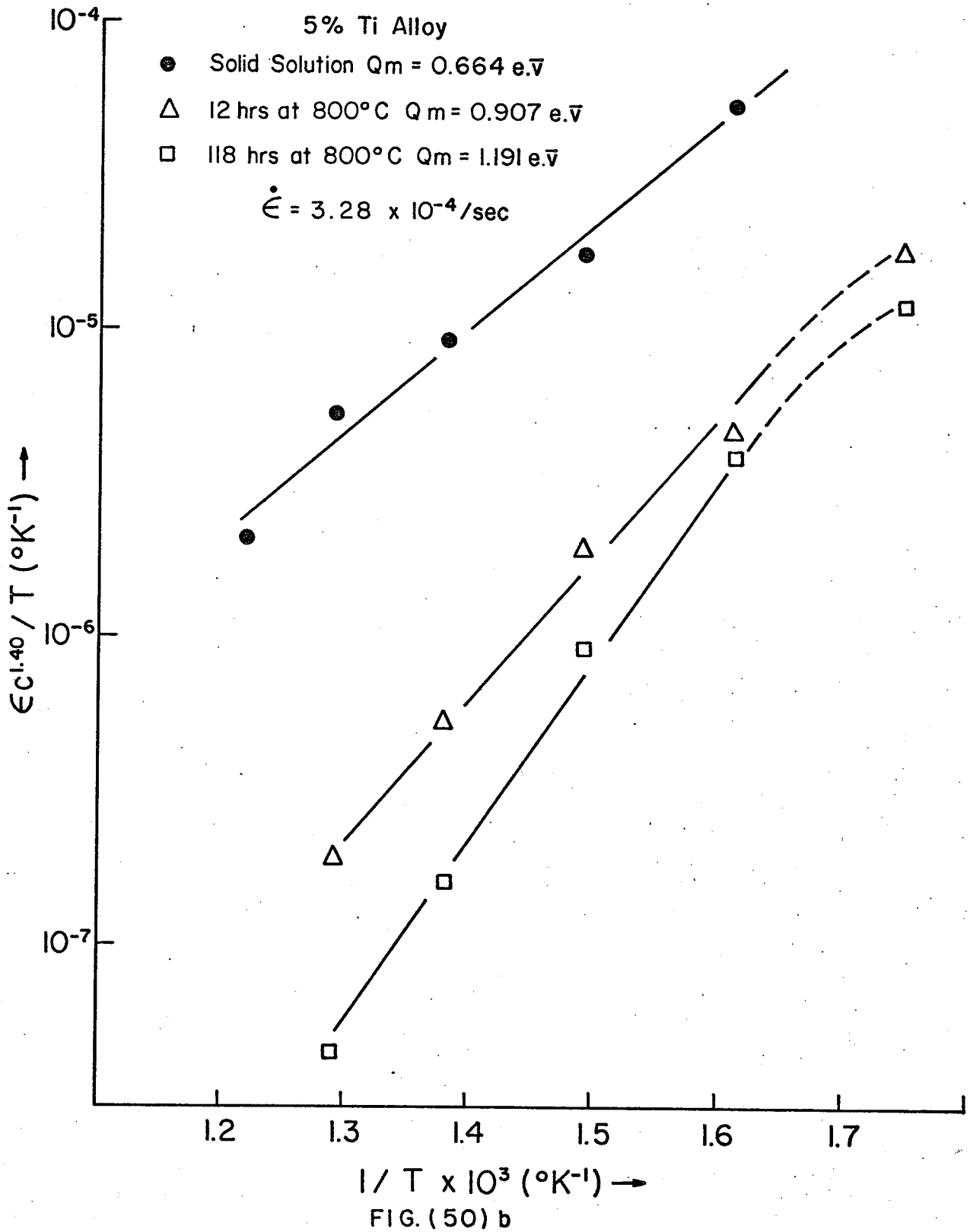
5% Ti Alloy
Solid Solution Qm = 0.664 e.v
12 hrs at 800°C Qm = 0.907 e.v
118 hrs at 800°C Qm = 1.191 e.v
$\dot{\epsilon}$ = 3.28 x 10^{-4}/sec
10^{-4}
10^{-5}
10^{-6}
10^{-7}
$\epsilon C^{1.40} / T$ ($°K^{-1}$) →
1.2
1.3
1.4
1.5
1.6
1.7
1/ T x 10^3 ($°K^{-1}$) →

FIG. (50) b

Figure (50)(c) The variation of log $\varepsilon_c^{1.4}/T$ with 1/T for 6% Ti alloy.

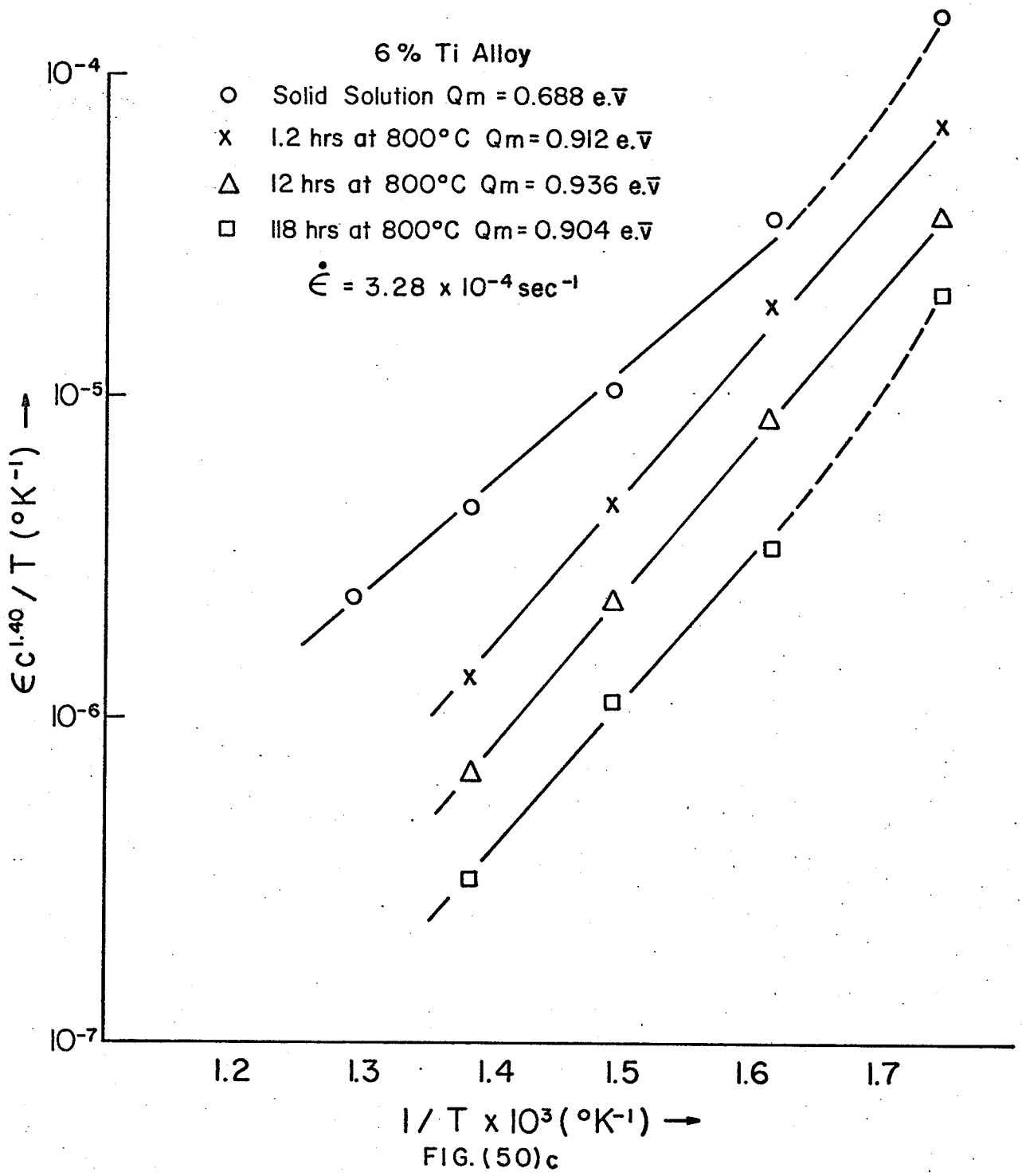
6 % Ti Alloy
O Solid Solution Qm = 0.688 e.v
X 1.2 hrs at 800°C Qm = 0.912 e.v
Δ 12 hrs at 800°C Qm = 0.936 e.v
□ 118 hrs at 800°C Qm = 0.904 e.v
$\dot{\epsilon}$ = 3.28 x 10^{-4} sec^{-1}
10^{-4}
10^{-5}
10^{-6}
10^{-7}
$\epsilon c^{1.40} / T$ ($°K^{-1}$) →
1.2
1.3
1.4
1.5
1.6
1.7
$1/T \times 10^3$ ($°K^{-1}$) →

FIG. (50)c

Figure (51) Plots of log C_o against 1/T for the various values of $\varepsilon_c{}^{1.4}/T$

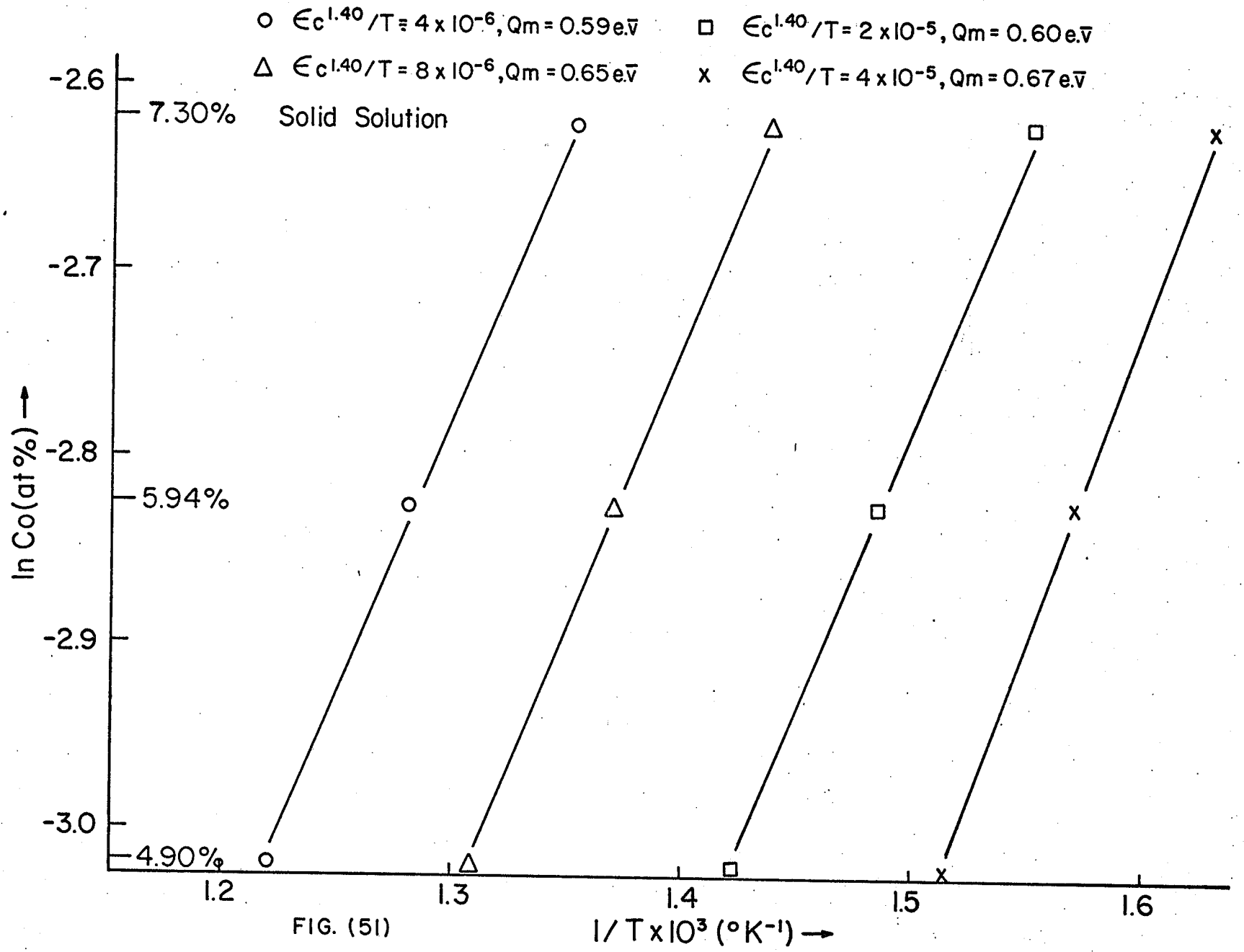
o $\epsilon c^{1.40}/T = 4 \times 10^{-6}$, Qm = 0.59 e.v
□ $\epsilon c^{1.40}/T = 2 \times 10^{-5}$, Qm = 0.60 e.v
Δ $\epsilon c^{1.40}/T = 8 \times 10^{-6}$, Qm = 0.65 e.v
x $\epsilon c^{1.40}/T = 4 \times 10^{-5}$, Qm = 0.67 e.v
Solid Solution
7.30%
5.94%
4.90%
-2.6
-2.7
-2.8
-2.9
-3.0
ln Co(at%) →
1.2
1.3
1.4
1.5
1.6
1/T x 10³ (°K⁻¹) →

FIG. (51)

Figure (52) Plots of log $\bar{L}$ against 1/T for the three values of $\varepsilon_c^{1.4}/T$.

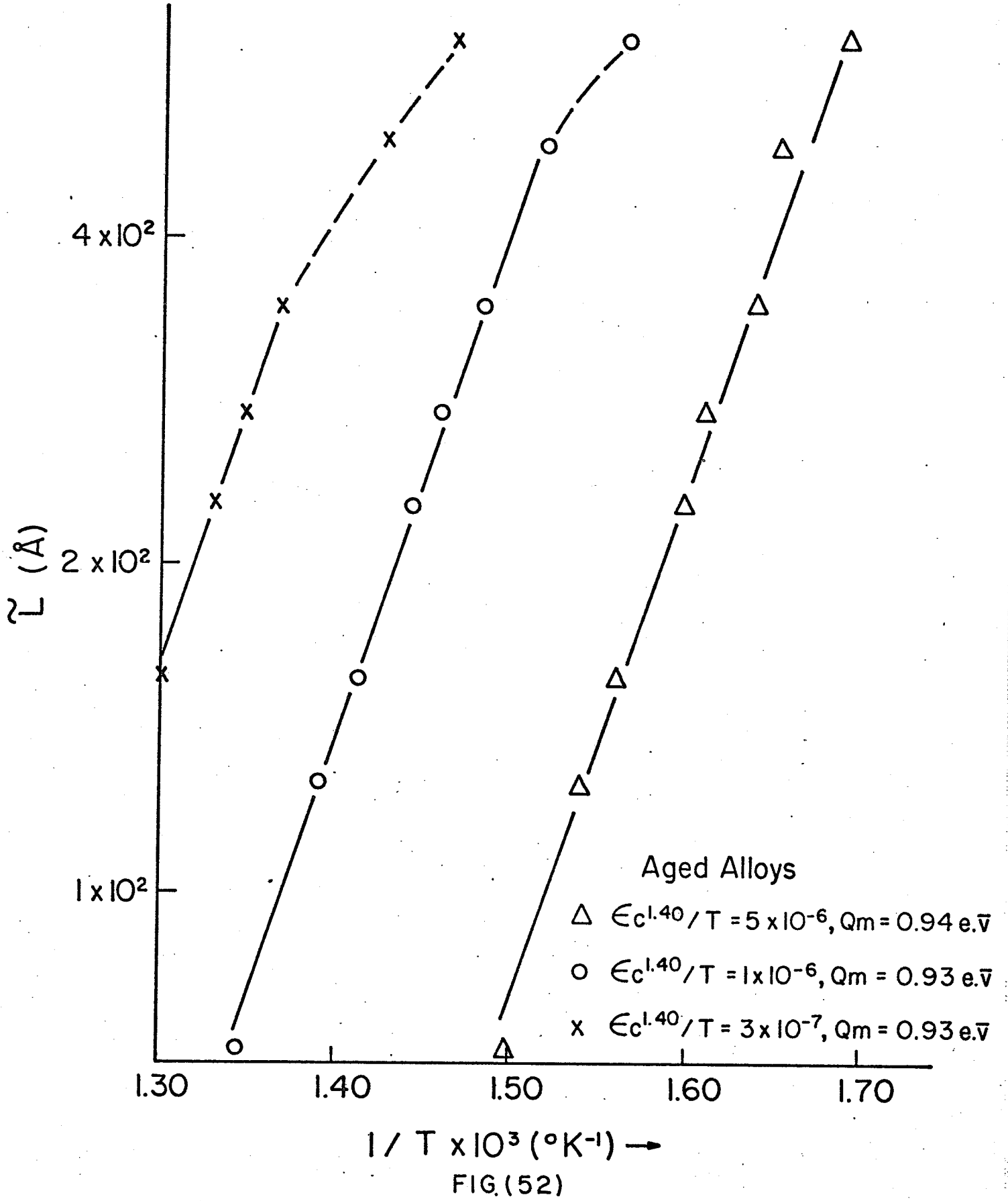
4 x 10²
2 x 10²
1 x 10²
L (Å)
1.30
1.40
1.50
1.60
1.70
1 / T x 10³ (°K⁻¹) →
Aged Alloys
Δ εc^1.40 / T = 5 x 10⁻⁶, Qm = 0.94 e.v
o εc^1.40 / T = 1 x 10⁻⁶, Qm = 0.93 e.v
x εc^1.40 / T = 3 x 10⁻⁷, Qm = 0.93 e.v

FIG. (52)

Table 4

Activation Energy for the onset of serration at various heat treatment conditions and alloying compositions.

Composition of Ti (wt%)	Heat treatment	r_s (Å)	Volume fraction of γ' (f_v)	Q_m (e.V)	Q_m' (e.V)
4	solid-solution	-----	-----	0.591	0.659
5	solid-solution	-----	-----	0.596	0.664
6	solid-solution	-----	-----	0.771	0.688
4	1.5 hrs at 800°C	35.9	0.103	0.770	0.918
4	12 hrs at 800°C	78.4	0.103	0.869	0.911
4	118 hrs at 800°C	171.5	0.103	1.142	1.094
5	12 hrs at 800°C	78.4	0.141	0.913	0.907
5	118 hrs at 800°C	171.5	0.141	1.159	1.191
6	1.5 hrs at 800°C	35.9	0.194	0.899	0.912
6	12 hrs at 800°C	78.4	0.194	0.915	0.936
6	118 hrs at 800°C	171.5	0.194	0.941	0.904

3.2.8 Electron microscopy.

Transmission electron microscopy revealed that slip was predominantly restricted to the primary slip plane with little evidence of cross-slip. This was the case regardless of the test temperature in the range 23° to 600° C or the ageing treatment. Fig. (23) shows the dislocation structure of a solid solution specimen strained 3.5% at room temperature.

The specimen with 1.5 hours ageing at 800° C shows super dislocation after deformation at room temperature, but single dislocation arrangement at 300° C and 500° C as shown in Figures (53) and (54) respectively.

Figure (53) Dislocation structure of 4% Ti alloy aged 1.5 hours at 800° C and strained 4% at 300° C.

Figure (54) The dislocation structure of 4% Ti alloy aged 1.5 hours at 800° C and deformed 4% at 500° C.

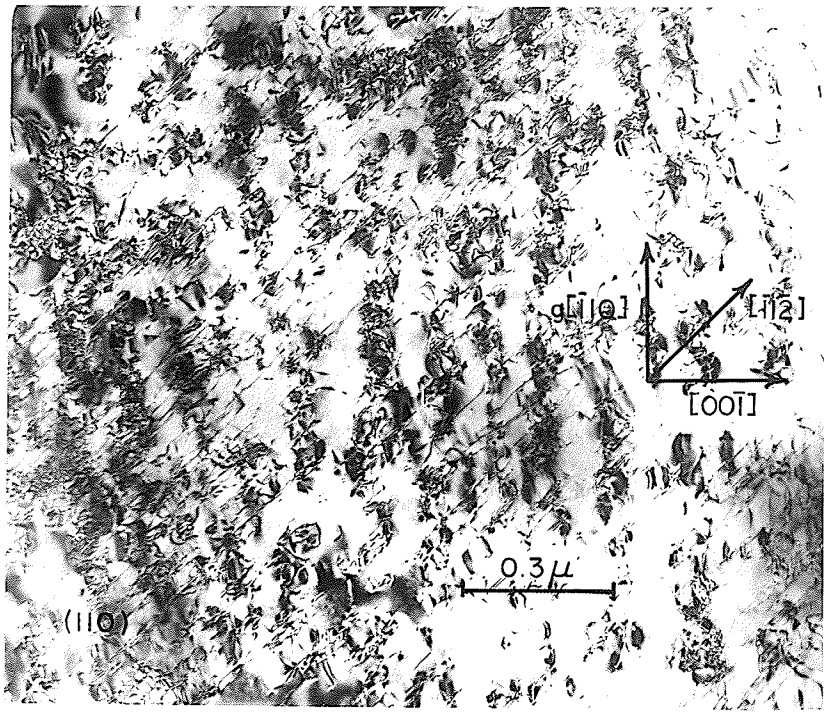

FIG. 53

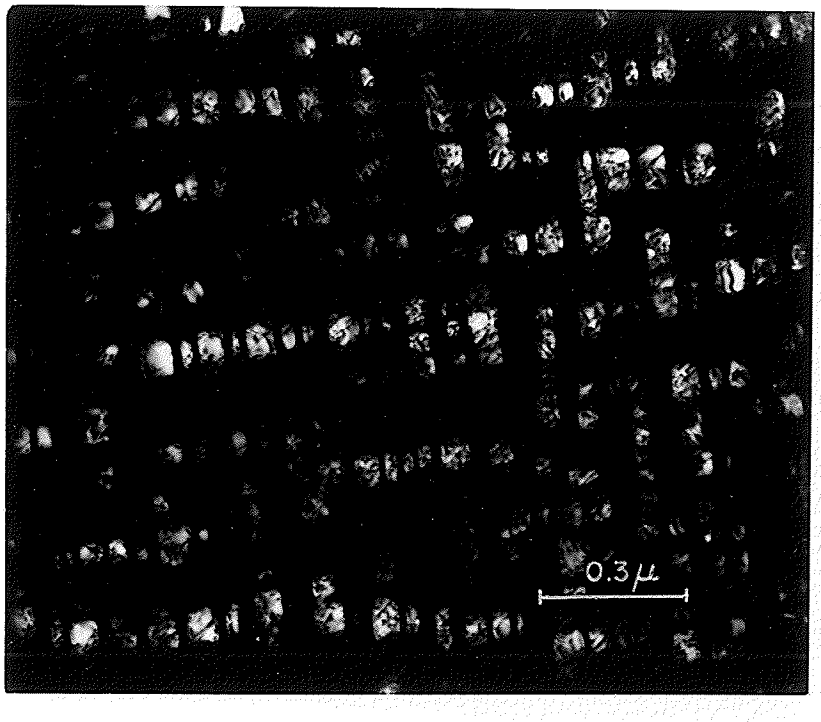

FIG. 54

Figure (28) shows the dislocation structure of a specimen aged 12 hours at 800° C and deformed 2.5% at room temperature. Note the planar slip arrays, the evidence of dislocation loop formation and the residual contrast at many particles. Figure (29) is a dark field of the same area; no evidence could be found for particle shearing at this stage. Thus, the dislocations appear to be by-passing the particle by Orowan looping.

Similar dislocation structures were observed in deformed specimens aged 118 hours at 800° C as observed in Figure (55) and (56).

Figure (55) The dislocation structure of 5% Ti alloy aged 118 hours at 800° C and strain 4% at 400° C

Figure (56) Dark field micrograph of structure shown in Figure (55), using (100) superalttice diffraction spot of γ'.

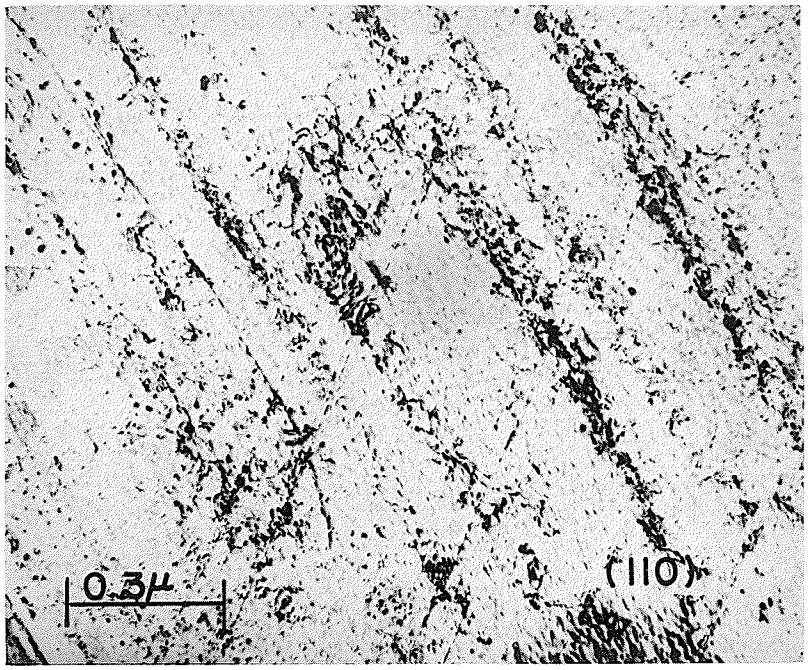

FIG. 55

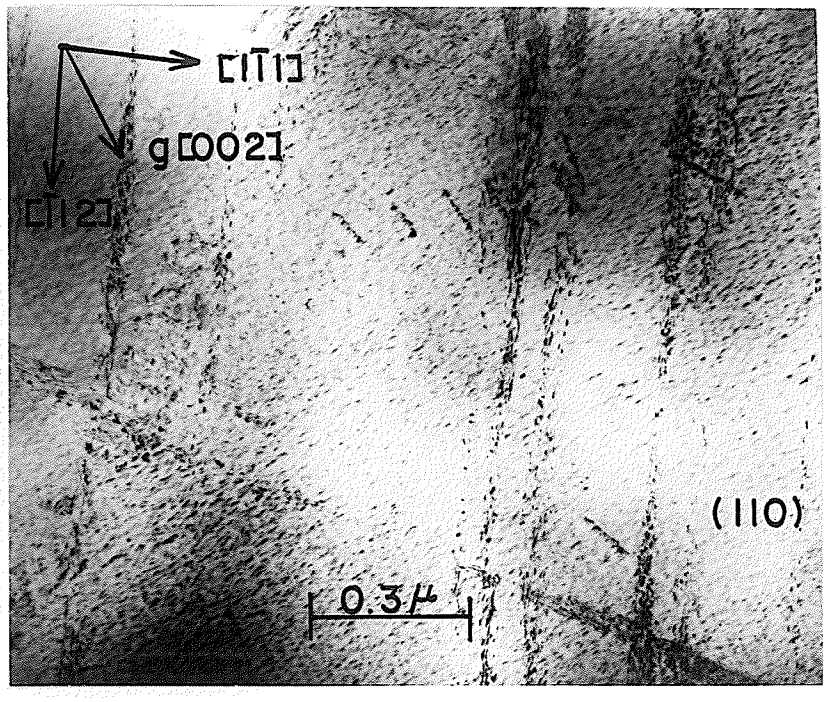

FIG. 56

V. DISCUSSION

The results obtained during the course of this investigation have shown that cobalt, nickel, chromium superalloys containing Ti are precipitation strengthened by γ'. The dislocation-precipitate interaction at the onset of yielding depends upon the particle size. It has also been observed that the serrated yielding phenomenon occurs in these alloys, not only in the solid solution condition, but also in the age hardened condition. In this chapter an attempt will be made to examine the current theories of the precipitate growth kinetics, onset of yielding and serrated yielding, in the light of the results presented in the previous chapter.

1. The growth kinetics of γ' phase.

The main precipitation reaction within the grains of all the three alloys studied was the formation of the γ' phase while, at the grain boundaries it was Ni_3Ti hexagonal η phase. The volume fraction of γ' determined metallographically was similar to that established by electrochemical extraction, though certain amount of η phase might have been included in the extracted precipitate. This suggests that the majority of the precipitate extracted was γ' phase. Therefore, the volume fraction and the composition of γ' which was determined by analysing the electrochemically extracted precipitate, and shown in Table (1), are fairly accurate. The composition of γ' in Udimet 700 (Ni - base superalloy) has been observed to be nearly independent of time and temperature of ageing. However it has also been suggested

that it may depend upon the temperature of ageing[122]. Although the data on the composition of γ' formed at the various temperatures of ageing in the present alloys are limited, they do suggest that the composition of γ' depends upon the temperature of ageing which is contrary to the behavior of γ' in Udimet 700[122].

The growth kinetics of γ' phase in the Co - Ni - Cr alloys studied follows the LSW theory of diffusion controlled growth over a wide range of time and temperature of ageing. The time dependence of particle size follows the growth equation very accurately in spite of the fact that hexagonal Ni_3Ti phase precipitates discontinuously at the grain boundaries in addition to γ' phase within the grains, as shown in Fig. (7) and (8). It is also observed that $\bar{a}_{(o)}$ values are not exactly zero which would suggest that the nucleation of γ' had occurred before the measurements were made. This is similar to the observations in Ni - Al alloys[4]. Since the particle size of γ' obeys the time law of coarsening, in spite of the complexity of the alloys, the particle size can be predicted for a given ageing treatment by the plots of Fig. (14) and/or (17). Also, these plots can be used to determine the heat treatment to develop a particular size and, hence, the mechanical properties of these alloys, as has been suggested for Udimet 700[122]. The activation energy for the growth process was calculated to be 3.1 e.V/molecule. This activation energy is dependent not only upon the diffusion of Ti in the matrix but may also depend upon the diffusion of Co and Cr atoms away from a growing γ' particle. The activation energy for the diffusion of Ti in Ni has been observed to be 2.67 e.V/molecule[123

and that for the self diffusion of Co, in the 772° C - 1048° C, and of Cr, in the 1300° C - 1600° C temperature range, have been found to be 2.83 e.V/molecule and 3.19 e.V/mole respectively. Therefore, the calculated value of 3.1 e.V/molecule for the coarsening of γ' particles in these superalloys is not unreasonable.

The distribution of particle size of γ' in these alloys differs considerably from the theoretical distribution of LSW theory. It is much broader than the theoretical distribution but slightly narrower than in the Ni - Ti binary alloy system[6]. The observed cut-off value of ρ_c in Ni - Cr - Al, Ni - Si, Ni - Al and Ni - Ti alloys have lead to the belief that the deviation of ρ_c from its theoretical value of 1.5 primarily depends upon the lattice misfit, Δ a/a, ie., as the lattice misfit increases so does the deviation of ρ_c from its theoretical value[7]. In the present alloy system, where the lattice mismatch is + 1.3%, the deviation in ρ_c was observed to be 36% as compared to Ni - Cr - Al system[39], where $\Delta a/a$ is + 0.5%, the deviation was 13.5%. Therefore, our results seem to be in agreement with this general trend. However, in Ni - Ti system[6], where the lattice mismatch is +0.9%, the deviation in ρ_c was 40%. A satisfactory explanation for this anomaly, i.e., a nearly similar deviation in ρ_c with widely different lattice mismatch, is not available. It may therefore be concluded that the average particle size in the present system is proportional to $t^{1/3}$ as predicted by the LSW theory of diffusion controlled growth but the distribution of particle size differs considerably from the theoretical distribution of precipitate particles.

1.2 Effect of volume fraction of γ' on coarsening process.

In the LSW theory it is assumed that the particles are spherical and the volume fraction is very small so that the mean distance between the particles is large as compared to their diameter. In spite of these assumptions the LSW theory has been successfully applied to the coarsening behavior of Cu in Fe - Cu[35], Mn in Mg - Mn[124], γ' in Ni - Al[5], Ni - Si[7], Ni - Ti[6], and in Ni - Co - Cr - Ti[25], and Fe_3Si in Fe - Si - Ti[125] systems. However, the basic expression of the LSW theory does not contain a volume fraction term. Ardell[32] has modified this theory to incorporate the volume fraction term, f_v, in the LSW expression. This modified theory predicts that the basic $t^{1/3}$ kinetics remain the same as the original LSW theory but the coarsening rates should increase with increasing volume fraction of the precipitate. It is observed that the growth of Co precipitate in the Cu - Co[32] system obeys the MLSW theory very well, however, the growth of γ' in Ni - Al, and Ni - Cr - Al alloys[126] is entirely in contradiction to the MLSW theory, and follows the original LSW theory which is independent of volume fraction.

The LSW as well as MLSW theories assume a steady state diffusion, but with a different geometry of diffusion. In the LSW theory, the volume fraction of the growing phase is assumed to be nearly zero which implies that the interparticle spacing, L, is much greater than the particle size (2r), ($L >> 2r$). In the MLSW theory, on the other hand, a steady state diffusion is assumed to occur through concentric spheres[32].

According to Brown and Ham[12], the interparticle spacing, L, for spherical particles of radii, r, is given by $L = [(\frac{\pi}{f_v})^{1/2} - 2]r$ where f_v is the volume fraction of the precipitate. In the present alloys, the particles are cubic and, as stated earlier, it is assumed that $r = \frac{a}{2}$. Therefore, in a 6% Ti alloy aged for 1 hour at 800° C, where $\frac{a}{2}$ = 82 Å, L is calculated to be 133 Å. This is less than the particle size, ie. 164 Å. Similarly, at higher volume fraction, the γ' particle size is always greater than the interparticle spacing. This is contrary to the assumption of the LSW theory, yet the growth of γ' particles follows the original LSW thoery, and not the MLSW theory. Therefore the assumption and approach of the MLSW theory are attractive but do not seem to apply to the growth of γ' particles in the present alloy system. A similar conclusion was also reached by Chellman and Ardell[126] while working on the Ni - Al and Ni - Cr - Al alloys.

2. Strengthening Mechanism.

The results of the structural examination of the aged and deformed alloys has indicated that at the onset of plastic flow two types of precipitate - dislocation interactions occur. When the γ' particles are smaller than 28 Å they are sheared by paired dislocations and when they are bigger than 56 Å they are by passed by the moving dislocations by the Orowan mechanism. It was also observed that when the γ' particle size is between 28 ∿ 56 Å both of these mechanisms are operative.

2.1 Strengthening mechanism during the early stage of ageing.

In general, when the precipitate particles are cut by glide dislocations the strengthening of the alloy can be due to the following sources:

1. Modulus hardening: This is due to the differences between the elastic moduli of the matrix and the particle.
2. Stacking fault hardening: This is caused by the differences between the stacking fault energy of the matrix and the particles.
3. Coherency hardening: This is introduced by the elastic coherency precipitate particles that do not fit the matrix exactly.
4. Surface hardening: This is due to the energy required to create additional matrix - particle interface when the particle is sheared by the dislocation.
5. Order hardening: This arises due to the additional work required to create an antiphase boundary when the precipitate particle is ordered.

It has been observed that the contribution of modulus hardening by γ' precipitate in Ni base alloys[127] and stainless steel[15] is very small and can be ignored. It has also been concluded that the contribution of surface hardening in these alloys is negligible and can, therefore, be ignored[127]. Similarly, the stacking fault hardening is not expected to contribute significantly to the total strength of the alloy. Therefore, only coherency and order hardening mechanisms are examined in detail.

2.1.1 Coherency strengthening.

Two theories have been advanced to account for the strengthening due to the coherent precipitate particles. The first theory which was

discussed in Chapter II, is due to Gerold and Haberkorn. According to this theory the increase in CRSS, $\Delta\tau$, due to coherency strains is given by

$$\Delta\tau = \beta_1 \; G \; (\varepsilon)^{3/2} \; (\frac{r}{b})^{1/2} \; f_v^{1/2} \qquad \ldots . \qquad (17)$$

where, ε is the matrix particle misfit,

r is the particle radius,

f_v is the precipitate volume fraction,

b is the Burger vector,

G is the shear modulus of the matrix,

β_1 is the constant (3 for edge and 1 for screw dislocation).

In deriving the above expression Gerold and Haberkorn assumed dislocations, interacting with the strain field around precipitate particles as rigid and straight. Gleiter disagreed with this assumption and by using a more rigorous treatment arrived at the following expression for $\Delta\tau$.

$$\Delta\tau = 11.8 \; G\varepsilon^{3/2} \; f_v^{5/6} \; (\frac{r}{b})^{1/2} \qquad \ldots . \qquad (55)$$

In the present investigation increase in the CRSS was calculated for 5% Ti alloy where $\varepsilon = 0.013$, $b = 2.506$ A^{o}. The values of f_v for various particle sizes were obtained from figure 9 and G was assumed to be 6000 kg/mm^2. Both, Gerold and Haberkorn's and Gleiter expressions were used. If either of the two mechanisms are operating a plot of observed and calculated CRSS values should be a straight line with unit slope. The data points obtained by using

Gerold and Haberkorn's expression for an edge dislocation are shown in figure 57. The slope of the best fitting straight line, obtained by the least square method, is 0.773 ± 0.046. The discrepancy, considering the assumptions involved, is not too unreasonable. The values of $\Delta\tau$ by Gleiter's expression will be about 4 times greater than those obtained by Gerold and Haberkorn's expression. Therefore, deviation from the observed values will be even greater. A similar analysis could not be made for the 4% and 6 Ti alloys as their volume fraction data for very early stages of ageing is not available. However, it may be concluded that if coherency strengthening mechanism was operative it follows the theory of Gerold and Haberkorn.

2.1.2 Order strengthening.

The physical model of order strengthening was discussed in Chapter II. According to Brown and Ham the increase in CRSS, for the particle size over which the particle shearing was observed during the present investigation, is given by

$$\Delta\tau = \frac{\gamma_{APB}}{2b}\left[\left(\frac{4\gamma_{APB}\, f_v\, r_s}{\pi T^*}\right)^{1/2} - f_v\right] \qquad \ldots \qquad (12)$$

where, γ_{APB} - antiphase boundary energy, and

T^* - line tension of the dislocation.

The other terms are the same as in the coherency mechanism expression. The values of γ_{APB}, f_v, r_s and b are known from the experimental results and by taking $T^* = \frac{3Gb^2}{8\pi}$ (12) the theoretical values of $\Delta\tau$ can be calculated by equation 12. The data points obtained by this calculation

Figure (57) Plots of the observed and calculated values of $\Delta\tau$ of 5% Ti alloys during the early stages of ageing.

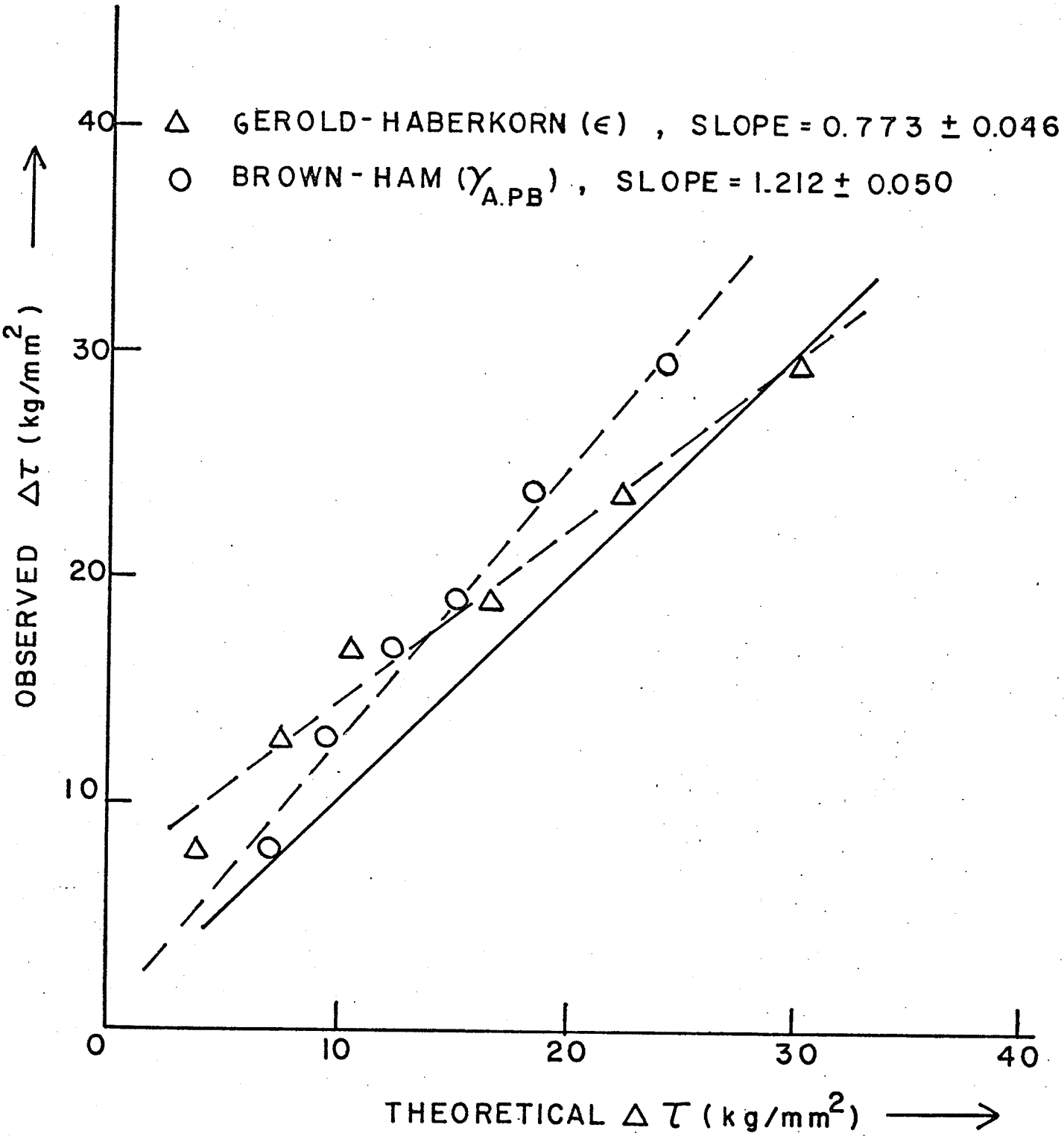
Δ GEROLD-HABERKORN (ϵ) , SLOPE = 0.773 ± 0.046
O BROWN-HAM ($\gamma_{A.PB}$) , SLOPE = 1.212 ± 0.050
OBSERVED Δτ (kg/mm²)
THEORETICAL Δ τ (kg/mm²)
0
10
20
30
40

FIG. (57)

are plotted against experimental observation in figure (57). The slope of the best fitting straight line, obtained by the least square method, is 1.212 $\pm$ 0.054. Once again the deviation between the two, considering the assumptions that have been made, is not too unreasonable.

2.1.3 Order strengthening vs. coherency strengthening.

The analysis of the results, presented in the previous two sections, has shown that the increase in the strength of the aged alloys, during the particle shearing process, can be either due to the coherency hardening mechanism or due to the order hardening mechanism. In the existing literature a great deal of doubt exists regarding the relative contribution of these two mechanisms to the strength of a precipitation hardened alloy. Mihalisin and Decker[13], Parker[128], and Parker and West[129] emphasize the coherency strains while Raynor and Silcock[15], Phillips[16], and Munjal and Ardell[127] consider APB to be the main factor. It should be noted that none of the γ - γ' systems studied by these workers has such a large misfit as the present alloys i.e. 1.3%. On the other hand Singhal and Martin[17] found the two factors to be additive. However, Singhal and Martin obtained the values of CRSS by dividing the value of yield stress, obtained by tensile testing polycrystalline specimen, by a factor of 2. It has since been pointed out that for the F.C.C. material the best estimate of CRSS can be obtained by using a factor of 3[130]. Therefore, in the present analysis a factor of 3 has been used. Now, if the contributions due to the coherency strains and order strengthening are added the theoretical values of CRSS are considerably more than the observed values[Table 5]. Therefore, it seems that the two values of CRSS should not be added together.

Table 5

	r_s (Å)	Δσ, (observed) (kg/mm^2)	ε Δσ, by Gerold-Haberkorn, coherency model (kg/mm^2)	γ_{APB} Δσ, by Gleiter-Hornbogen, APB model (kg/mm^2)	γ_{APB} Δσ, by Brown-Ham, APB model (kg/mm^2)
1	10	8	4.268	2.118	6.64
2	15	13	7.547	2.86	9.043
3	21	17.3	10.437	3.558	12.076
4	28	19	16.958	4.253	15.068
5	33.5	24	21.957	4.882	18.307
6	54	29.3	30.200	6.410	23.420

Figure 21 shows the plots of $\Delta\tau$ vs $r_s^{1/2}$ for all the three alloys. During the early stages of ageing these plots are straight lines which cannot be extrapolated to pass through the origin. According to Gerold and Haberkorn's expression for $\Delta\tau$ due to coherency hardening $\Delta\tau$ vs $r_s^{1/2}$ plot should be a straight line passing through the origin (Equation 17). On the other hand the expression for $\Delta\tau$ due to order strengthening (Equation 12) can be rewritten as:

$$\Delta\tau = B\, r_s^{1/2} - \delta \qquad \ldots \quad (56)$$

That is, the $\Delta\tau$ vs $r_s^{1/2}$ plot should be a straight line with a negative value of the intercept of the y-axis of the plot. Figure 21 shows that the experimental plots can be described by the expression (56) and hence, by the expression due to order strengthening. This would suggest that order strengthening is operative in this alloy system.

If equations 12 and 56 are compared it is seen that the constant B is a function of γ_{APB}, f_v and T* and δ is a function of γ_{APB} and f_v, i.e.

$$B = \gamma_{APB}^{3/2} \left(\frac{f_v}{\pi T}\right)^{1/2} \quad \ldots\ldots \quad (57)$$

and

$$\delta = \frac{\gamma_{APB} f_v}{2b} \quad \ldots\ldots \quad (58)$$

Therefore, since the values of various factors in the above two equations are known, and B and δ can be obtained from figure 21, γ_{APB} can be calculated. The value of γ_{APB} was calculated to be 215 ergs/cm^2 by equation 57 and 186.3 ergs/cm^2 by equation 58. The average value of the two, 200 ergs/cm^2, is fairly close to the value of 193 ergs/cm^2 obtained by the minimum loop method and 196 ergs/cm^2 calculated by using Flinn's expression[63]. This analysis also suggests that the order strengthening mechanism of Brown and Ham is operative in the present alloy system.

The calculated and observed flow stress are plotted against the particle size in figure 58. It is seen that as the particle size is increased the deviation of the theoretical yield stress from the

observed values becomes significant i.e. the theoretical values are greater than the observed values. This may be due to the fact that in this region both the looping and shearing mechanism are operative because of the distribution of particle size over a large range.

The contribution of coherency strains to the strength of these alloys can only be established by studying the temperature dependence of yield stress in single crystals. This was not possible due to time restraint. However, the above analysis does suggest that the order strengthening has a greater probability of being the main strengthening mechanism than the coherency strengthening.

2.2 Strengthening mechanism in overaged alloys.

Figures 21 and 58 show that as the γ' particle size is increased the strength of the alloy decreases i.e. overaging sets in. It has also been observed that during this stage the deformation proceeds by the Orowan looping mechanism (eg. Fig. 26). Ashby[57] has suggested that the increase in CRSS by Orowan looping will be different for the screw and edge dislocations. The modified expressions for increase in CRSS, as discussed in Chapter II, are

$$\Delta\tau_{edge} = 0.85 \frac{Gb}{2\pi L_o} \ln\left(\frac{2r_s}{r_o}\right) \quad \ldots\ldots \quad (21)$$

$$\Delta\tau_{screw} = 0.85 \frac{Gb}{2\pi L_o(1-\nu)} \ln \frac{2r_s}{r_o} \quad \ldots\ldots \quad (22)$$

Figure (58) A comparison between the experimental and the theoretical $\Delta\tau$ during Orowan bowing process (overaged stages).

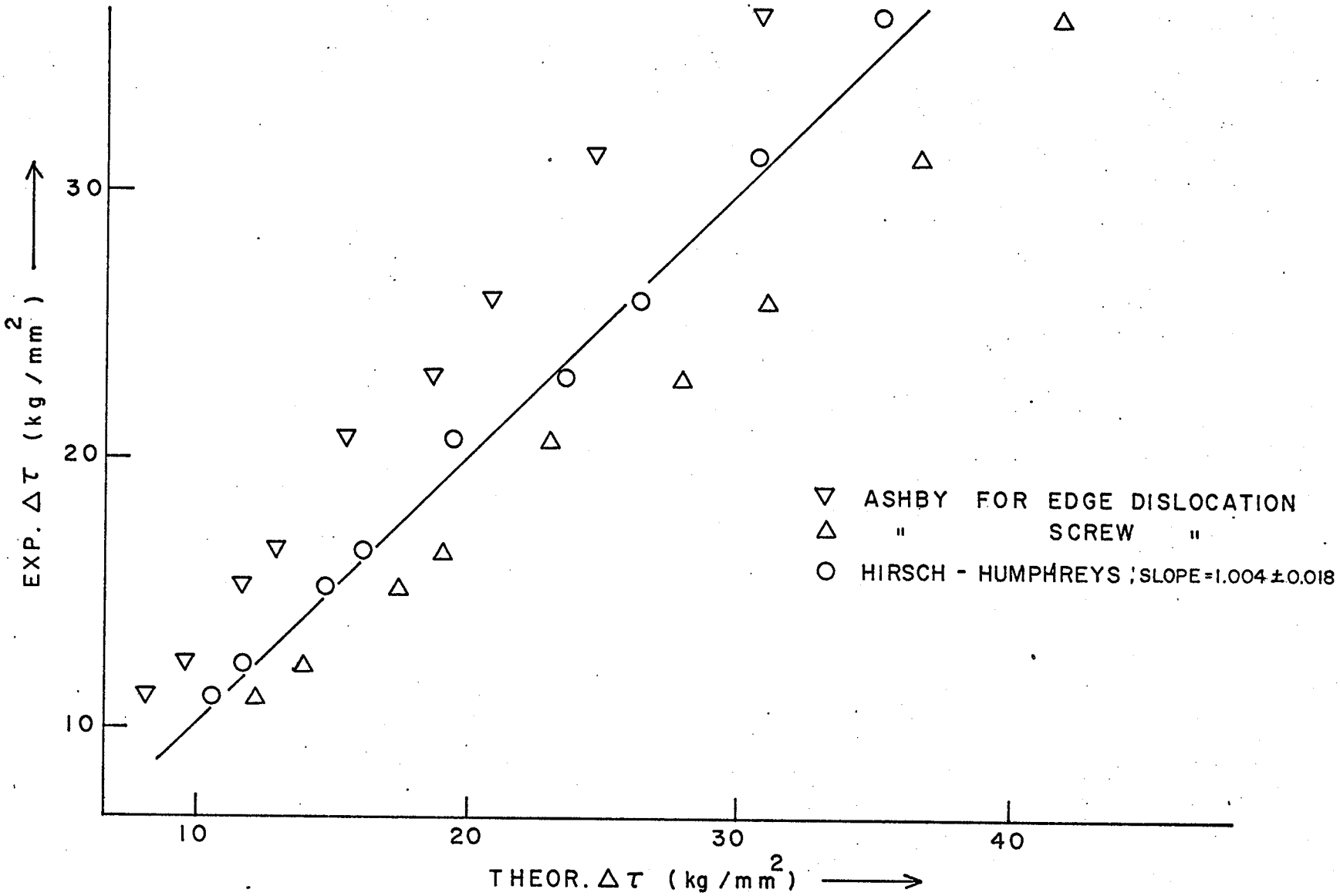
EXP. Δτ (kg / mm²)
30
20
10
10
20
30
40
THEOR. Δτ (kg / mm²)
ASHBY FOR EDGE DISLOCATION
" SCREW "
HIRSCH - HUMPHREYS ; SLOPE = 1.004 ± 0.018

FIG. (58)

Hirsch and Humphreys[58] have, however, suggested that both edge and screw dislocations will by-pass particles at the same stress. This stress is given by the following expression

$$\Delta\tau = \frac{0.81\ Gb}{2\pi\ L_o\ (1-\nu)^{1/2}} \ln\left(\frac{2r_s}{r_o}\right) \qquad \ldots\ (23)$$

All the three expressions suggest that a plot of $\Delta\tau$ against $\frac{1}{L_o} \ln\left(\frac{2r_s}{r_o}\right)$ should be a straight line. Figure 22 shows that by taking the value of r_o, the inner cut off radius, to be b, the Burgers vector, this plot is a straight line. In order to determine whether the theory of Hirsch and Humphreys applies to our alloys, or the Ashby mechanism controls the yield stress of the overaged alloys theoretical CRSS were calculated by using expressions 21, 22 and 23. These values were plotted against the observed values, as shown in figure 59. It is seen that there is a deviation between the two if Ashby's suggestions are followed. Whereas, the plot between the theoretical values, based on Hirsch and Humphrey's suggestions and the observed value is a straight line with a slope of 1.004 ± 0.018. This is an excellent fit and it may be concluded that, as suggested by Hirsch and Humphreys, both edge, and screw dislocations require the same stress to by-pass γ' particles in the overaged Co - Ni - Cr - Ti alloys.

3. Serrated yielding.

The results presented in Chapter III have shown that when the tensile tests are carried out at elevated temperatures the stress-strain diagrams of all the three alloys, in both solution-treated as well as in aged condition, show serrations. In this section those results will be analysed to evaluate the present theories of serration yielding.

Figure (59) The theoretical and experimentally observed flow stresses against particle size for the three alloys aged at 800° C.

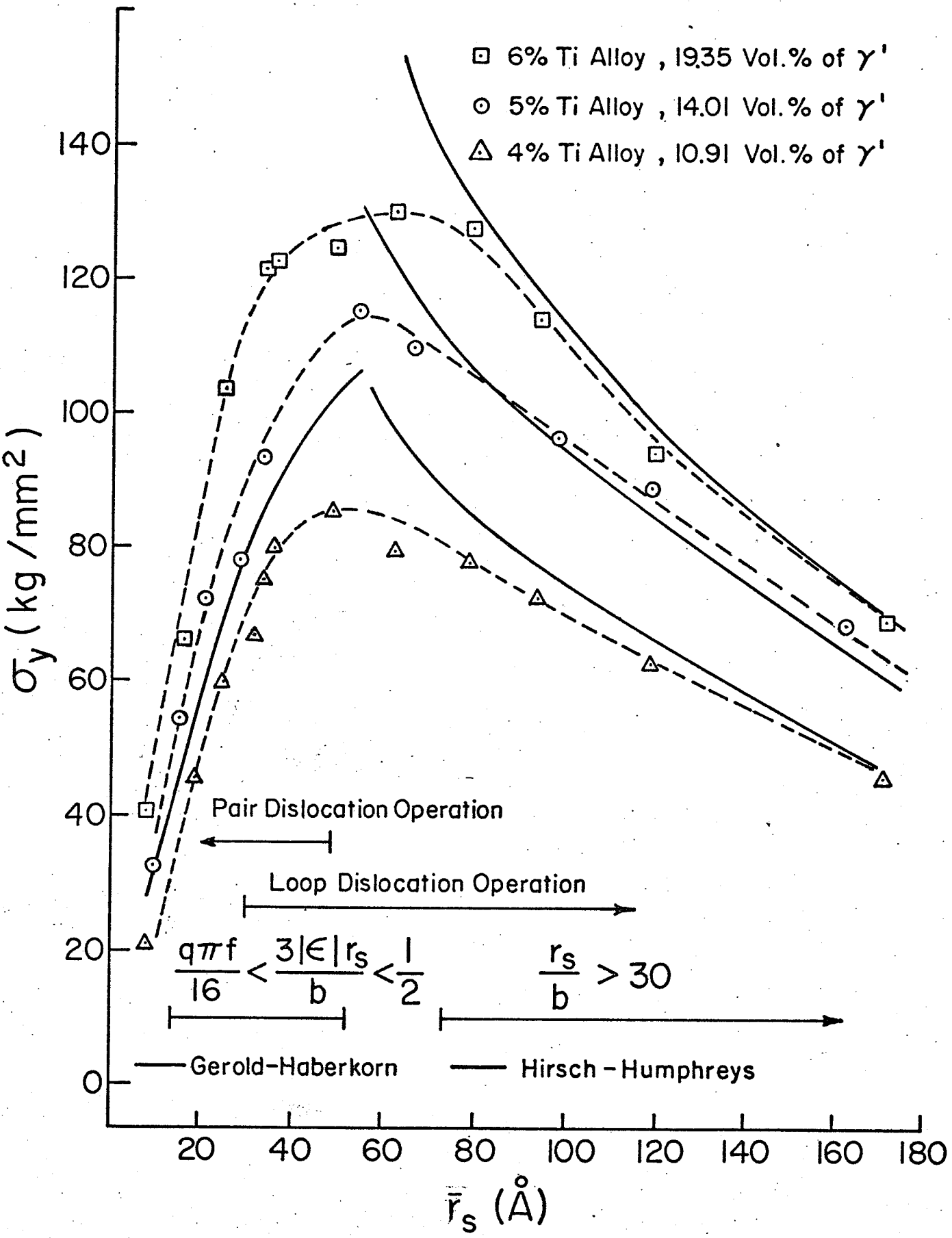
6% Ti Alloy , 19.35 Vol.% of γ'
5% Ti Alloy , 14.01 Vol.% of γ'
4% Ti Alloy , 10.91 Vol.% of γ'
σy (kg /mm2)
140
120
100
80
60
40
20
0
Pair Dislocation Operation
Loop Dislocation Operation
qπf/16 < 3|ε|rs/b < 1/2
rs/b > 30
Gerold-Haberkorn
Hirsch - Humphreys
20
40
60
80
100
120
140
160
180
r̄s (Å)

FIG. (59)

3.1 Critical strain to serrations, ε_c.

The results on serrated yielding clearly show that the basic relationships of linearity between $\log \dot{\varepsilon}/\log \varepsilon_c$ and $\log \varepsilon_c/\frac{1}{T}$ predicted by equations (30) and (35) are confirmed in the present alloys for temperatures in the range 300 to 550° C (Figs. 41 and 43). Deviations in the $\log \varepsilon_c/\frac{1}{T}$ plots are observed at lower temperatures (Fig. 41). However, contrary to previous work[22, 23] the results show that ageing decreases the critical strain to serrations. It is difficult to explain this behavior in terms of the dynamic strain ageing model of equation (30), but a reasonable rationale can be suggested in terms of the static strain ageing model equation (34).

The results also show that if solute atoms are the main obstacles then the relationship obeys $\varepsilon_c \propto 1/C_o$ and thus $L \propto C_o^{-1/2}$ similar to that in Cu - Sn alloy[82,84], whereas if precipitate are the major obstacles then $L \propto \bar{L}$ and thus L can be represented by the interparticle spacings. Therefore in the case of solid solution condition the solute atoms, Ti, are considered to be the main obstacles, while in aged condition the γ' precipitate particles are the main obstacles.

3.2.1 Vacancy production and mobile dislocation density - $(m+\beta)$.

The average value of $m+\beta$ obtained from all the data is 1.4 and is independent of the heat treatment. From an analysis of the smooth portion of the stress-strain curve over a range of temperatures and strain, an average value of n in $\sigma = A_2 \varepsilon^n$ expression was found to

be 0.45, for all the alloys. From equation (45) one can obtain a value of $m = n + 1 = 1.45$, which compares with $(m+\beta) = 1.4$ obtained from the critical strain data. Hence the Saada's model for vacancy accumulation is in agreement with the present result if $\beta = 0$, ie. the mobile dislocation density is effectively independent of strain. This is in agreement with the recent computer simulations of plastic flow[131].

An alternative model of vacancy production [equation (47)], predicts $m = 1.72$, which is inconsistent with the present serrated yielding results. However, this model may be operating at lower temperatures ie., 280° C, when the critical strain is lower than expected on the basis of the Saada's model. Equation (48) predicts a higher vacancy production rate and hence a lower ε_c.

3.3 The influence of solute content, C_o.

Since it has been shown that $(m+\beta)$ is effectively independent of Ti content, and it will be shown in section 3.5 that so is Q_m, in the solution treated condition equation (51) should be valid i.e.,

$$\varepsilon^{(m+\beta)} \propto C_o^{(\alpha_1 - 3/2)}$$

Therefore a plot of log ε_c against log C_o should be linear with a slope of $(\alpha_1 - 3/2)/m+\beta$. Figure (60) shows that such a plot is indeed linear with a slope of -1.5. Substituting for $(m+\beta) = 1.4$, one can obtain $\alpha_1 = -0.6$ which compares with $\alpha_1 = -0.5$ expected on the basis of solution hardening theories with $L \propto C_o^{-0.5}$. In Cu - Sn Russell[84]

Figure (60) Log plots of critical strain ε_c against concentration of Ti, C_o in solid solutions at various temperatures.

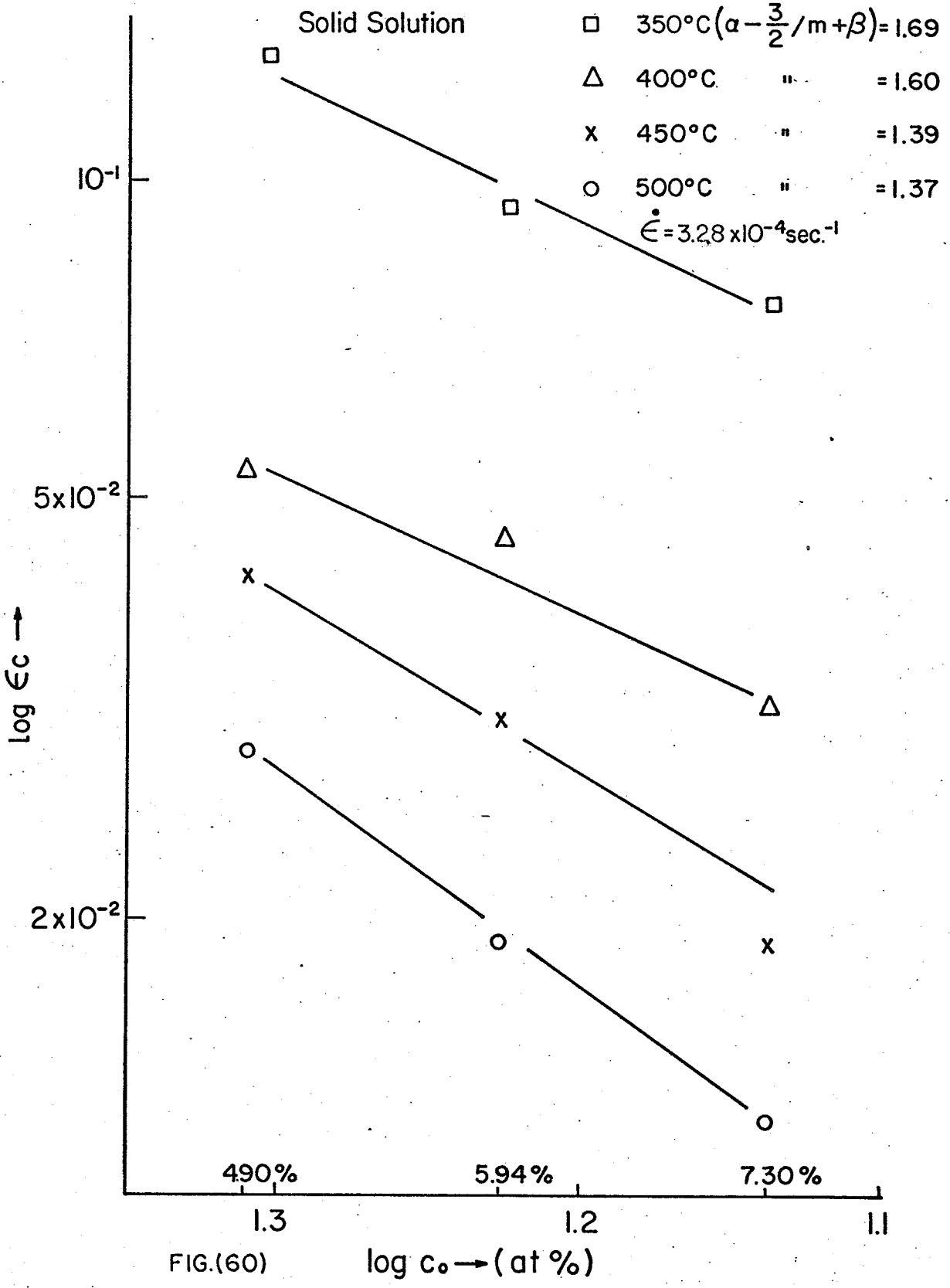
Solid Solution
□ 350°C $(\alpha - \frac{3}{2}/m + \beta) = 1.69$
△ 400°C " = 1.60
x 450°C " = 1.39
o 500°C " = 1.37
$\dot{\epsilon} = 3.28 \times 10^{-4} sec.^{-1}$
10^{-1}
5×10^{-2}
2×10^{-2}
log ϵ_c →
4.90%
5.94%
7.30%
1.3
1.2
1.1
log c_o → (at %)

FIG.(60)

found $\varepsilon_c \propto C_o^{-1/2}$ for $m+\beta = 2.2$, and Vohringer and Macherauch[82] found $\varepsilon_c \propto C_o^{-1/2}$ for $m+\beta = 2.8$. These results support the contention that the solutes are the major barriers to dislocation motion in the solution treated alloys.

In going from the solid solution to the aged condition, the concentration of Ti is reduced from 5.94 at % to 2.52 at %. Hence, if it is assumed that Ti is responsible for serrated yielding, and it should be noted that the concentration of Ni, Co and Cr in the matrix is also changing, one would expect a corresponding change in ε_c. On the basis of equation (35) and assuming the obstacle spacing and ρ_m remain constant, ε_c should increase from 4.5% for the solid solution deformed at 400° C and $\dot{\varepsilon} = 3.28 \times 10^{-4}$/sec. to about 11.5%. Clearly this is contrary to experimental results. Furthermore, the concentration dependence cannot explain the difference in ε_c between the 12 hours and 118 hours ageing treatments, where the concentration of solute remains approximately constants. In this arguement it has been assumed that the nature of the obstacles and its spacing remains constant. This is not expected to be so, since in aged specimens the precipitates are probably the obstacles. A comparison of the two ageing treatments should clarify this.

3.4.1 The influence of particle spacing, $\bar{L}$.

From equations (35) and (54) it is seen that the static strain ageing model predicts a change in ε_c with a change in the particle spacing $\bar{L}$. Assuming that the particles are the major dislocation

barriers, and the concentration of solute in the matrix is constant. (In the present alloys C_o = 0.027 Ti when aged at 800° C). Knowing the particle size, $\bar{a}$, and the volume fraction of the particle, f_v can obtain $\bar{L}$ from[12].

$$\bar{L} = \left[\left(\frac{\pi}{f_v}\right)^{1/2} - 2\right] \frac{\bar{a}}{6}$$

The influence of $\bar{L}$ on ε_c is shown in Figure (61) for the three alloys over a range of strain rates. It is apparent that, in agreement with equations (35) and (54), the critical strain ε_c decreases as $\bar{L}$ increases. From equation (54), assuming A_p and Q_m are constant, a plot of log ε_c against log $\dot{\varepsilon}/L$ should be linear with a gradient of $(m+\beta)$. (In fact the activation energy results show a slight variation in Q_m but the variation is within experimental uncertainty.) Figure (62) shows that such a plot is linear with a gradient of $(m+\beta) = 1.44 \pm 0.03$, which is in good agreement with the previous value of $(m+\beta) = 1.4$ obtained from the strain experiments. These results therefore show that the influence of the volume fraction of precipitate particles can be fully accounted for on the basis of its influence on the dislocation barrier spacing.

3.5 Activation energy.

From equation (35), a plot of log $\dot{\varepsilon}^{m+\beta}/T$ against $1/T$ yields Q_m value at constant $\dot{\varepsilon}$. From this plot an average value of Q_m = 0.67 e.V for the solid solution conditions was obtained.

Figure (61) The relationship between ε_c and the interparticle spacing $\overline{L}$.

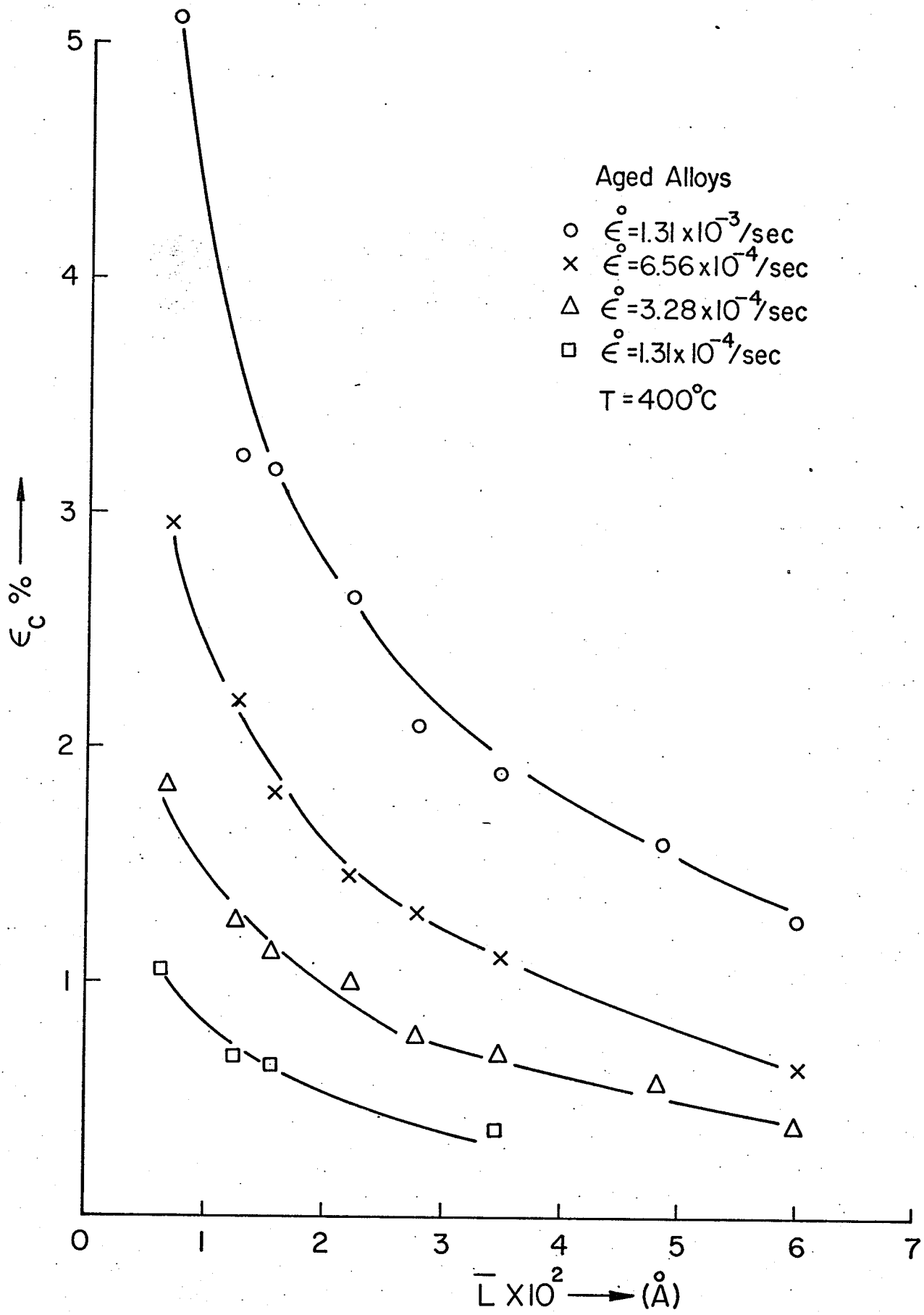
Aged Alloys
○ $\dot{\epsilon}^{\circ}$=1.31 x10^{-3}/sec
× $\dot{\epsilon}^{\circ}$=6.56x10^{-4}/sec
△ $\dot{\epsilon}^{\circ}$=3.28x10^{-4}/sec
□ $\dot{\epsilon}^{\circ}$=1.31x10^{-4}/sec
T=400°C
ϵ_c %
$\bar{L}$ X10^{2} → (Å)
0
1
2
3
4
5
6
7

FIG. (6 I)

Figure (62) A log plot of ε_c against $\dot{\varepsilon}/\overline{L}$ for the aged alloys.

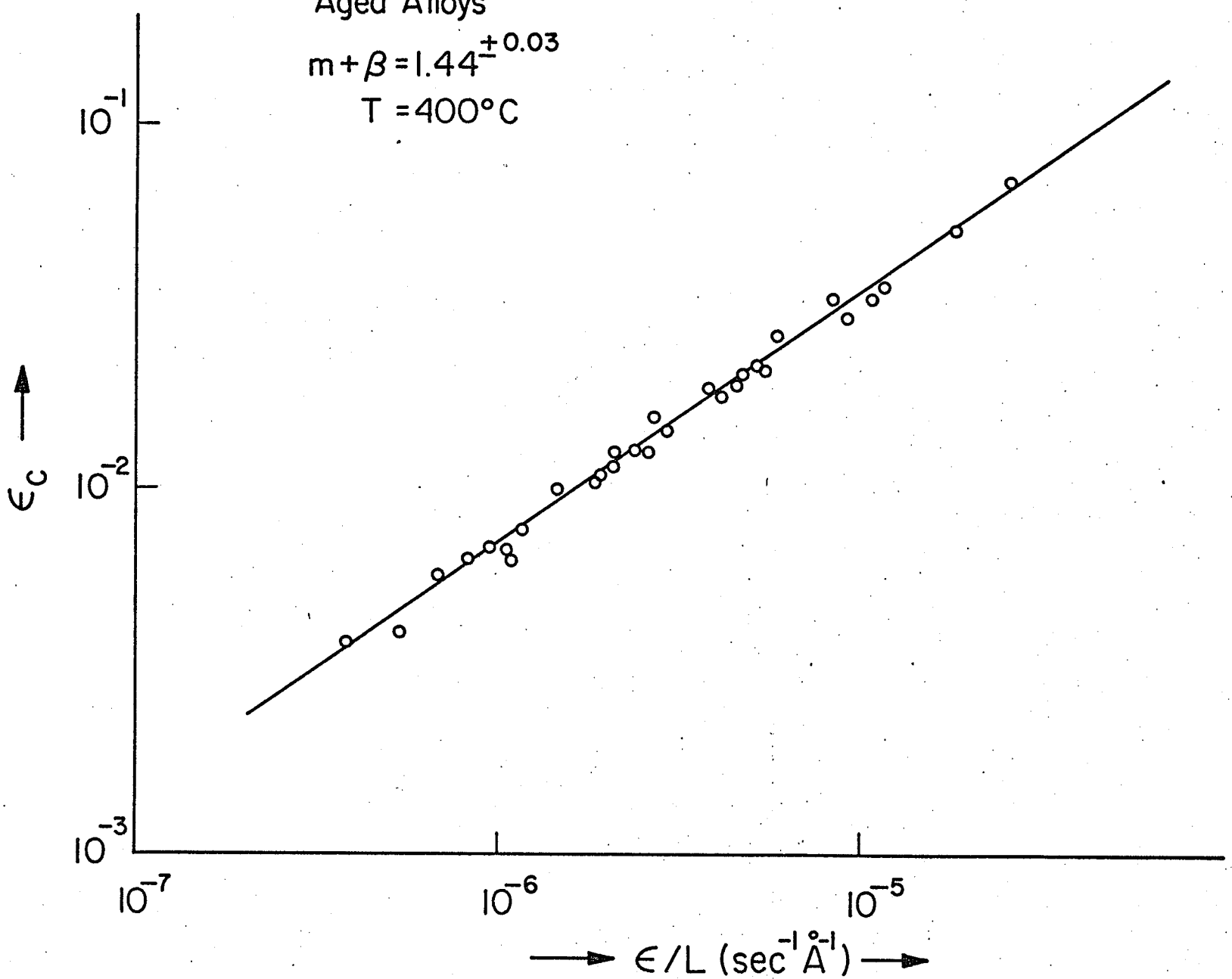
Aged Alloys
m + β = 1.44 ± 0.03
T = 400°C
10^{-1}
10^{-2}
10^{-3}
ϵ_c
10^{-7}
10^{-6}
10^{-5}
ϵ/L (sec^{-1} Å^{-1})

FIG.(62)

The migration energy for Ti atoms in Ni is not known but it should be about the same as that of Al atoms in Ni which is about 1.0 e.V. (Swalin and Martin[123] give a value of 2.8 e.V. for the activation energy for diffusion of Al in Ni and the formation energy of vacancy in Ni is about 1.8 e.V.[44]. As a result the discrepancy between the values is about 0.33 e.V. This indicates a binding energy between Ti and a vacancy and/or between Ti and other impurity atoms. In fact the present alloys contain about 0.01% carbon atoms[25] as an impurity, forming carbide (TiC) at about 600 to 800° C and when these alloys are solution treated at 1250° C these carbon atoms remain in solution and act as interstitials. Therefore, this impurity interaction seems to result in lowering of the Q_m value.

The activation energy for aged alloys are somewhat higher than that of solid solution treated alloys. Q_m obtained from equation (54) with temperature factor also gives an average value of Q_m = 0.97 e.V. for aged alloys. This value is close to the available diffusion data (1.0 e.V.). The agreement seems to be clear from the following point of view; when alloys are aged at 800° C the most of the impurities in solution should precipitate out at this temperature (800° C), little impurities will remain in solution and hence little impurity interaction with Ti and/or vacancy in the matrix are expected to occur.

3.6 Comparison with previous experiments.

As stated in the literature review, previous results on Al alloys[22,23] and on alpha - beta brass[24] show an increase in ε_c

with ageing. A similar result in the H.C.P. system of Mg - 10% Ag has been found by Chaturvedi et al[132]. The present results are in direct contradiction to this. The explanation lies in the static strain ageing expression[94] (35). When a material is aged the value of C_o in equation (35) is decreased which results in an increase in ε_c. This duplex result appears to be the dominant effect in the work previously reported in the literature

No details of analysis in those alloys was given in terms of ageing process between solute decomposition and precipitate growth. However, if ageing results in a change in L through precipitation of a second phase which then becomes the major obstacles, ε_c can decrease provided $L_{ppt} >> L_{solute}$. This is the dominant effect in the results reported here.

VI CONCLUSIONS

1. On the coarsening behavior.

(1) The γ' phase in the Co - Ni - Cr base alloys precipitates coherently along <100> matrix directions and is of cuboid shape. The lattice parameter mismatch between γ' and the F.C.C. matrix was +1.3%. A hexagonal Ni_3Ti, η, phase precipitates discontinuously at the grain boundaries. However, the major part of the total precipitate was found to be the γ' phase.

(2) The chemical composition of the γ' phase is not independent of temperature of ageing, unlike Udimet 700[122]. The volume fraction of γ' precipitate decreases linearly with ageing temperature.

(3) The results of this investigation show that the coarsening kinetics of γ' in Co - Ni - Cr - Ti alloys follow the time-law prediction of the Lifshitz-Wagner theory of diffusion-controlled coarsening.

(4) The particle-size distribution at all the ageing temperature is a great deal broader than the theoretical distribution of the Lifshitz-Wagner theory. This could be due to a large lattice mismatch between γ' and the matrix[25].

(5) The effect of volume fraction on the growth kinetics of γ' in the three alloys was also studied. The growth of γ' in the present alloys is entirely in contradiction to the MLSW,

which takes into consideration the volume fraction of the growing phase, and follows the original LSW theory which is independent of volume fraction.

2. On strengthening mechanism.

(1) During the early stages of ageing, when the γ' particles are smaller than 28 Å, the deformation occurs due to the precipitate particles being sheared by the glide dislocations which move in pairs. When the precipitate particles are larger than 56 Å they are by-passed by the glide dislocations which leave a loop around them.

(2) During the particle shearing stage it was not possible to determine conclusively whether coherency hardening mechanism was operative or if the strengthening was due to order hardening. However, the results seem to favor the order hardening mechanism of Brown and Ham.

(3) In the overaged alloys, where the deformation occurs by the Orowan looping mechanism, the tensile test results seem to favour the suggestion of Hirsch and Humphreys that both the edge and screw dislocations require the same stress to by-pass the precipitate particles.

3. On serrated yielding.

(1) When tensile tests were conducted at elevated temperatures the stress-strain curves of both solution treated and aged alloys exhibited serrations in the temperature range of 300-600° C.

(2) In the temperature region where these serrations were observed the 0.2% offset yield stress shows a characteristic temperature independence and an inverse strain rate effect.

(3) The serrated yielding behavior, in the alloys investigated, can be explained on the basis of McCormick's static strain ageing model if the solute atoms are considered to be the main obstacles in the path of dislocations in the solution treated alloys and γ' precipitates in the aged alloys.

(4) It has also been shown that the results are consistent with Saada's model of vacancy production and negligible change in the mobile dislocation density with strain.

(5) The activation energy for serrations were found to be 0.6 e.V. in the solution treated alloys and 0.93 e.V. in the aged alloys.

VIII REFERENCES

1. C. T. Sims, J. Metals, 21 (1969) 27.

2. I. M. Lifshitz and V. V. Slyozov, J. Physics Chem. Solids, 19 (1961) 35.

3. C. Wagner, Z. Electrochem., 65 (1961) 581.

4. A. J. Ardell and R. B. Nicholson, Acta Met., 14 (1966) 1295.

5. A. J. Ardell and R. B. Nicholson, J. Physics Chem. Solids, 27 (1966), 1793.

6. A. J. Ardell, Met. Trans., 1 (1970) 525.

7. P. K. Rastogi and A. J. Ardell, Acta Met., 19 (1971) 321.

8. W. I. Mitchell, Z. Metallk., 57 (1966) 586.

9. E. H. Van Der Molen, J. M. Oblak and O. H. Kriege, Met. Trans., 12 (1971) 1627.

10. H. Gleiter and H. Hornbogen, Mater. Sci. Eng., 2 (1967/68) 285.

11. R. F. Decker, Steel Stren. Mech. Symp. Zurich 506 (1969) 1-23.

12. L. M. Brown and R. K. Ham, Stren. Meth. Crys., Elsevier (1971) 9 Ed. by A. Kelly and R. B. Nicholson.

13. J. R. Mihalisin and R. F. Decker, Trans. A.I.M.E. 218 (1960) 507.

14. M. E. Fine, N. P. L. Symp. Rel. Str. Mech. Prop. Met. (HMSO) 1963.

15. D. Raynor and J. M. Silcock, Met. Sci. J., 4 (1970) 121.

16. V. A. Phillips, Phil. Mag., 16 (1967) 103.

17. L. K. Singhal and J. W. Martin, Acta Met., 16 (1968) 947.

18. B. J. Brindley and P. J. Worthington, Met. Rev., 145 (1970) 101.

19. H. Dio and Y. Shimanuki, "Proc. 2nd Int. Conf. Superalloys - Processing", P. 0-1, Metals and Ceramics Inf. Center (1972).

20. G. Thomas, D. Schmatz and W. Gerberich, "High Strength Mats.", ed. V. F. Zackay, Wiley (1965) 251.

21. M. Chaturvedi, Met. Trans., 3 (1972) 583.

22. V. A. Phillips, J. Inst. Met. 81 (1952/53) 649.

23. K. Matsuura, T. Nishiyama and S. Koda, Trans. J.I.M. 10 (1969) 429.

24. S. M. Adams, Scrip. Met. 7 (1973) 173.

25. D. W. Chung and M. Chaturvedi, Met. Sci. J., 6 (1972) 134.

26. W. Ostwald, Z. Phy. Chem., 34 (1900) 495.

27. G. W. Greenwood, "Mech. Phase Trans. Cry. Sols., Inst. Met. Monograph, London 33 (1969) 103.

28. Che-Yu Li and R. A. Oriani, Oxide disp.str., Met. Soc. Conf. Ed. G. S. Ansell, T. D. Cooper and F. V. Lenel, Gordon, New York, 47 (1968) 431.

29. A. J. Ardell, P. 111 in ref. 27.

30. C. Zener, J. Appl. Phys., 20 (1949) 950.

31. S. Sarian and H. W. Weart, J. Appl. Phys. 37 (1966) 1675.

32. A. J. Ardell, Acta Met., 20 (1972) 61.

33. J. D. Livingston, Trans. AIME 215 (1959) 566.

34. I. S. Servi and D. Turnbull, Acta Met., 14 (1966) 161.

35. G. R. Speich and R. A. Oriani, Trans. AIME, 233 (1965) 623.

36. J. W. Cahn, Acta Met., 10 (1962) 907.

37. J. W. Cahn, Acta Met., 14 (1966) 83.

38. R. A. Oriani, Acta Met., 12 (1964) 1399.

39. E. Hornbogen and M. Roth, Z. Metallk, 58 (1967) 842.

40. J. D. Eshelby, Acta Met., 14 (1966) 1306.

41. O. H. Kriege and J. M. Baris, Trans. ASM, 62 (1969) 195.

42. O. H. Kriege and C. P. Sullivan; Trans. ASM 61 (1968) 278.

43. E. H. Van Der Molen, J. M. Oblak and O. H. Kriege, Met. Trans., 2 (1971) 1627.

44. J. Friedel, "Dislocations", Pergamon Press Oxford, (1964).

45. K. H. Westmacott, C. W. Fountaini and R. J. Stirton, Acta Met., 14 (1966) 1628.

46. U. F. Kocks, Acta Met., 14 (1966) 1629.

47. U. F. Kocks, Phil. Mag., 13 (1966) 541.

48. U. F. Kocks, Canad. J. Physics, 45 (1967) 739.

49. A. J. E. Foreman and M. J. Makin, Phil. Mag., 14 (1966) 911.

50. A. J. E. Foreman and M. J. Makin, Canad. J. Phys., 45 (1967) 511.

51. R. K. Ham, "Ordered Alloys", Struct. Appl. Phys. Met., Claitors, Baton Rouge, Louisiana (1970) 365.

52. H. Gleiter and E. Hornbogen, Phys. Stat. Sol., 12 (1965) 235 and 251.

53. N. F. Mott and F. R. N. Nabarro, Rep. Conf. Str. Sol., Phy. Soc. (1948) 1.

54. V. Gerold and H. Haberkorn, Phy. Stat. Sol. 16 (1966) 675.

55. R. L. Fleischer, The Strength. Met., Reinhold, New York, (1964) 93.

56. E. Orowan, Symposium on Inter. Stress. in Met. and Alloys, London, The Inst. of Met. (1948) 451.

57. M. F. Ashby, Proc. Soc. Bolton Landing Conf. on Oxide Disp. Str., New York, Gordon and Breach.

58. P. B. Hirsch and F. J. Humphreys, Physics of Strength and Plasticity, ed. by Argon (1969) 189.

59. D. J. Bacon, U. F. Kocks and R. O. Scattergood, Phil. Mag. 28 (1973) 1241.

60. R. G. Davies and N. S. Stoloff, Trans. Met. Soc. AIME 233 (1965) 714.

61. V. A. Phillips, Acta Met., 14 (1966) 1533.

62. S. M. Copley and B. H. Kear, Trans. AIME 239 (1967) 977 and 984.

63. P. A. Flinn, Trans. AIME 218 (1960) 145.

64. E. Hornbogen and M. Mukherjee, Z für Metall., 55 (1964) 293.

65. J. L. Castagné, A. Pineau, and M. Sindzingre C. R. Acad. Sci. C263 (1966) 1465.

66. R. W. Guard and J. H. Westbrook, Trans. AIME 215 (1959) 807.

67. C. F. Bilsby, Ph.D. Thesis, Univ. of Camb. (1966).

68. J. L. Castagné, F. Lecroisey and A. Pineau, C. R. Acad. Sci., C266 (1968) 510.

69. M. H. Lewis and J. W. Martin, Acta Met., 11 (1963) 1207.

70. M. H. Lewis and J. W. Martin, Acta Met., 12 (1964) 753.

71. R. Ebeling and M. F. Ashby, 13 (1966) 805.

72. R. L. Jones and A. Kelly, Proc. of Soc. Bolt. Land. Conf. on Oxide Disp. Str. (1968).

73. A. Kelley and R. B. Nicholson, Prog. Mat. Sci., 10 (1963) 151.

74. A. H. Cottrell, Phil. Mag., 44 (1953) 829.

75. R. K. Ham and D. Jaffrey, Phil. Mag., 15 (1967) 245.

76. J. J. Gilman, "Nature of dislocations", Mech. Beh. of Mat. at elev. temp., McGraw Hill, New York (1961) 17.

77. A. M. Cottrell, Vacancies and Other point defects in Metals and alloys, Inst. Met. (1958) 1.

78. H. G. Van Bueren, Acta Met., 3 (1955) 519.

79. S. R. MacEwen and B. Ramaswami, Phil. Mag., 22 (1970) 1025.

80. K. Mukherjee, C. D'Antonio and R. C. Maciag, Scripta Met. 4 (1970) 209.

81. D. Munz and E. Macherauch, Z. Metallk, 57 (1966) 552.

82. O. Vöhringer and Macherauch, Z. Metallk., 58 (1967) 317.

83. J. R. Soler - Gomez and N. J. McG. Tegart, Phil. Mag., 20 (1969) 495.

84. B. Russell, Phil. Mag., 8 (1963) 615.

85. S. Miura and H. Yamauchi, Trans. JIM 13 (1972) 82.

86. H. M. Tensi and W. Piess, Z. Metallk., 63 (1972) 479.

87. H. M. Tensi, P. Dropmann and H. Borchers Acta Met., 20 (1972) 87.

88. W. Roberts, C-G, Lenasson and Y. Bergström, Scripta Met., 7 (1973) 395.

89. K. Mukherjee, C. D'Antonio, R. Maciag and G. Fischer, J. Appl. Phys., 39 (1968) 5434.

90. W. Rauchle, O. Vohringer and E. Macherauch, Z. Metallk., 64 (1973) 296.

91. F. Seitz, Advanc. Phys., 1 (1952) 43.

92. N. F. Mott, Phil. Mag., 43 (1952) 1151.

93. A. W. Sleeswyk, Acta Met. 6 (1958) 598.

94. P. G. McCormick, Acta Met., 20 (1972) 351.

95. G. Saada, Acta Met. 9 (1961) 166, 965.

96. G. Saada, Elect. Mic. and Strength of Crys., ed. by G. Thomas and J. Washburn, Interscience (1963) 651.

97. G. Saada, Physica 27 (1961) 657.

98. C. G. Lenasson, Scripta Met. 6 (1972) 1125.

99. G. F. Bolling, Phil. Mag., 4 (1959) 537.

100. B. Russell and P. Vella, Phil. Mag., 8 (1963) 677.

101. J. G. Rider and C. T. B. Foxon, Phil. Mag., 13 (1966) 289.

102. J. N. Lomer and H. M. Rosenberg, Phil. Mag., 4 (1959) 467.

103. W. Roberts, S. Karlsson and Y. Bergström, Mat. Sci. Eng., 11 (1973) 247.

104. W. G. Johnston and J. J. Gilman, J. Appl. Phys., 30 (1959) 129.

105. D. J. Lloyd, Scripta Met., 8 (1974) 1025.

106. M. C. Chaturvedi and D. J. Lloyd, Phil. Mag., 30 (1974) 1199.

107. D. J. Lloyd, P. J. Worthington and J. D. Embury, Phil. Mag., 21 (1970) 1147.

108. B. J. Brindley and P. J. Worthington, Acta Met., 17 (1969) 1357.

109. W. Charnock, Phil. Mag., 18 (1968) 89.

110. B. J. Brindley and P. J. Worthington, Scripta Met., 4 (1970) 295.

111. L. K. Singhal, Scripta Met., 5 (1971) 959.

112. T. Muto and Y. Takagi, "Solid State Physics", ed. by F. Seitz and D. Turnbull, 1 (1955) 193.

113. M. J. Marcinkowski, "Electron Micros, and Strength of Crys.", ed. by G. Thomas and J. Washburn, Interscience Pub., (Wiley and Sons), (1963) 333.

114. P. G. McCormick, Acta Met., 19 (1971) 463.

115. A. H. Cottrell, Phil. Mag., 8 (1963) 615.

116. A. Wijler, M. M. A. Vrijoff and A. Van Den Beukel, Acta Met. 22 (1974) 13.

117. Z. S. Basinski and S. Saimoto, Can. J. Phys., 45 (1967) 1161.

118. D. Tseng, M.Sc. thesis, Univ. of Man., (1974).

119. Z. S. Basinski, R. A. Foxall and R. Pascual, Scripta. Met., 6 (1972) 807.

120. J. E. Milliard, Quantitative Relation Between Prop. and Microstr., ed. by D. G. Brandon and A. Rosen, Israel Univ. Press (1969) 3.

121. P. M. Kelly, Inter. Metall. Rev. 18 (1973) 31.

122. E. H. Van Der Molen, J. M. Oblak and O. H. Kriege, Met. Trans., 2 (1971) 1627.

123. R. A. Swalin and A. Martin, Trans. Met. Soc. AIME, 206 (1956) 567.

124. A. F. Smith, Acta Met., 15 (1967) 1867.

125. E. N. Bower and J. A. Whiteman, "The Mech. of Pha. Trans., in Crys. Sol., " Inst. Met. Mon. 33 (1969) 119.

126. D. J. Chellman and A. J. Ardell, Acta Met., 22 (1974) 577.

127. V. Munjal and A. J. Ardell, Acta Met., 23 (1975) 513.

128. B. A. Parker, J. Autra. Inst. of Met. 14 (1969) 321.

129. B. A. Parker and D. R. F. West, J. Aut. Inst. Met. 14 (1969) 102.

130. G. I. Taylor, Met. Trans., 5 (1974) 39.

131. Y. Bergström and W. Roberts, Acta Met., 19 (1971) 1243.

132. M. Chaturvedi, D. J. Lloyd and K. Tangri, Met. Sci. J. 6 (1972) 16.

133. F. A. Mohamed, K. L. Murty and T. G. Langdon, Acta Met., (in press).

APPENDIX

Order strengthening by a pair of superlattice dislocations

It has been observed through equation (9) and (11) that the stress necessary to force the dislocation line 1 through the particle is given by

$$\tau_1 = \frac{\gamma_{APB}^{3/2}}{b} \left(\frac{4 f_v r_s}{\pi T^*}\right)^{1/2} \quad \ldots. \quad (a)$$

The fraction of dislocation line 1 cutting particles is then

$$\frac{2r_s}{L_1} = \left(\frac{4\gamma_{APB} f_v r_s}{\pi T^*}\right)^{1/2}, \quad \frac{\pi T^* f_v}{4\gamma_{APB}} \leq r_s \leq \frac{T^*}{\gamma_{APB}} \ldots. \quad (b)$$

The upper limit on this fraction for increasingly bent dislocation is set by the condition $r_s = T^*/\gamma_{APB}$ for which $L_1 = L$, that is, just at the point of Orowan bowing:

$$\frac{2r_s}{L_1} = \frac{2r_s}{L} = \left(\frac{4f_v}{\pi}\right)^{1/2}, \quad r_s = \frac{T^*}{\gamma_{APB}} \quad \ldots. \quad (c)$$

At and above this critical fraction, the stress to shear a particle becomes

$$\tau_1 = \frac{\gamma_{APB}}{b} \left(\frac{4f_v}{\pi}\right)^{1/2} \quad \ldots. \quad (d)$$

This stress must be less than the Orowan bowing stress in order for particle shear to continue.

The lower limit of $2r_s/L_1$, equation (b) is given by the value of L_1 for a perfectly straight dislocation and corresponds to the case of very small particles, that is

$$\frac{2r_s}{L_1} = f_v, \quad r_s \leq \frac{\pi T^* f_v}{4\gamma_{APB}} \quad \ldots. \quad (e)$$

As the first dislocation is just shearing the particles, as suggested by Fig. 4, the second dislocation is pulled forward by the Anti-phase boundary remaining in all particles cut by the first dislocation. If the two dislocations have the same shape and the separation X between the two dislocation is sufficiently small, but larger than r_s, the second dislocation may lie outside of all the particles. Then, at equilibrium, the total forward stress on the second dislocation τ_{II} balances the repulsive force between the two dislocations for edge component,

$$\tau_{II}\, b = \frac{Gb^2}{2\pi(1-\nu)x} \qquad \text{11..} \qquad \text{(f)}$$

Provided that the second dislocation does come into contact with A.P.B. and is nearly straight. The more A.P.B. is cut by the second dislocation, the less effective the particles become as obstacles. Then, referring to Fig. (4), the force balances as follows:

dislocation I,

$$\tau b + \frac{Gb^2}{2\pi(1-\nu)x} - \frac{\gamma_{APB}\, d_1}{L_I} = 0 \qquad \text{....} \qquad \text{(g)}$$

dislocation II

$$\tau b + \frac{\gamma_{APB} d_{II}}{L_{II}} - \frac{Gb^2}{2\pi(1-\nu)x} = 0 \qquad \text{....} \qquad \text{(h)}$$

Solving equation (g) and (h) simultaneously one obtain for the forward stress on the first dislocation:

$$2\tau b + \frac{\gamma_{APB} d_{II}}{L_{II}} = \frac{\gamma_{APB} d_1}{L_I} \qquad \text{....} \qquad \text{(i)}$$

Since the second dislocation is observed to be straight during shear by the first dislocation, one may substitute equation (e) for d_{II}/L_{II} and equation (b) for d_1/L_1 so that:

$$2\tau b + \gamma_{APB} f_v = \left(\frac{4 \gamma_{APB} f_v r_s}{\pi T^*}\right)^{1/2} \gamma_{APB} \quad \ldots\ldots \quad (j)$$

Leading to the following relation for the applied stress τ:

$$\tau = \frac{\gamma_{APB}}{2b} \left[\left(\frac{4 \gamma_{APB} f_v r_s}{\pi T^*}\right)^{1/2} - f_v\right]$$